Brain Tumor Classification and Watermarking of MRI Using Nonsubsampled Contourlet Transform

By

Chandan Saha

A thesis submitted in partial fulfillment of the requirements for the degree of
M.Sc. Engineering
in the Department of Electronics and Communication Engineering

Department of Electronics and Communication Engineering
Khulna University of Engineering & Technology
Khulna 9203, Bangladesh

November, 2018

Declaration

This is to certify that the thesis work entitled "*Brain Tumor Classification and Watermarking of MRI Using Nonsubsampled Contourlet Transform*" has been carried out by *Chandan Saha* in the Department of Electronics and Communication Engineering, Khulna University of Engineering & Technology, Khulna, Bangladesh. The above thesis work or any part of this work has not been submitted anywhere for the award of any degree or diploma. Except where states otherwise by reference or acknowledgement, the work presented is entirely my own.

Signature of Supervisor

Signature of Candidate

Approval

This is to certify that the thesis work submitted by *Chandan Saha* entitled "*Brain Tumor Classification and Watermarking of MRI Using Nonsubsampled Contourlet Transform*" has been approved by the board of examiners for the partial fulfillment of the requirements for the Degree of *M.Sc. Engineering* in the Department of *Electronics and Communication Engineering*, Khulna University of Engineering & Technology, Khulna, Bangladesh in November, 2018.

BOARD OF EXAMINERS

1. Dr. Md. Foisal Hossain — Chairman (Supervisor)
Professor
Department of Electronics and Communication Engineering
Khulna University of Engineering & Technology

2. Head, — Member
Department of Electronics and Communication Engineering
Khulna University of Engineering &Technology

3. Dr. Md. Mostafizur Rahman — Member
Professor
Department of Electronics and Communication Engineering
Khulna University of Engineering & Technology

4. Dr. A. B. M. Aowlad Hossain — Member
Professor
Department of Electronics and Communication Engineering
Khulna University of Engineering & Technology

5. Prof. Dr. Kazi Khairul Islam — Member (External)
Dean,
School of Science & Engineering
Uttara University

Abstract

Automatic or semi-automatic brain tumor classification scheme is demanded in today's medical system to get rid of human involvement of classification of brain tumor images. So, here we propose nonsubsampled contourlet transform (NSCT) based MRI brain tumor classification using support vector machine (SVM) and artificial neural network (ANN) classifier. In this scheme, K-means clustering is used for segmentation of region of interest. NSCT is applied to the region of interest of brain image in order to obtain its low and high subband coefficients. Then from the coefficients of NSCT, twelve features are extracted from the region of interest. SVM which incorporates two stages is trained with these twelve features. 1st stage of SVM is able to classify brain image as normal or abnormal and then 2nd stage of SVM classifies grade of tumor as low grade, where tumor is slowly growing or high grade, where tumor is rapidly growing. The grade of tumor is also classified using the ANN classifier based on feed forward back propagation. Furthermore, when the multimedia contents like MRIs or other images are transferred through a communication channel, sometimes the whole content or its part may be modified or deteriorated by hackers. In order to protect this content from unauthorized user, digital watermarking is considered to be a promising tool. So another purpose of this research is to develop image watermarking scheme which ensures higher security, imperceptibility and robustness against different distortion attacks. In first proposed scheme of image watermarking, NSCT is also used because most of the perceptual content of an image focuses on low frequency subband of NSCT. Singular value decomposition (SVD) is also applied on low frequency subband of NSCT, because the singular values taken from low frequency subband have certain stability. Besides, game of life (GOL) cellular automata is used to scramble binary watermark so that no one can recover the watermark without secret scrambling keys. So in this scheme, NSCT and SVD ensure the imperceptibility and robustness as well as cellular automata improves the security. In second proposed scheme of watermarking, multiple chaotic maps, NSCT and discrete cosine transform (DCT) are used. Here, an arranged chaotic sequence which is created by logistic map is used to shuffle the pixel positions of MRI. Patient information, watermark is encrypted by two chaotic maps, like Arnold's Cat map and tent map. Then, DCT coefficients of encrypted watermark are embedded into the DCT coefficients of NSCT's approximation band of shuffled MRI. Both proposed watermarking schemes are tested on varieties of MRIs and their associated results reveal that the two schemes have promising improvements in imperceptibility and robustness against noise and geometric attacks. Overall, NSCT is used in both brain tumor classification and watermarking in this research.

Keyword: Magnetic resonance imaging, K-means clustering, nonsubsampled contourlet transform, support vector machine, artificial neural network, game of life cellular automata, singular value decomposition.

Acknowledgement

First and foremost, I am thankful to the Almighty Creator. It is His plan and my belief in Him that helped me finish all steps for completing my M. Sc. Engineering degree.

My sincere appreciation goes to my respected thesis supervisor Prof. Dr. Md. Foisal Hossain for accepting me as his student and giving me the directions to finish my studies. I am grateful to him for his kind inspiration and supports throughout the entire time.

I wish to thank the course teachers of my M. Sc. Engineering degree – Prof. Dr. Md. Mostafizur Rahman. Prof. Dr. Md. Faruque Hossain, Prof. Dr. A.B.M. Aowlad Hossain, Prof. Dr. Monir Hossen, Prof. Dr. Sheikh Md. Rabiul Islam, with Course Co-coordinator Prof. Dr. Md. Foisal Hossain, Department of Electronics and Communication Engineering, Khulna University of Engineering & Technology (KUET) and all of the examiners for their time to review the thesis and attend in my defense as a board member.

I thank my family for their love and affection. They taught me the importance of education and always inspired me to work harder and better to succeed in my academic and professional pursuit.

Author

Contents

CHAPTER II Literature Review 11-34

List of Tables

List of Figures

List of Abbreviations

ACS	American Cancer Society
ANN	Artificial Neural Network
CA	Cellular Automata
CSF	Cerebrospinal Fluid
CT	Contourlet Transform
CT	Computed Tomography
DWT	Discrete Wavelet Transform
DFB	Directional Filter Bank
FN	False Negative
FP	False Positive
GLCM	Gray Level Co-occurrence Matrix
GM	Gray Matter
GOL	Game of Life
GRB	Gaussian Radial Basis
IDM	Inverse Difference Moment
JPEG	Joint Photographic Expert Group
KNN	K-Nearest Neighbor
KSVM	Kernel Support Vector Machine
LBP	Local Binary Pattern
LSB	Least Significant Bit
NBTF	National Brain Tumor Foundation
MRI	Magnetic Resonance Imaging
MRI	Mean Square Error
NC	Normalized Correlation
NSCT	Nonsubsampled Contourlet Transform
NSDFB	Nonsubsampled Directional Filter Bank

NSFB	Nonsubsampled Filter Bank
NSP	Nonsubsampled Pyramid
PET	Positron Emission Tomography
PNG	Portable Network Graphics
PSNR	Peak Signal to Noise Ratio
RGB	Red, Green and Blue
RMS	Root Mean Square
ROI	Region of Interest
SD	Standard Deviation
SVM	Support Vector Machine
SVD	Singular Value Decomposition
DCT	Discrete Cosine Transform
TN	True Negative
TP	True Positive
WHO	World Health Organization

CHAPTER I

INTRODUCTION

1.1 Introduction

Brain tumor is one of most dangerous diseases which results from the rampant augmentation of cells in human brain which is regarded as one leading causes of death among people. According to the statistics of American Cancer Society [1] and National Brain Tumor Foundation (NBTF) [2], the rate of death caused by brain tumor is rising alarmingly. Among various types of brain tumors, glioma is the most common and hostile in nature which is found in glial cells in brain. World Health Organization (WHO) and American Brain Tumor Association uses a grading scale from I to IV in which grade I and II glioma are called low grade glioma and grade III and IV are called high grade glioma [3]. Low grade glioma shows less aggressiveness than high grade glioma [4]. People affected with low grade glioma require serial monitoring and sometimes surgical excursion of tumor can be a solution for them [4]. Whereas current treatments for the people affected with high grade or grade III and IV tumor are the radiotherapy, chemotherapy or coalition of thereof [3]. However, with the advance of medical diagnosis, different imaging tools like magnetic resonance imaging (MRI), computed tomography (CT), positron emission tomography (PET) are used by physicians for detection of tumor. Among them, MRI is widely used, because it is non-invasive, no involvement of radiation and also provides greater contrast of soft tissue [5] than other imaging tools. However, discriminating tumor region from other normal tissues like gray matter (GM), white matter (WM), cerebrospinal fluid (CSF) [3] and further classifying of tumors is highly problematic for any physician. Besides, this process of manual investigation of MRI image is accurate and also a time consuming task [6] which results in misdiagnosis of patients. On the other hand, the chance of survival rate of brain tumor affected patient largely depends on the accurate detection of tumor and its area of spreading region. The process of treatment like surgical operation, chemotherapy and radiotherapy entirely depends on the classification of tumor. So, there is a need to develop a fast and accurate scheme which will reduce this type of human involvement for detecting and classifying tumor.

While transferring the multimedia content like magnetic resonance images (MRIs) or other normal images, sometimes the whole content or its part may be modified or deteriorated by hackers. In order to protect this content from unauthorized user, digital watermarking is a promising tool [7]. Digital watermarking is an emerging data hiding tool which is applied in various multimedia applications in order to protect the content from unauthorized user, to ensure data authenticity [8]. It usually embeds secret information called watermark into multimedia data like image, audio and video in an effective way that it is imperceptible to human visual system and extracts it later to prove authentication. So there is a need to develop an image watermarking scheme which ensures higher security, imperceptibility and robustness against different distortion attacks while transferring the magnetic resonance images or other images.

1.2 Related Works

1.2.1 Related Works on Brain Tumor MRI Classification

Different researchers have proposed various schemes in order to classify the MRI brain images as normal, where tumor is absent or abnormal, where tumor is present. Chaplot *et al.* [9] proposed a scheme for classification of MRI brain images in which discrete wavelet transform (DWT) is used for extracting features. Artificial neural network (ANN) and support vector machine (SVM) were used for classification of normal and abnormal MRI image. Dahshan *et al.* [10] proposed hybrid intelligent techniques in which features were extracted using DWT and then features were reduced by principal component analysis (PCA). In this approach, two classifiers like feed forward back propagation artificial network (FP-ANN) and K-nearest neighbor were applied for classification of MRI brain image. Kharrat *et al.* [11] proposed wavelet and genetic algorithm (GA) based MRI brain image classification scheme. Wavelet was used for extracting features and then genetic algorithm was used for selecting features. SVM was then used for classification of MRI brain image. Ahmad *et al.* [12] proposed DWT and PCA based normal or abnormal MRI image classification scheme. In this approach, the linear and radial basis kernel functions were used to classify MRI brain images. Ellah *et al.* [13] kernel SVM based brain images classification scheme. Here, K-means clustering was applied to segment MRI and then and features were extracted from segmented image. Then kernel SVM was used to classify normal or abnormal MRI image. In some approaches, features are extracted from MRI image directly without applying wavelet transform. Nandpuru *et al.* [14] proposed a scheme in which gray scale, symmetrical and texture features were extracted directly MRI brain image. These features were used to classify normal or abnormal MRI image using linear, quadratic and polynomial kernel SVM. Kumar *et al.* [15] proposed a scheme in which MRI brain image is segmented using region growing algorithm and morphological operation. Histogram and textural features are extracted and then SVM is used. Zacharaki *et al.* [16] proposed a machine learning scheme for classification of tumor grade using MRI texture and shape. In their scheme, features like tumor shape, intensity characteristics and rotation invariant texture features were extracted. SVM with recursive feature elimination was used for feature subset selection. Suhag *et al.* [17] proposed automatic brain tumor detection and classification of different types of tumor using SVM classifier. In their scheme, Fuzzy C-means clustering was used for performing the segmentation of brain MRI. Multi-SVM was used to classify the types of tumors like Gliomas, Metastasis, Astrocytoma etc. Latif *et al.* [18] proposed Random Forest classifier based brain glioma classification using 3D discrete wavelet transform (DWT) features. Here, a technique was proposed for classification and segmentation of low-grade and high-grade glioma tumors in multimodal MRI. MRI is divided into small blocks and features were extracted using DWT from each block. Random Forest classifier was applied for the classification of multiple Glioma tumor classes. By reconstructing the MRI based on classified blocks, the desired segmentation was performed. Queen *et al.* [19] proposed a survey on brain tumor classification using ANN. This technique used back propagation ANN classifier was used for classifying brain tumor as benign, grade I, grade II and malignant tumor.

1.2.2 Related Works on Image Watermarking

Different researchers have proposed different watermarking schemes in different frequency domains. Lee *et al.* [20] proposed DWT and bit plane base region of interest (ROI) medical image watermarking. In this scheme, the host image is segregated to ROI and NROI. Then 3-level DWT was applied to the ROI image in order to obtain low frequency subband LL_3. The wave coefficients of LL_3 were represented to 8 bit plane. Each of bit plane information was used as the watermark which was the embedded into the NROI using the embedding information. The proposed scheme was tested for its effectiveness on MRIs under JPEG compression attacks. Li *et al.* [21] DWT and Arnold transform based medical images watermarking. In their scheme, Arnold transform was used for scrambling the binary watermark which enhanced the security of watermarking. Then DWT was employed on the original medical image for obtaining approximated coefficients subband LL_1 and DCT was applied on these approximated coefficients. Then DWT-DCT coefficients were arranged in order to form a feature vector. Then using the encrypted watermark and feature vector, a public key sequence was generated following Hash cryptography which preserved the ownership of original image. Nedooshan *et al.* [22] proposed medical image watermarking based on SVD-DWT technique. In their method, a threshold technique was used for ROI areas form NROI areas of the original image. Then 2-level DWT is applied on the host image and then detailed coefficient's subband was divided into 8*8 sunblock. The energy of each sub-block is computed and the block with highest energy was selected. Then SVD was applied used embedding the watermark. Dharwadkar *et al.* [23] proposed non-blind watermarking method for color images using DWT-SVD. Bhagyashri *et al.* [24] proposed a robust color images watermarking technique in YUV color space using all frequency band DWT-SVD. Nasir *et al.* [25] proposed image normalization based a robust color image watermarking. Gunjal *et al.* [26] proposed DWT-SVD based color image watermarking technique in different color spaces.

1.3 Motivation

Among different types of brain tumors, gliomas are the most aggressive with the highest mortality rate [2]. However, for the anatomical examination of tumor in brain, magnetic resonance imaging (MRI) is widely used [3]. But manual investigation of MRI images like tumor detection, image or tumor classification from a large number of MRI images is a time consuming process and also susceptible to errors [6]. One of the purposes of this research is to develop a fast, accurate scheme for classifying brain tumor MRIs. In proposed brain tumor image classification scheme, nonsubsampled contourlet transform (NSCT) which was first proposed by Cunha, Zhou and Do in 2006 [27] is used. NSCT has multiscale, multidirection, shift invariance properties and provides better performance than contourlet transform (CT) and DWT in image analysis applications such as edge detection, contour characterization, image denoising [28-29]. It has also better frequency selectivity and regularity than CT [29]. In proposed brain tumor image classification scheme, NSCT can be applied for extracting features from segmented brain image. These features can be applied to support vector machine (SVM) and artificial neural network classifier (ANN) classifier in order to classify the type of tumor as low grade or high grade.

Furthermore, while transferring the multimedia content like magnetic resonance images (MRIs) or other normal images, sometimes the whole content or its part may be modified or deteriorated by hackers. In order to protect this content from unauthorized user, digital watermarking is a promising tool [7]. Another purpose of this research is to develop an image watermarking scheme which ensures higher security, imperceptibility and robustness against different distortion attacks. In proposed first watermarking scheme, NSCT can also be used along with cellular automata and singular value decomposition (SVD). A cellular automaton can be used for improving security. As Most of the perceptual content of an image focuses on low frequency subband of NSCT and the singular values taken from low frequency subband have certain stability. NSCT along with SVD will ensure imperceptibility and robustness against different distortion attacks. Besides, the strength of scrambling of an image can be increased by using multiple chaotic maps and secret keys associated with this scrambling process can also increase the security of watermarking. So, another watermarking is proposed, where patient information can scrambled using multiple chaotic maps and NSCT along with discrete cosine transform (DCT) can be used for embedding. This scheme also will give promising performance for imperceptibility and robustness test of watermarking.

1.4 Objectives

One of the objectives of this research work is to classify normal or abnormal brain images and then to classify low or high grade tumor images. Because of outstanding features of NSCT, like multiscale, multidirection, shift invariance and varieties of applications, NSCT is used in this work. In brain tumor classification, NSCT is mainly used for extracting features which applied to SVM and ANN classifier in order to classify the type of tumor as low grade or high grade. Another objective of this research is to develop an image watermarking scheme which ensures higher security, imperceptibility and robustness against different distortion attacks. Here, two watermarking schemes are proposed, where NSCT is used for embedding of watermark. Cellular automata and multiple chaotic maps are used separately in these schemes. In proposed first watermarking scheme, NSCT is used along with cellular automata and SVD. A cellular automaton is used for improving security. In second watermarking, multiple chaotic maps are used for ensuring security and NSCT with DCT is also applied for embedding patient's information.

1.5 Challenges

Discriminating tumor region from other normal tissues like gray matter (GM), white matter (WM), cerebrospinal fluid (CSF) [3] and further classifying of tumors is highly problematic for any physician. Besides, proper classification of grade of tumors is also problematic task. But automatic or semiautomatic detection of brain tumor and further classification of tumor into different grades is not simple work. An automatic scheme faces some challenging issues like noise of MRI image produced by scanner [30], patient to patient tumor variation, various tumor types etc. For overcome these problems, automatic tumor detection and classification scheme consists of several stages like preprocessing, features or attributes extraction, features classification. Although different researchers have proposed different aforementioned schemes for accurate detection of tumor region and classification of tumor, but there is no universal method that can be applied to all kinds of images; so brain tumor detection and classification of tumor remains a challenging issue in biomedical image processing fields.

In image watermarking, security, imperceptibility and robustness against different distortion attacks are very important factors. Specially, in case of medical image watermarking imperceptibility of watermarked image is the crucial factor. The region of interest of medical image like tumor region of MRI should be not being changed during embedding of watermark. Different researchers have proposed different aforementioned watermarking schemes in order to ensure the security, imperceptibility and robustness The aforementioned watermarking schemes don't provide the desired level of security, imperceptibility and robustness against various image processing and geometric attacks like Gaussian white noise, salt and pepper noise, median filtering, JPEG compression, cropping and rotation.

1.6 Contribution of This Research

In brain tumor classification scheme, median filter is used for removing noise and enhancing resolution of MRI brain images. Median filter is chosen, because it preserves the information of edges, when denoising is performed on MRIs. Then K-means clustering is used for segmenting MRI brain images, due to its faster segmentation capability. NSCT is used for extracting twelve features [14] from region of interest of segmented brain MRI. NSCT has shift invariance, multiscale and multidirectional properties and it gives more geometric information in various directions of an image rather than contourlet transform (CT) and discrete wavelet transform (DWT). So, features are extracted from the low and high subband coefficients of NSCT of segmented MRI. These features are used to train the support vector machine (SVM) for the classification of MRI brain images as normal or abnormal and also for the further classification of type of tumor as low grade or high grade. Using these features, the grade of tumor as low grade or high grade is also classified using the ANN classifier based on feed forward back propagation. The effectiveness of the proposed hybrid scheme is evaluated in terms of sensitivity, specificity and accuracy. The brain tumor images which are used for evaluating the performance of the classification scheme are collected from standard database, called BRATS (Multimodal Brain Tumor Segmentation Challenges).

In image watermarking, NSCT is also used along with cellular automata and singular value decomposition (SVD). Game of life (GOL) cellular automata is used to scramble binary watermark, where the initial parameters of this scrambling process are considered as secret keys. This keys play pivotal role for the security improvement of this watermarking technique. Because of the salient features like multiscale, multidirection and shift invariance of NSCT, 2-level NSCT is applied to magnetic resonance images. Most of the perceptual content of an image focuses on low frequency subband of NSCT and the singular values of low frequency subband have certain stability to any modest change. In this proposed scheme, each singular value of scrambled binary watermark is embedded in fixed location of singular value matrix of low frequency subbands of NSCT of magnetic resonance image. This watermarking scheme is also applied on RGB color image which is used as a cover image. The scheme offers security, imperceptibility and robustness against various image processing and geometric attacks like Gaussian white noise, salt and pepper noise, median filtering, JPEG compression, cropping and rotation. The proposed scheme is compared with existing watermarking schemes in terms of Peak Signal to Noise ratio (PSNR), Normalized Correlation (NC) and provides satisfactory performance than other schemes. Here, another watermarking is proposed, where patient information is scrambled using multiple chaotic maps. Here, three chaotic maps, such as Arnold’s cat map, logistic map and tent map are used in ways. The number of iterations and the initial values of parameters of these maps are used as confidential keys, which strengthen the security of proposed watermarking. Besides, the approximation band of NSCT contains considerable visual information of an image. DCT is applied on this approximation band, because NSCT along with DCT makes watermarking technique more imperceptible and robust. This scheme is also evaluated with PSNR, NC and gives promising performance for imperceptibility and robustness test of watermarking.

1.7 Outlines of Thesis

- **Chapter 2** contains literature review of brain tumors, MRI, watermarking, NSCT, image segmentation, SVM, ANN, Arnold's cat map, logistic map, tent map, game of life cellular automata, SVD and DCT.
- **Chapter 3** consists of proposed methodologies of brain tumor classification and watermarking.
- **Chapter 4** comprises with results and discussion of proposed methodologies.
- **Chapter 5** concludes the total work with clear illustration of applicability, benefits and limitations of the proposed schemes. The scope of future work is also analyzed in this section.

References

[1] E. Dandıl, M. Çakıroğlu, and Z. Ekşi, "Computer-aided diagnosis of malign and benign brain tumors on MR images," *ICT Innovations*, vol. 311, pp. 157-166, 2015.

[2] M.K. Abd-Ellah, A.I. Awad, A.A.M. Khalaf, and H.F.A. Hamed, "Classification of brain tumor MRI brain images using a kernel support vector machine," *Communications in Computer and Information Science*, vol. 636, pp. 151-160, Sep. 2015.

[3] N.B. Bahadure, A.K. Ray, and H.P. Thethi, "Image analysis for MRI brain tumor detection and feature extraction using biologically inspired BWT and SVM," *International Journal of Biomedical Imaging*, vol. 2017, pp.1-12, 2017.

[4] S. Pereira, A. Pinto, V. Alves, and C.A. Silva, "Brain tumor segmentation using convolutional neural networks in MRI images," *IEEE Transactions on Medical Imaging*, vol. 35 (5), pp. 1240-50, May 2016.

[5] P.M.S. Kumar and S. Chatterjee, “Computer aided diagnostic for cancer detection using MRI images of brain,” in Proc. *India Conference (INDICON)*, Dec. 2016.

[6] A. Aslam, E. Khan, and M.M.S. Beg, “Improved edge detection algorithm for barin tumor segmentation,” *Procedia Computer Science*, vol. 58, pp.430-437, 2015.

[7] W.H. Lin, Y.R. Wang, S.J. Horng, T.W. Kao, and Y. Pan, “A blind watermarking method using maximum wavelet coefficeint quantization,” *Expert Systems with Applications*, vol. 36, no. 9, pp.11509-11516, November 2009.

[8] A.A. Haj, “Providing integrity, authenticity and confidentiality for header and pixel data of dicom images,” *Journal of Digital Imaging*, vol. 28, no. 9, pp.179-187, April 2015.

[9] S. Chaplot, L.M. Patnaik and N.R. Jagannathan, “Classification of magnetic resonance brain images using wavelets as input to support vector machine and neural machine,” *Biomedical Signal Processing and Control*, vol. 1, pp.86-92, Jan. 2006.

[10] E.S.A. El-Dahshan, T. Hosny and A.B.M Salem, “Hybrid intelligent techniques for MRI brain images classification,” *Digital Signal Processing*, vol. 20, pp. 433-441, 2010.

[11] A. Kharrat, K. Gasmi, M.B. Messaoud, N. Benamrane and M. Abid, “A hybrid approach for automatic classification of brain MRI using genetic algorithm and support vector machine,” *Leonardo Journal of Sciences* (ISSN 1583-0233),” pp. 71-82, 2010.

[12] M. Ahmad, M.U. Hassan, I. Shafi and A. Osman, “Classification of tumors in human brain MRI using wavelet and support vector machine,” *IOSR Journal of Computer Engineering (IOSRJCE)*, vol. 8(2), pp. 25-31, 2012.

[13] M.K. Abd-Ellah, A.I. Awad, A.A.M. Khalaf, and H.F.A. Hamed, “Classification of brain tumor MRI brain images using a kernel support vector machine,” *Communications in Computer and Information Science*, vol. 636, pp. 151-160, Sep. 2015.

[14] H.B. Nandpuru, S.S. Salankar, and V.R. Bora, “MRI brain cancer classification using support vector machine,” in Proc. of *IEEE Students’ Conference on Electrical, Electronics and Computer Science*, March 2014.

[15] P. Kumar and B. Vijayakumar, “Brain tumor MR image segmentation and classification using by PCA and RBF kernel based support vector machine,” *Middle-East Journal of Scientific Research*, vol. 23(9), pp. 2106-2116, 2015.

[16] E.I. Zacharaki, S. Wang, S. Chawla, D.S. Yoo, R. Wolf, E.R. Melhem, and C. Davatzikos, “Classification of brain tumor type and grade using MRI texture and shape in a machine learning scheme,” *Magnetic Resonance in Medicine*, vol. 62, pp. 1609-18, 2009.

[17] S. Suhag and L.M. Saini, “Automatic brain tumor detection and classification using SVM classifier,” *International Journal of Advances in Science Engineering and Technology*, ISSN: 2321-9009, pp. 121-25, October 2015.

[18] G. Latif, M.M. Butt, A.H. Khan, O. Butt, and D.N.F.A. Iskandar, “Multiclass brain glioma tumor classification using block-based 3D wavelet features of MR images,” in Proc. of *4th International Conference on Electrical and Electronics Engineering*, pp.33-37, April 2017.

[19] M. Queen and T.M. Babi, “A survey on brain tumor classification using artificial neural network,” *International Journal of Advanced Research in Computer Engineering & Technology (IJARCET)*, vol. 3, no. 11, 2014.

[20] H.K. Lee, H.J. Kim, K.R. Kwon, and J.K. Lee, “ROI medical image watermarking using DWT and bit plane,” in Proc. of *Asia-Pacific Conference on Communications*, October, 2017.

[21] J. Li, M. Huang, H. Zhang, C. Dong, and Y. Bai “ The medical images watermarking using DWT and Arnold,” in Proc. of *International Conference on Computer Science and Automation Engineering (CSAE)*, 2012.

[22] A.S. Nedooshan, K. Yaghmaie and R.S. Nadooshan, “Medical image watermarking based on SVD-DWT technique,” *International Congress on Informatics, Environment, Energy and Applications (IEEA)*, vol. 38, 2012.

[23] N.V. Dharwadkar, B.B. Amberker and A. Gorai, “Non-blind watermarking scheme for color images in RGB space using DWT-SVD,” in Proc. of International Conference on Communications and Signal Processing (ICCSP), pp. 489-493, February 2011.

[24] S.K. Bhagyashri and M.Y. Joshi, “All frequency band DWT-SVD robust watermarking technique for color images in YUV color space,” in Proc. of International Conference on Computer Sciecne and Automation Engineering (ICCSAE), pp. 292-299, June 2011.

[25] I.A. Nasir and A.B. Abdurrman, “A robust color image watermarking scheme based on image normalization,” in Proc. of World Congress on Engineering (WCE), vol. 3, July 2013.

[26] B.L. Gunjal and S.N. Mali, “Comparative performance analysis of DWT-SVD based color image watermarking technique in YUV, RGB and YIQ color spaces,”Internatioal Journal of Computer Theory and Engineering, vol. 3, no. 6, pp. 714-179, December 2011.

[27] A.L. Cunha, J. Zhou, and M.N. Do, “The nonsubsampled contourlet transform: theory, design and applications,” IEEE Transactions on Image Processing, vol. 15, no. 10, pp. 3089-3101, 2006.

[28] M.F. Hossain, M.R. Alsharif, and K. Yamashita, “LMMSE-based image denoising in onsubsampled contourlet transform domain,”Lecture Notes in Computer Science, vol. 6134, pp. 36-43, 2010.

[29] J. Zhou, A.L. Cunha, and M.N. Do, “Nonsubsampled contourlet transfrom: construction and application in enhancement,” in Proc. of International Conference on Image Processing (ICIP), Septermber 2005.

[30] M. Havaei, P.M. Jodoin, and H. Larochelle, “Efficient interactive brain tumor segmentation within-brain KNN classification,” in Proc. of 22nd International Conference on Pattern Recognition (ICPR), pp.556-561, August 2015.

CHAPTER II

LITERATURE REVIEW

2.1 Introduction

This chapter presents the overview of brain tumors, MRI, watermarking, nonsubsampled contourlet transform (NSCT), image segmentation, support vector machine (SVM), artificial neural network (ANN), Arnold's cat map, logistic map, tent map, cellular automata, singular value decomposition (SVD), discrete cosine transform (DCT). Firstly, brain anatomy, tumors, types of tumor and MRI are described. Then types, requirements and techniques of watermarking are outlined. The structural description of NSCT illustrated. Then, Image segmentation using K-means clustering is described here. Machine learning based classifier like SVM and feed forward back propagation ANN are described. Arnold's cat map, logistic map, tent map, Game of life cellular automata, SVD and DCT are outlined.

2.2 Brain Anatomy Overview

The human brain is an amazing organ with a very swift processing capability; it is able to collect and process concurrently thousands of sensory and cognitive inputs through our five sensory organs, store information in the brain and dominant our movements, actions, thoughts, and speech [1-2]. The brain collects all information using our five senses: sight, touch, taste, smell, and hearing [2]. Figure 2.1 demonstrates the vertical cross section of the human brain. The brain consists of 3 vital parts: The cerebrum, the cerebellum, and the brainstem (or medulla) [2]. Figure 2.2 shows the position of lobes of human brain [2].

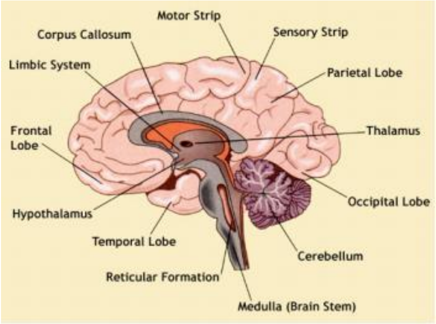

Figure 2.1: Vertical cross section of the human brain [2].

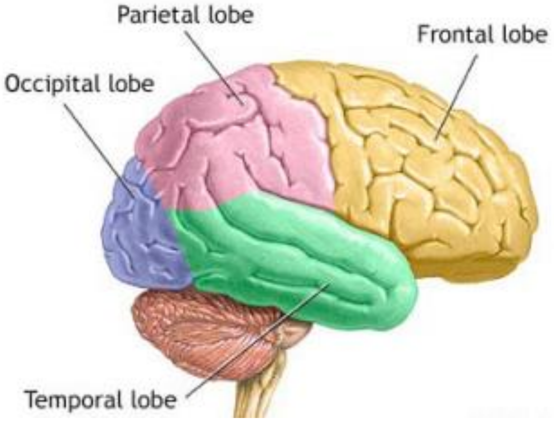

Figure 2.2: Lobes of human brain [2].

- **Functions of Frontal lobe:** Personality, behavior, emotions, judgment, planning, problem solving, speaking, writing, body movement (motor strip), intelligence, concentration, self-awareness [2].
- **Functions of Temporal lobe:** Understanding language (Wernicke's area), memory, hearing, sequencing and organization [2]
- **Functions of Parietal lobe:** Interpreting language, sense of touch, pain, temperature (sensory strip), signals from vision, hearing, motor, sensory and memory [2].
- **Functions of Occipital lobe:** Interprets vision (color, light, movement) [2]

2.3 Brain Tumors

Normally new cells are born in the adult body only when they are required to replace old or damaged ones. New cells are created in the children in order to accomplish their development in addition to those needed for repair. But unnecessary multiplication of normal or abnormal cells creates tumor in living creatures [3].

Brain tumor is one of most dangerous diseases which results from the rampant augmentation of cells in human brain which is regarded as one leading causes of death among people. According to the statistics of American Cancer Society [4] and National Brain Tumor Foundation (NBTF) [5], the rate of death caused by brain tumor is rising alarmingly. It is the second main reason of cancer death for children (< 15 years) and young adults (~34 years) [4]. The incidence rate of all brain and other central nervous tumors is 22.64 cases per 100,000 for a total count of 379,848 incident tumors [6]. The rate is higher in females than in males. An approximated 78,980 new cases of brain and other central nervous tumors are assumed to be diagnosed in the United States in 2018 [6].

Causes and risk factors of brain tumor can be *environmental or genetic*. Many studies have looked at a wide spectrum of environmental factors as possible causes of brain tumors including but not limited to [3]:

- Being exposed to air pollution, residential power lines, second hand smoke, agricultural chemicals and industrial formaldehyde
- Working in synthetic rubber manufacturing or petroleum refining/production
- Smoking cigarettes, smoking cigarettes while pregnant and consuming alcohol
- Using common medications like birth control pills, sleeping pills, headache remedies, over-the-counter pain treatments and antihistamines
- Experiencing viruses and common infections
- Having a history of head trauma, epilepsy, seizures or convulsions
- Consuming cured foods (nitrites)

2.4 Types of Brain Tumors

Scientists have classified brain tumor according to the location of the tumor, type of tissue involved, whether they are noncancerous or cancerous. The site of the origin (primary and secondary) and other factors involved. Brain tumors can be cancerous (malignant) or noncancerous (benign). The benign brain tumor has uniform structure which does not contain cancer cells, whereas malignant brain tumor has non-uniform structure which contains cancer cells [7]. When tumors grow, they create the pressure inside our skull. This can cause our brain damage, and very often it could be life-threatening [8].

Brain tumors are categorized as primary or secondary. A primary brain tumor originates in our brain. A secondary brain tumor, also referred to as metastatic brain tumor, occurs when cancer cells spread to our brain form another organ, like lung or breast [8].

2.4.1 Primary Brain Tumors

Primary brain tumors can develop in our brain cells, the membranes that surround our brain, nerve cells and glands [8]. Primary tumors can be benign or cancerous. In adults, the most common types of brain tumors are gliomas and meningiomas [8].

2.4.1.1 Gliomas

Gliomas are tumors that develop from glial cells [8]. These cells normally support the structure of our central nervous system, provide nutrition, clean cellular waste and break down dead neurons [8]. Gliomas can develop from different types of glial cells. Among various types of brain tumors, glioma is the most common and hostile in nature [9]. World Health Organization

(WHO) and American Brain Tumor Association uses a grading scale from I to IV in which grade I and II glioma are called low grade glioma and grade III and IV are called high grade glioma [7]. Low grade glioma shows less aggressiveness than high grade glioma [9]. People affected with low grade glioma require serial monitoring and sometimes surgical excursion of tumor can be a solution for them [7]. Whereas current treatments for the people affected with high grade or grade III and IV tumor are the radiotherapy, chemotherapy or coalition of thereof [7, 9].

2.4.1.2 Meningiomas

These tumors results from the arachnoid mater which is one of the layers of the meninges of brain. Very often these tumors are occurred in middle aged woman and 38% of primary brain tumors are meningiomas. The most of meningiomas are benign, grade I, slow-growing tumors [3]. Meningiomas are most often found between the cerebral hemispheres; within the meninges; at the base of the skull; and in the back, lower part of the brain [3]. Although a single tumor is found in most of the patients, but sometimes multiple meningiomas also occur. Risk factors for meningioma are a genetic disorder and prior radiation exposure to the head [3].

2.4.2 Secondary Brain Tumors

Most of the brain cancers results from secondary brain tumors. They initialize from one part of the body and then spread to the brain [8]. The majority of malignant or cancerous tumors are secondary brain tumors. The following can metastasize or spread to the brain [8]:

- Lung cancer
- Breast cancer
- Kidney cancer
- Skin cancer

2.5 Magnetic Resonance Imaging (MRI)

MRI is a sophisticated and non-invasive imaging technology in which no damaging radiation is used and it produces 3D anatomical images of human body [10]. Raymond V. Damadian invented MRI in 1969 and was the first person to use MRI to investigate the human body [11]. Most often it is used for detecting disease and monitoring treatment [10].

However, different medical Imaging techniques like Magnetic Resonance Imaging (MRI), Computed Tomography (CT), Positron Emission Tomography (PET) etc. play an indispensable role in detection of different types of brain tumor and diagnosis, but MRI has promising advantages like non-invasive, providing greater contrast of tumors [9] than others. Multimodal MRI (T1, T2, T1C, FLAIR) images are preferred over other imaging tools for classification of brain tumors, because they provide numerous information on tumors [9].

2.6 Digital Watermarking

The security of information is one of crucial issues in our modern era of information and communication technology. Digital watermarking is one of the effective solutions for ensuring the security of information. It is applied in various multimedia applications in order to protect the content from unauthorized user, to ensure data authenticity, data ownership and copyright proof [12-14]. It usually embeds secret information called watermark into multimedia data like image, audio and video in an effective way that it is imperceptible to human visual system and extracts it later to prove authentication. The basic model of watermarking is shown in Figure 2.3 which is composed of four stages like generation, embedding, distribution and detection. In generation and embedding stage, watermark is generated and then it is embedded in the cover data in a sophisticated way that it is imperceptible to our human eye. In the distribution stage, when data is transmitted through the distribution channel, the data may be corrupted by different types of intentional or accidental attacks. The detection stage provides information to the identified owner about the extraction of watermark. The block diagram of simple embedding and extraction process for digital image watermarking is demonstrated in Figure 2.4.

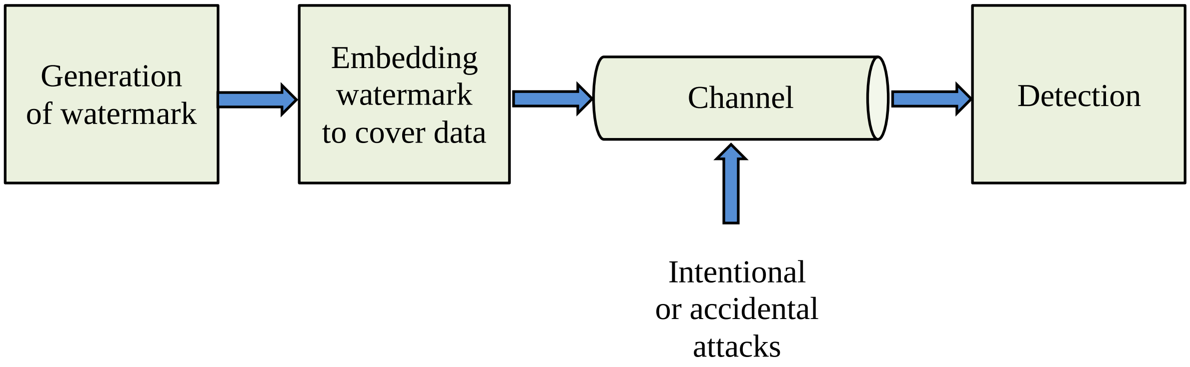

Figure 2.3: Basic model of watermarking scheme.

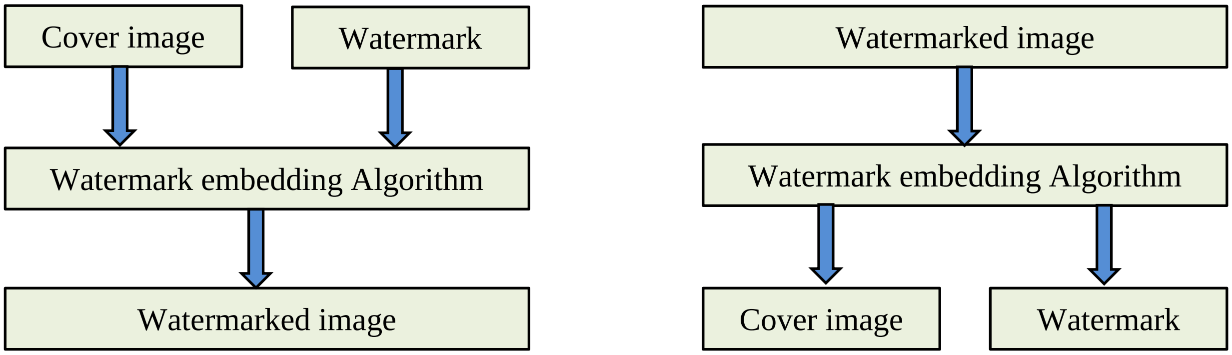

Figure 2.4: Block diagram simple embedding and extraction process

2.7 Types of Digital Watermarking

Watermarking techniques can be divided into four categories according to the type of document to be watermarked like text watermarking, image watermarking, audio watermarking and video watermarking. Watermarking is further classified as visible and invisible watermarking, informed and blind watermarking, fragile watermarking and robust watermarking.

- **Visible and Invisible Watermarking:** In visible watermarking, if the watermark is embedded into the most significant bits (MSB) of the host image, then can not perceived by our human visual system. But in invisible watermarking, if the watermark is embedded into least significant bits (LSB) of the cover image, then it can not be perceived by our human visual system. Figure 2.5 (a) shows the original or cover image and Figure 2.5 (b) shows the watermark image. Visible and invisible watermarking approach depending on embedded bit planes are shown in Figure 2.6.

- **Informed and Blind Watermarking:** In informed watermarking, the original un-watermarked cover image is needed in order to extract the watermark from the watermarked image. In blind watermarking, the original un-watermarked cover image is not required to extract the watermark from the watermarked image.

- **Fragile watermarking:** Fragile watermarking, called hard authenticate, is normally used for tamper detection which does not permit any kind of modification and the watermark will be invalid with a slight modification in the watermarked image [14].

- **Robust Watermarking:** Robust watermarking has the ability to resist different distortion attacks like noise, compression, rotation etc. in the watermarked images and thus is used for copyright protection and owner issues [14].

2.8 Watermarking Requirements

In this section, the basic four requirements of watermarking system are given below:

- **Security:** The security of watermarking implies that the watermark is so arduous that it cannot be removed without damaging the host multimedia data. It can be considered as the ability to ensure privacy and integrity of the watermark information, and resist different kinds of noise attacks [16].
- **Imperceptibility:** The imperceptibility of watermarking implies that there exists no perceptible difference between the watermarked and original or host signal [17, 18].

- **Capacity:** The capacity of watermarking implies that how amount of watermark bits are embedded into a host signal. Generally, a higher capacity deteriorates either the imperceptibility or the strength of robustness or both

- **Robustness:** The robustness of watermarking is referred to as the capability of the watermark to survive against different kinds of malicious attacks.

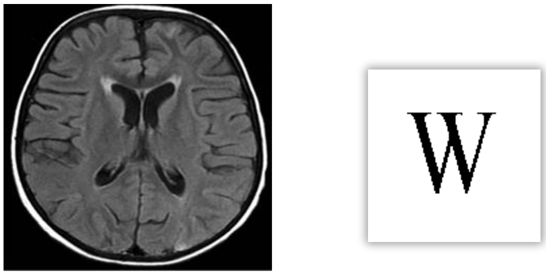

(a) (b)

Figure 2.5: (a) original image or cover image, (b) watermark image

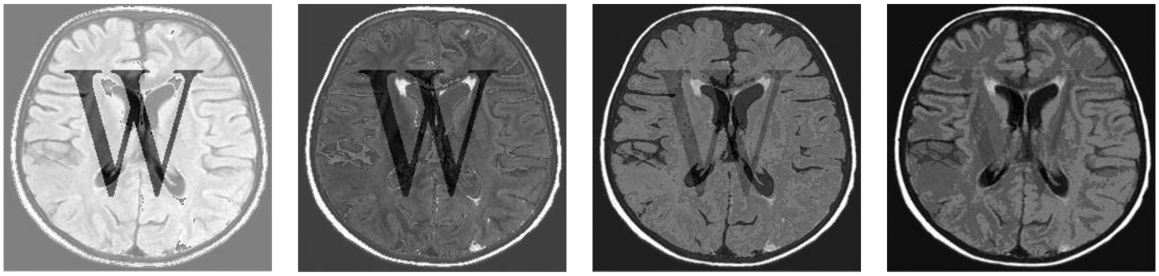

8th bit substitution 7th bit substitution 6th bit substitution 5th bit substitution

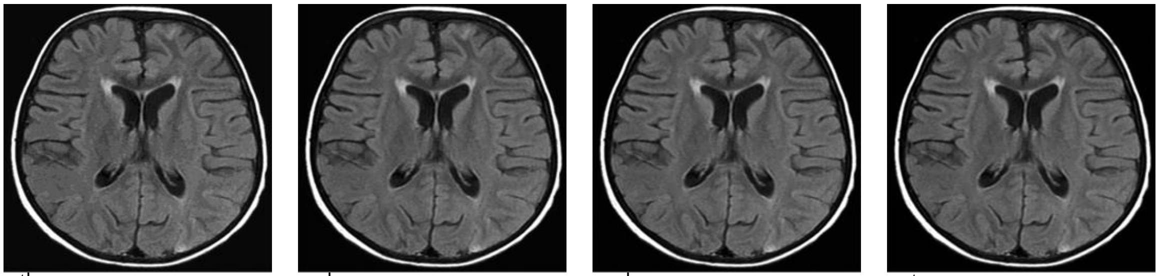

4th bit substitution 3rd bit substitution 2nd bit substitution 1st bit substitution

Figure 2.6: Visible and invisible watermarking approach depending on embedded bit planes

2.9 Watermark Embedding Techniques

- **Spatial watermarking:** As watermark is directly embedded into the bit planes of cover image in spatial domain such as least significant bit (LSB) [19], local binary pattern (LBP) [20], so spatial domain based watermarking techniques have low computational complexity but they can’t exhibit robustness against distortion attacks.

- **Transform or Frequency Domain Watermarking:** frequency domain based watermarking provides better imperceptibility and higher robustness against various image processing and geometric attacks; but it needs rigorous computational manipulations. Varieties of transforms like discrete cosine transform [21], discrete wavelet transform [22], singular value decomposition [23] are frequently used in frequency domain based watermarking schemes.

2.10 Nonsubsampled Contourlet Transform (NSCT)

NSCT has justified its potentiality as a powerful image decomposition scheme as it provides outstanding performance than contourlet transform (CT) and discrete wavelet transform (DWT). At first, a multiscale and multidirectional image transform scheme named contourlet transform (CT) is proposed by [24]. But it is not shift invariant which results in Pseudo-Gibbs phenomena around singularities. It does not provide desirable performance in contour characterization, edge detection, image enhancement, denoising. So, Contourlet transform (CT) is ameliorated and developed a modified version of CT, named nonsubsampled contourlet transform (NSCT) [25].

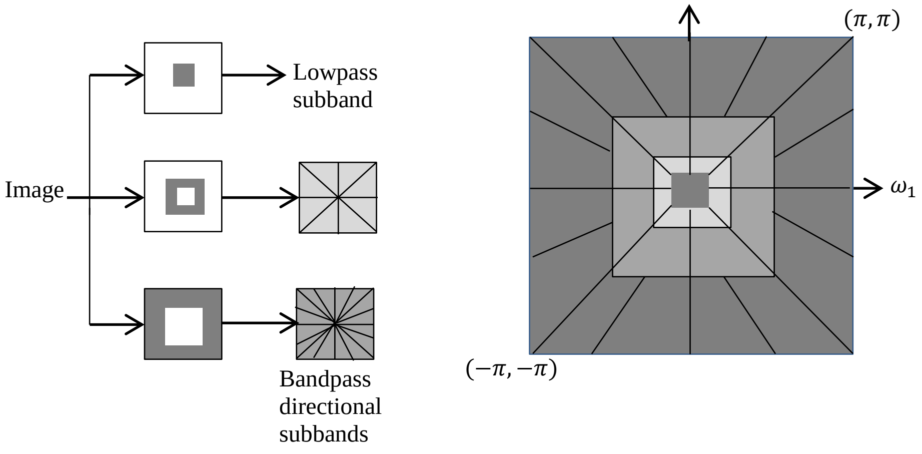

(a) (b)

Figure 2.7**:** Nonsubsampled contourlet trasform: a) NSFB structure that implements the NSCT, (b) Idealized frequency partitioning [25]

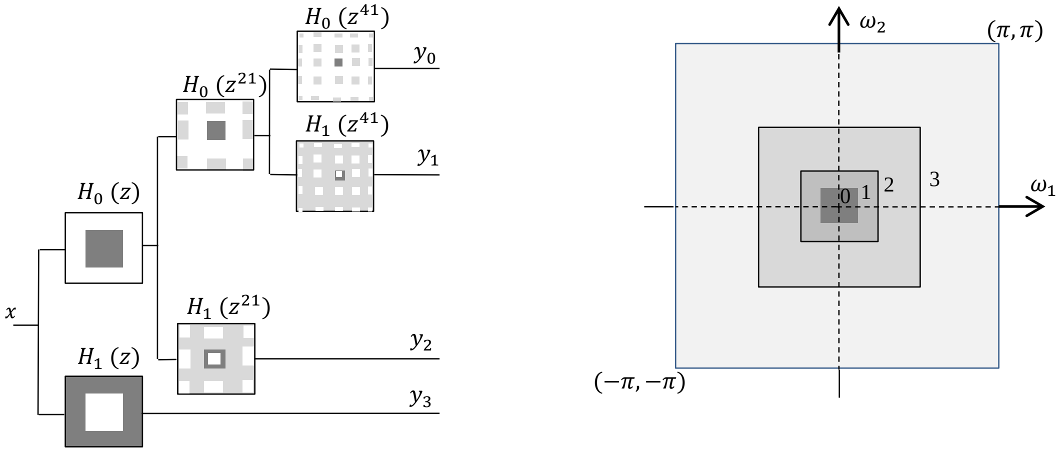

(a) (b)

Figure 2.8**:** (a) NSP decomposition for stage three, (b) subbands on the 2-D frequency plane [25]

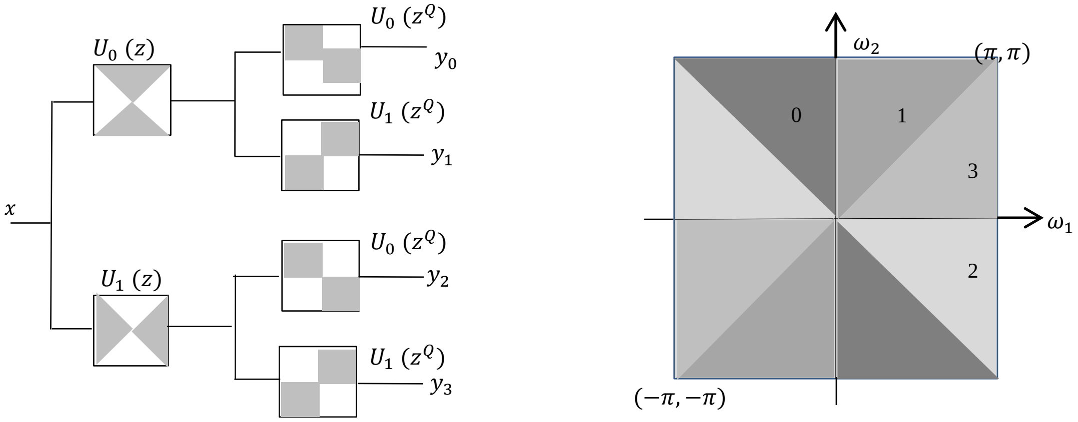

(a) (b)

Figure 2.9**:** Four channel nonsubsampled directional filter bank composed with two channel fan filter banks. (a) Filtering structure which depicts the equivalent filter in each channel, (b) Corresponding frequency decomposition [25]

Figure 2.7 (a) and Figure 2.7 (b) shows the complete vies of NSCT and idealized frequency partitioning, respectively. Now NSCT provides shift invariant feature along with multiscale and multidirectional feature. It is based on nonsubsampled pyramid (NSP) structure and nonsubsampled directional filter bank (NSDFB). The NSP and the NSDFB ensures the multiscale and multidirectional feature, respectively. NSP partitions the input image into a low and high pass subband. Then the high pass subband is decomposed into some directional subbands by NSDFB. The technique is reiterated on the outputs of low pass subband of NSP [26]. Figure 2.8 (a) and Figure 2.8 (b) demonstrate the NSP decomposition for stage three and subbands on the 2-D frequency plane, respectively [25]. This type of expansion is theoretically alike to the one dimensional nonsubsampled wavelet transform (NSWT) with the *à trous* algorithm and has redundancy of *J+1*, where *J* represents the number of stages of decomposition [25]. $[-(\pi/2^j),(\pi/2^j)]^2$ is the region of the ideal support of low-pass filter in the *j*th stage. Similarly, The ideal equivalent support of the high-pass filter is the complement of the low-pass, i.e., the region $[(-\pi/2^{j-1}),(\pi/2^{j-1})]^2\backslash[(-\pi/2^{j}),\ (\pi/2^{j})]^2$. NSDFB is built by excluding the down samplers and upsamplers in the DFB. Specifically, the nonsubsampled filter bask (NSFB) can be constracted from low-pass filter $H_0(z)$. Then one sets

$$H_1(z) = 1 - H_0(z) \tag{2.1}$$

The corresponding synthesis filters are

$$G_0(z) = G_1(z) = 1 \tag{2.2}$$

where, $G_0(z)$ and $G_1(z)$ are the low-pass and high-pass filters which eliminate specific parts of the noise in the processed pyramid coefficients.

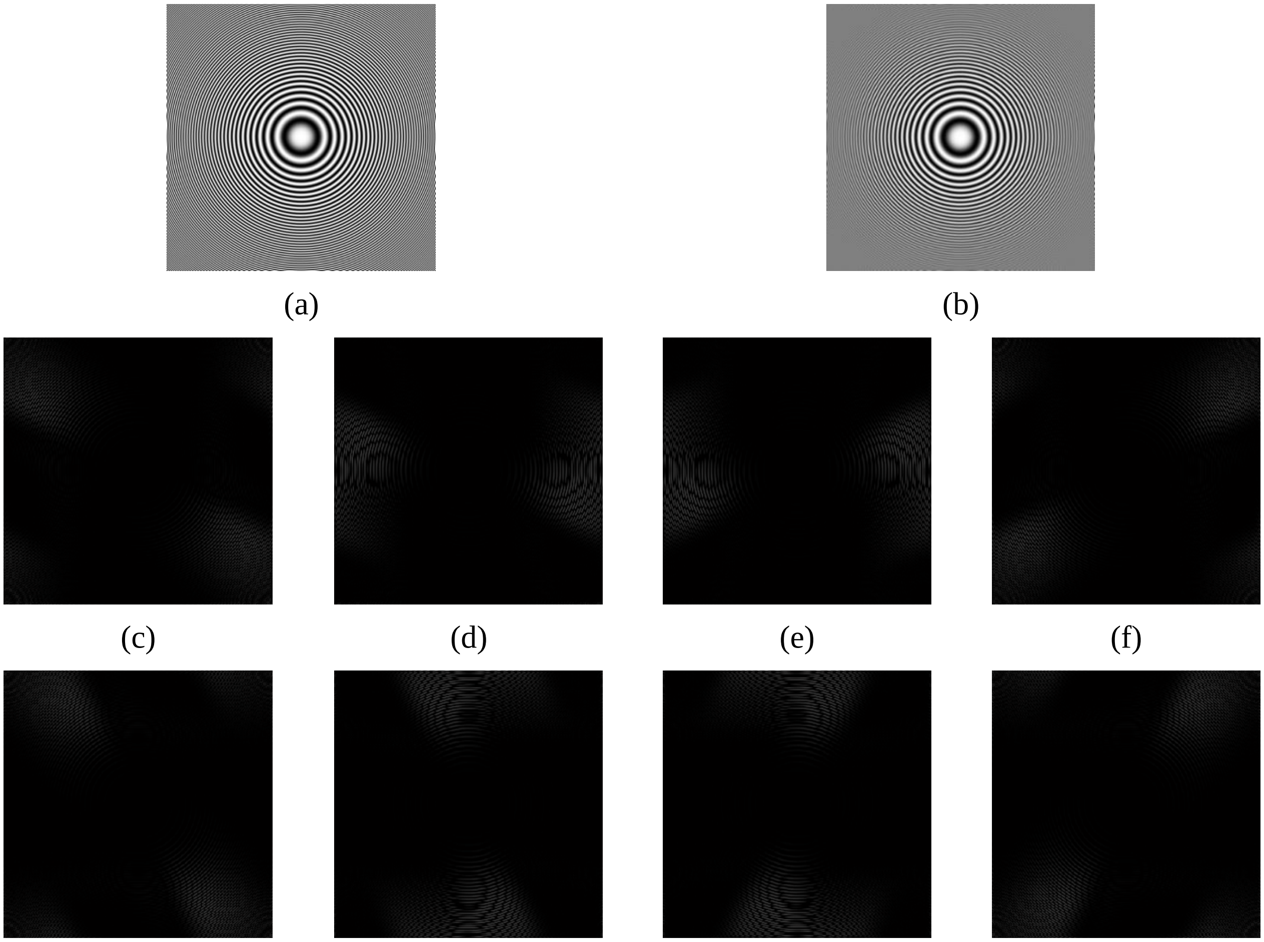
(a) (b)
(c) (d) (e) (f)
(g) (h) (i) (j)

Figure 2.10: Scenario after applying NSCT on Zoneplate image: (a) Original Zoneplate image, (b) lowpass subband of Zoneplate image, (c)-(j) Zoneplate's high pass subbands.

The nonsubsampled directional filter bank (NSDFB) is accomplished by switching off the downsamplers/upsamplers in each two channel filter bank in DFB tree structure and upsampling the filters accordingly [25]. Figure 2.9 explains four channel nonsubsampled directional filter bank composed with two channel fan filter banks [25]. Figure 2.9 (a) depicts the filtering structure which shows the equivalent filter in each channel. Figure 2.9 (b) shows the corresponding frequency decomposition [25]. Perfect reconstruction condition is obtained as follows:

$$H_0(z)G_0(z) + H_1(z)G_1(z) = 1 \tag{2.3}$$

This condition is much simpler to satisfy than the ideal reconstruction for critically sampled filter banks, and thus allows better filters to be designed. Figure 2.10 demonstrates scenario after applying of NSCT on Zoneplate image which gives one low pass subband image and eight high pass subbands image in eight directions.

2.11 Image Segmentation

Image segmentation is referred to as technique that splits an image into various regions having similar attributes like edge, texture etc. Depending of various characteristics of an image, segmentation is performed on the image on the basis of discontinuity and similarity [27]. Discontinuity based segmentation like edge detection partitions an image by detecting abrupt variation of intensity and does not need threshold or information about the contents of the image. It does not need a priori information about the contents of an image and has swift computation [28]. Similarity based segmentation like region growing, thresholding, clustering segments an image on the basis of predefined criteria [28]. Region based segmentation is comparatively simple and shows greater noise immunity when it is compared with edge detection based image segmentation technique. Thresholding based segmentation is a simple and effective technique which needs a priori information about the contents of an image [28].Clustering is referred to as unsupervised learning algorithm which separates high density of data points by increasing intra-class similarity or by decreasing inter-class similarity from other regions with low density of data points [29].

2.11.1 K-means Clustering

Clustering is a technique of grouping pixels of an image according to their intensity values which can be classified into two types: one is hard clustering and the other is soft clustering. In hard clustering, data points belong to exactly one cluster. On the other hand, data points belong to more than one cluster in soft clustering.

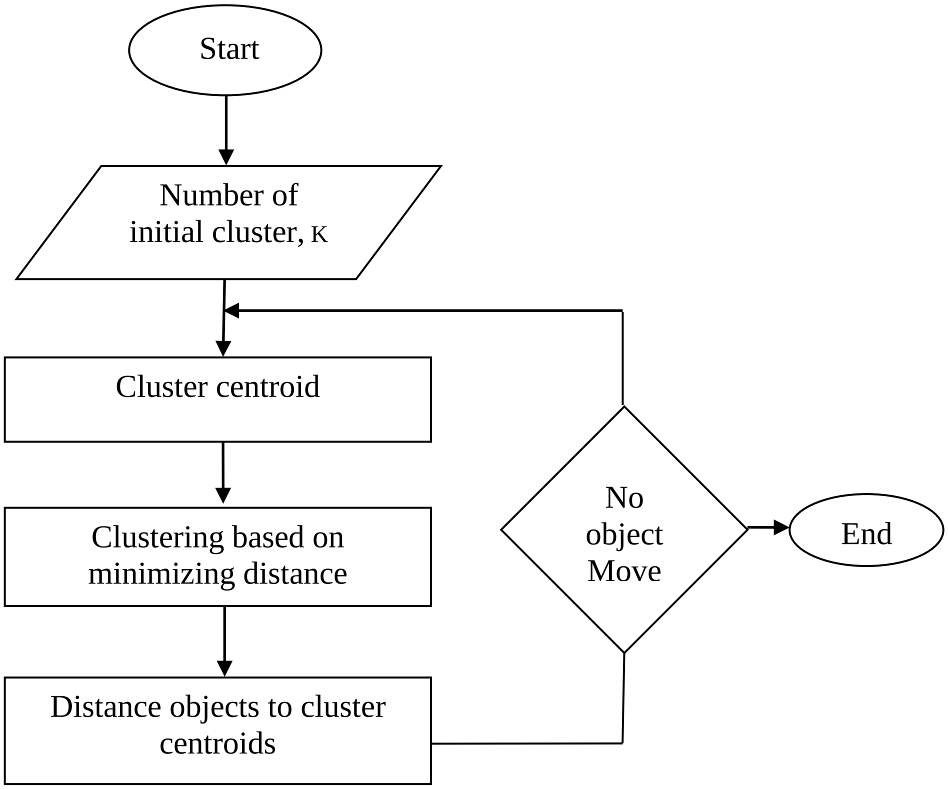

Figure 2.11**:** Flow chart of simple K-means clustering algorithm [31]

K-means clustering is one of the prominent examples of unsupervised learning algorithm which has the capability to solve the clustering problem [29] of a given data set with a fixed number of clusters, say K. It was first proposed by J. MacQueen in 1967 [30]. The flow chart of simple K-means clustering algorithm [31] is shown in Figure 2.11. The clustering procedure follows a simple way: at first it selects *k* number of centroids from data points, one for each cluster and then it assigns other data points to the nearest cluster centroid [4]. After completing this first step with no data point is remaining, K-means calculates *k* new centroids and the same process is repeated until the clustering satisfies convergence criterion

2.12 Support Vector Machine (SVM)

SVM is a promising classification tool for solving two class problems which was firstly developed by Vapnik and Lerner in 1963 [33]. Basically, it is a binary classification scheme which separates a set of binary labeled data by constructing a hyper-plane [33] in feature space. Because of its promising characteristics like sophisticated mathematical tractability, high accuracy, and direct geometric interpretation [34], SVM is widely used in various areas of biomedical image processing. There are two steps called training and testing which are involved in SVM. A finite training set consists of known data and defined decision values which are used to fed the SVM [35]. After feeding the SVM, SVM is able to perform the classification of unknown data from testing set. SVM can be partitioned into linear and non-linear SVM [33].

2.12.1 Linear SVM

Linear SVM is the simplest type, in which the input data samples are linearly separable, but because of small margin in feature space, linearly separable data samples are not well performed. A linear function is defined by following [33]

$$f(x_i) \geq 0 \;\; if \; y_i = +1 \tag{2.4}$$

$$f(x_i) < 0 \;\; if \; y_i = -1 \tag{2.5}$$

The desired optimal hyperplane can be defined by following (2.4) if the data samples are linear separable.

$$f(x) = \boldsymbol{w}^T + bx = 0 \tag{2.6}$$

Where, $\boldsymbol{w}$ and b represent the weight vector or normal to the hyperplane and distance from the origin to the hyperplane, respectively.

2.12.2 Non-linear SVM

In linear SVM, a straight line is drawn for separating data points, but in case of non-linear SVM, the original data set is transformed to upper dimensional data and a nonlinear operator is used to map the input data samples. However, different non-linear kernel functions like polynomial, radial Gaussian basis (RBF) are used in SVM but (RBF) kernel based SVM with proper scaling factor outperforms others [36]. Polynomial, radial Gaussian basis (RBF) kernels are defined as following (2.5)-(2.6).

$$K\left(x_p, x_q\right) = (\alpha x_p^T x_q + c)^d \tag{2.7}$$

$$K\left(x_p, x_q\right) = \exp\left(-\frac{\left\|x_p - x_q\right\|^2}{2\sigma^2}\right) \tag{2.8}$$

2.13 Artificial Neural Network (ANN)

Artificial neural network (ANN) is a set of biologically inspired computing system which imitates the neural architecture of human brain [37]. It is described as a group of interconnected artificial neurons that are organized in parallel layers. However, multilayer feed forward artificial neural network has justified its potentiality to be used in numerous applications like prediction, controlling, pattern recognition, signal processing etc. [38]. It was first developed by Rumelhart [39] and because of its simple structure, less mathematical analysis, it has become popular than other existing neural networks like recurrent networks, Hopfield networks etc.

The information processing unit of a neural network is called neuron. It is the fundamental unit for the operation of neural network. Figure 2.12 depicts the model of a neuron which has three basic elements: a set of synapses or connecting links, adder and activation function [40]. A connecting link is represented by a weight. A signal x_j at the input of connecting link j connected to neuron k is multiplied by a weight w_{kj}. The summing of input signals, weighted by the corresponding synapses the neuron is performed by an adder. Then the amplitude of the output of the neuron is limited by an activation function [40]. This function is also called the squashing function whose main function is to limit the amplitude of the output of the neuron to some finite value. The neuronal model has bias, denoted by b_k, which increases or decreases the net output of the activation function [40].

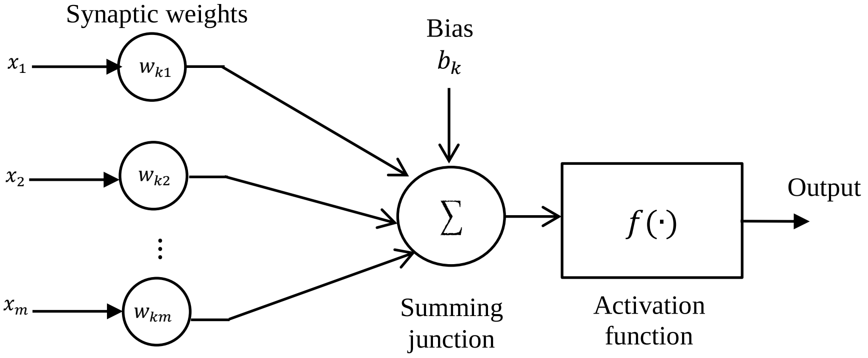

Figure 2.12: Model of a neuron [40]

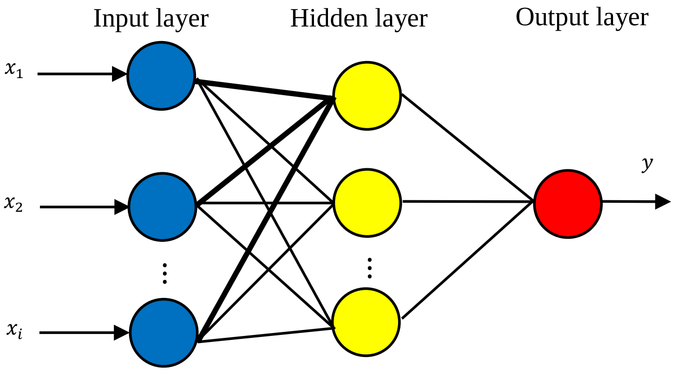

Figure 2.13: Structure of feed forward artificial neural network

Feed forward artificial neural network is composed of input layer, hidden layer and output layer with single neuron which is demonstrated in Figure 2.13. Blue, yellow and red circles of Figure 2.13 represent the input, hidden and output neurons of three layers, respectively. Information enters at the input layers and then passes through the hidden layers of neurons for intermediate computations that lie between input and output layers of network. Each of the connections between the layers of neurons is associated with a weight. For adjusting the weights of connections between the layers of neurons and the bias of network, back propagation algorithm is used. Rumelhart first proposed [39] back propagation algorithm for the training of feed forward network.

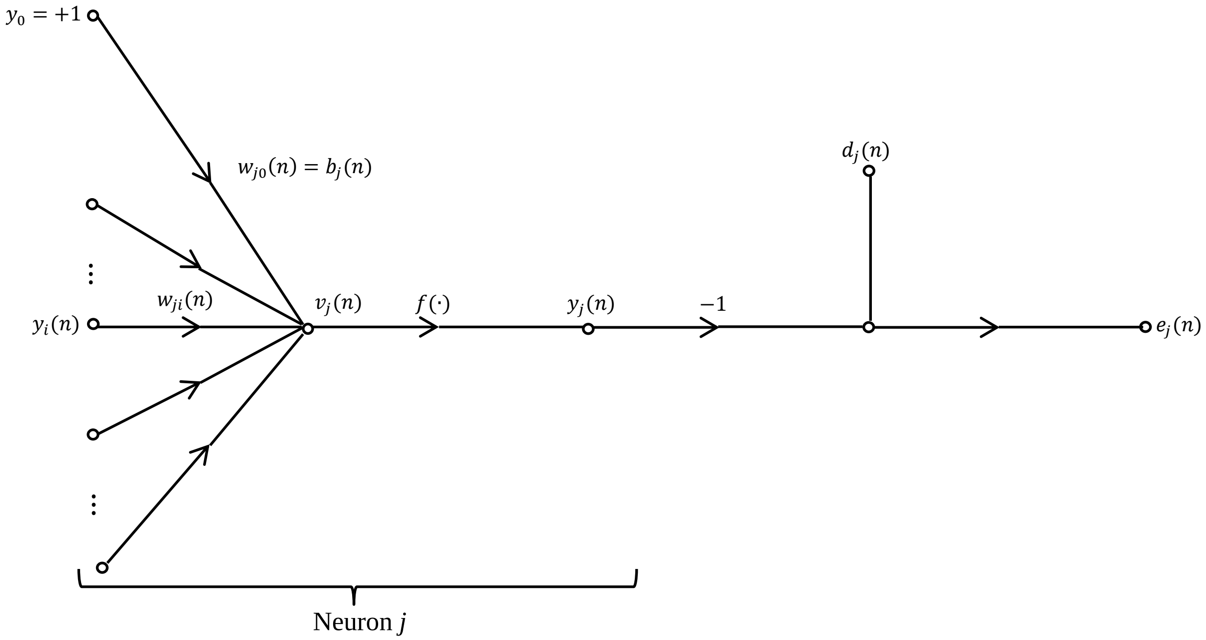

Figure 2.14: Signal-flow graph highlighting the details of output neuron *j* [40]

Consider the Figure 2.14, where neuron j being fed by a set of signals generated from a layer of neurons to the left [40]. The induced local field $v_j(n)$ produced at the input of the activation function associated with neuron *j* is

$$v_j(n) = \sum_{i=0}^{m} w_{ji}(n) y_i(n) \tag{2.9}$$

where, m denotes the total number of inputs applied to neuron *j*. The function signal $y_i(n)$ appearing at the output of neuron *j* at iteration *n* is

$$y_j(n) = f(v_j(n)) \tag{2.10}$$

The error signal at the output of neuron, j is the difference between desired output $d_j(n)$ and calculated network output $y_j(n)$.

$$e_j(n) = d_j(n) - y_j(n) \tag{2.11}$$

The instantaneous value of error energy for neuron *j* is defined as following

$$E(n) = \frac{1}{2}\sum_{j=C} e_j^2(n) \tag{2.12}$$

Where, *C* represents all the neurons in the output layer of network. If *N* is the total number samples of the training set, then average squared error energy is defined by following

$$E_{av} = \frac{1}{N}\sum_{n=1}^{N} E(n) \tag{2.13}$$

The adjustment of weights of connections is achieved by performing the gradient operation on the error with respect to weight [37] which is defined by following

$$\Delta w_{ji}(n) = -\eta \frac{\partial E(n)}{\partial w_{ji}(n)} \tag{2.14}$$

where, η is the convergent speed controlling parameter.

2.14 Arnold's Cat Map

This map has a periodic scrambling nature which is enormously used in different information hiding applications [41]. It is used in the first level of shuffling process of the watermark which is defined as

$$\left(\frac{x'}{y'}\right) = \begin{pmatrix} 1 & 1 \\ 1 & 2 \end{pmatrix} \left(\frac{x}{y}\right) mod\ M \quad x, y \in \{1,2 \dots \dots \dots M\} \tag{2.15}$$

Where, (x, y) is the position of pixel of an image before shuffling and (x', y') is the position of pixel of the same image after shuffling using Arnold's cat map.

2.15 Logistic Map

Logistic map is widely used for image scrambling in watermarking area, which generates one dimensional random sequence [42] which is defined by

$$x_{n+1} = \alpha x_n(1 - x_n) \tag{2.16}$$

Where, the initial values of x_n and α can be used as confidential keys. α is tuning parameter which regulates the randomness and usually stays in the range [3,4].

2.16 Tent Map

Tent map exhibits dynamical behavior [42] which can also be used to produce random sequence. The initial values of α and x_n has been used as confidential key of this proposed scheme. Its behavior is defined as following

$$x_{n+1} = \begin{cases} \alpha x_n, & for\ x_n < \frac{1}{2} \\ \alpha(1 - x_n), & for\ \frac{1}{2} \le x_n \end{cases} \tag{2.17}$$

where, α is a positive number.

2.17 Game of Life Cellular Automata

Cellular Automata show the complex characteristics which are proposed by Stani-slaw Ulam and John Von Neumann in the 1940s [43]. The applications of cellular automata are in the fields of random number generation, pattern recognition, games etc. Game of life is a paradigm of cellular automata which is applied to change the position of pixels of an image. [43].

In order to apply game of life (GOL) rules, a primary matrix (G) which is equal to size of cover image, is formed by logistic map in this proposed scheme. Here each pixel of initial matrix is called cell and each cell has either of the two states say, dead (0) or alive (1). The rules of GOL are applied to G in order to produce 1st generation G_1 , then the rules are applied to G_1 in order to produce 2nd generation G_2; thus this process is executed for K times to produce K generations and this K is used as one of the secret keys in the scrambling technique. Each cell upgrades its state by gathering information from states of eight neighbor cells (Moore neighborhood) according to the predefined game of life rules in order to scramble image. The game of life has four rules: the rule of birth, rule of death by overcrowding, rule of death by exposure and the rule of survival [43]. These rules are demonstrated in Figure 2.15.

Figure 2.15 (a, b) shows the rule of birth [43] which states that *"if at time T there are 3 alive (1) neighbor cells around a dead (0) center cell; at time T+1 the center cell will change its status to alive (1).*

Figure 2.15 (c, d) shows the rule of death by overcrowding [43] which states that *"if at time T there are 4 or more alive (1) neighbor cells around an alive (1) center cell; at time T+1 the center cell will change its status to death (0).*

Figure 2.15 (e, f) shows the rule of death by exposure [43] which states that *"if at time T there is 1 or no alive (1) neighbor cell around an alive (1) center cell; at time T+1 the center cell will change its status to death (0).*

Figure 2.15 (g, h) shows the rule of survival [43] which states that *"if at time T there is 2 or 3 alive (1) neighbor cell around an alive (1) center cell; at time T+1 the center cell will not change its Status"*.

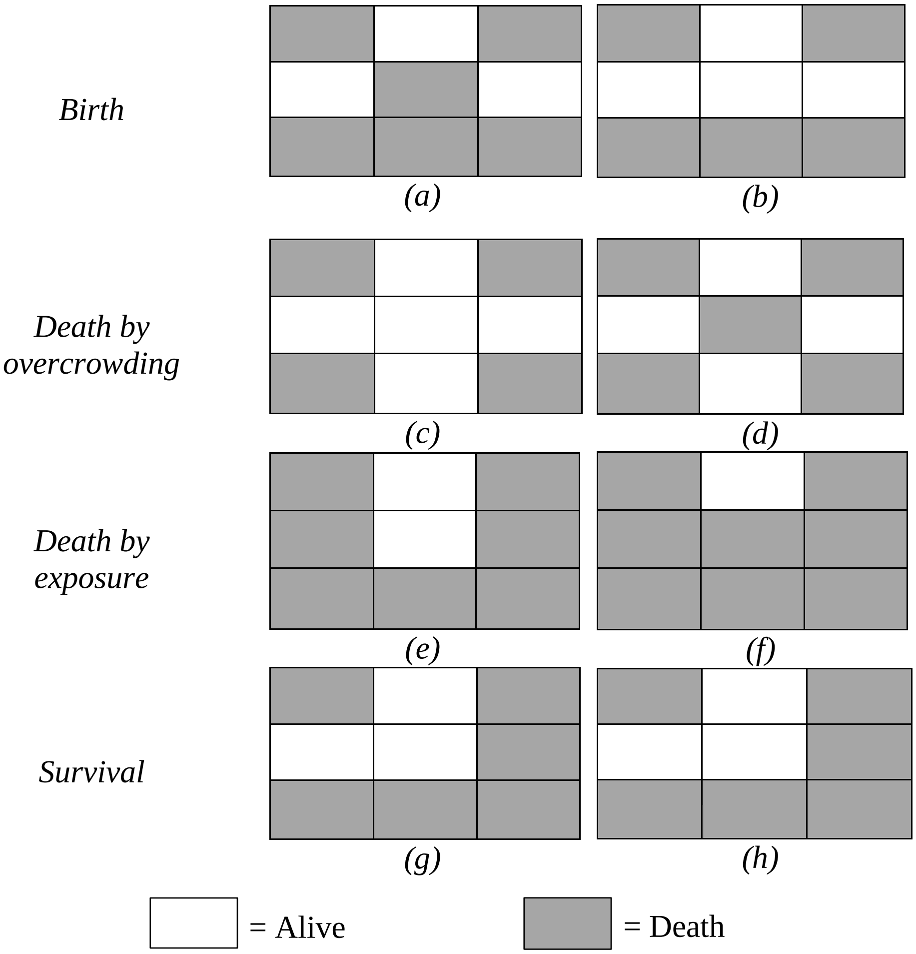

Figure 2.15: Rules of game of life cellular automata: (a, b) Rule of birth, (c, d) Rule of death by overcrowding, (e, f) Rule of death by exposure, (g, h) Rule of survival.

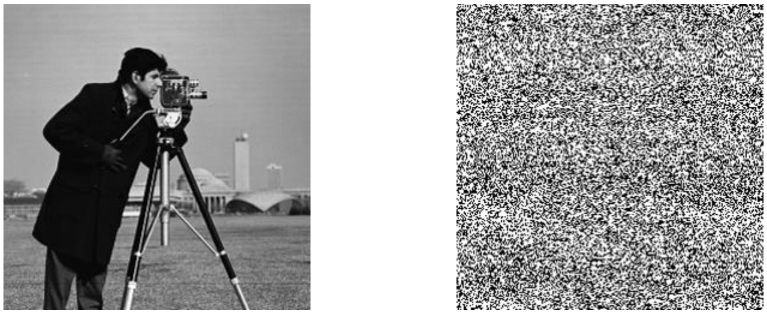

(a) (b)

Figure 2.16: Scrambling image using game of life cellular automata: (a) cameraman image, (b) Scrambled image after 5th generation of GOL.

Figure 2.16 (a) demonstrates the original cameraman image and Figure 2.16 (b) exhibits the Scrambled image after 5th generation of game of life cellular automata.

2.18 Singular Value Decomposition (SVD)

Singular value decomposition (SVD) is an effective numerical analysis scheme which has versatile applications of image processing. SVD has some merits in digital image processing. Firstly, the matrix size from SVD is not fixed which can be square or rectangle. Secondly, the singular values of an image are modestly affected if normal image processing operations are performed on the image. Thirdly, singular values preserve the algebraic characteristics of an image [44-45].

Consider an image A of size $N\times N$ with rank R, $A(R<N)$. Using SVD, A can be mathematically presented as follows, where U and V are $N\times N$ orthogonal matrices and the S is $N\times N$ diagonal matrix with singular values in decreasing order [45].

$$A = USV^T = \sum_{i=1}^{R} u_i s_i v_i^T \tag{2.18}$$

$$U = [u_1, u_2, \dots, u_N] \tag{2.19}$$

$$V = [v_1, v_2, \dots, v_N] \tag{2.20}$$

$$S = \begin{bmatrix} s_1 & \cdots & 0 \\ \vdots & \ddots & \vdots \\ 0 & \cdots & s_N \end{bmatrix} \tag{2.21}$$

2.19 Discrete Cosine Transform (DCT)

DCT is a block based transform method which splits an image into various frequency bands [45] which is used in numerous image processing areas. It produces a finite sequence in terms of function of cosine at several oscillation frequencies [47]. It is a block-based transformation scheme that partitions an image into $N \times N$ non-overlapping blocks. If $f(x, y)$ and $f'(p, q)$ is the input image and output image after applying DCT, respectively, DCT coefficients are calculated as following [47].

$$f'(p,q) = \sqrt{\frac{2}{x}}\sqrt{\frac{2}{y}}\alpha \sum_{x=0}^{M-1}\sum_{y=0}^{N-1} f(x,y)\,K \tag{2.22}$$

Where,

$$K = cos\frac{(2x+1)p\pi}{2x} cos\frac{(2y+1)q\pi}{2y}$$

$$\alpha = \frac{1}{\sqrt{2}} \quad for, p \,\&\, q = 0$$

$$\alpha = \frac{1}{\sqrt{2}} \quad for, p \,\&\, q = 1, 2, \dots \dots . M - 1$$

The DCT partitions the input image into three bands, namely low, high and middle frequency band. Our human visual system is very sensitive to the low frequency components of DCT. Besides, the high frequency components of DCT are vulnerable against image processing attacks [47]. So, middle frequency components are chosen in order to obtain a tradeoff between imperceptibility and robustness. DCT has the ability to present a signal with lowest number of coefficients that ensures better performance with respect to continuities rather than Discrete Fourier Transform (DFT) [47].

2.20 Summary

This chapter outlines a brief description of brain tumors, MRI, watermarking, nonsubsampled contourlet transform (NSCT), image segmentation, support vector machine (SVM), artificial neural network (ANN), Arnold's cat map, logistic map, tent map, cellular automata, singular value decomposition (SVD) and discrete cosine transform (DCT). NSCT, image segmentation using K-means clustering, SVM and ANN are used in our proposed hybrid brain tumor classification scheme. Arnold's cat map, logistic map, tent map, game of cellular automata, NSCT, SVD and DCT are used in our proposed two image watermarking schemes. In proposed brain tumor classification and watermarking schemes, NSCT is used due to its outstanding performances in image processing applications.

References

[1] https://www.mayfieldclinic.com/PE-AnatBrain.htm >; [accessed 29.12.17]

[2] https://biology.mit.edu/sites/default/files/Brain%20Anatomy%20OverviewRev.pdf>; [accessed 29.12.17]

[3] About brain tumors-a primer for patients and caregivers, American Brain Tumor Association, IL 60631, Chicago.

[4] E. Dandıl, M. Çakıroğlu, and Z. Ekşi, "Computer-aided diagnosis of malign and benign brain tumors on MR images," *ICT Innovations*, vol. 311, pp. 157-166, 2015.

[5] M.K. Abd-Ellah, A.I. Awad, A.A.M. Khalaf, and H.F.A. Hamed, "Classification of brain tumor MRI brain images using a kernel support vector machine," *Communications in Computer and Information Science*, vol. 636, pp. 151-160, Sep. 2015.

[6] http://www.cbtrus.org/factsheet/factsheet.html >; [accessed 29.12.17]

[7] N.B. Bahadure, A.K. Ray, and H.P. Thethi, "Image analysis for MRI brain tumor detection and feature extraction using biologically inspired BWT and SVM," *International Journal of Biomedical Imaging*, vol. 2017, pp.1-12, 2017.

[8] https://www.healthline.com/health/brain-tumor >; [accessed 29.12.17]

[9] S. Pereira, A. Pinto, V. Alves, and C.A. Silva, "Brain tumor segmentation using convolutional neural networks in MRI images," *IEEE Transactions on Medical Imaging*, vol. 35 (5), pp. 1240-50, May 2016.

[10] https://www.nibib.nih.gov/science-education/science-topics/magnetic-resonance-imaging-mri >; [accessed 29.12.17]

[11] R. Damadian, M. Goldsmith, and L. Minkoff, "NMR in cancer: XVI. FONAR image of the live human body," *Physiological Chemistry and Physics*, vol. 9 (1), pp. 97-100, May 1977.

[12] W.H. Lin, Y.R. Wang, S.J. Horng, T.W. Kao and Y. Pan, "A blind watermarking method using maximum wavelet coefficient quantization," *Expert Systems with Applications*, vol. 36 (9), pp.11509-11516, November 2009.

[13] A. Al-Haj, “Providing integrity, authenticity and confidentiality for header and pixel data of dicom images,” *Journal of Digital Imaging*, vol. 28 (9), pp.179-187, April 2015.

[14] L. Laouamer, M. AlShaikh, L. Nana and A.C. Pascu, “Robust watermarking scheme and tamper detection based on threshold versus intensity*,” Journal of Innovation in Digital Ecosystems*, vol. 2 (1-2), pp.1-12, December 2015.

[15] G. W. Braudaway, et. al., “Protecting publicly available images with a visible image watermark”, *Proc. SPIE Conf. Optical Security and Counterfeit Deterrence Technique*, Vol. SPIE- 2659, pp.126-132, Feb. 1996.

[16] C.-T. Li and F.M. Yang, “One-dimensional neighborhood forming strategy for fragile watermarking”, *Journal of Electronic Imaging*, vol. 12, no. 2, pp. 284-291, 2003.

[17] C. Podilchuk and W. Zeng,“Image-adaptive Watermarking using visual models”, *Journal of Areas of Communications*, IEEE vol. 16, pp. 525-539, May 1998.

[18] C. Podilchuk and E. Delp, “Digital watermarking algorithms and applications*”, IEEE Signal Processing Magazine*, vol. 18, no. 4, July 2001.

[19] G.J. Lee, E.J. Yoon and K.Y. Yoo, “A new LSB based digital watermarking scheme with random mapping function,” in proc. of *International Symposium on Ubiquitous Multimedia Computing*, pp.130-134, October 2008.

[20] J.D. Chang, B.H. Chen and C.S. Tsai “LBP- based fragile watermarking scheme for image tamper detection and recovery,” in proc. of *2nd International Symposium on Next-Generation Electronics (ISNE)*, pp. 173-176, February 2013.

[21] Z.J. Xu, Z.Z. Wang and Q. Lu, “Research on image watermarking algorithm based on DCT,” *Procedia Environmental Sciences*, vol. 10, pp. 1129-1135, 2011.

[22] Z. Dawei, C. Guanrong and L. Wenbo,“A chaos based robust wavelet domain watermarking algorithm,” *Chaos, Solutions & Fractals*, vol. 22, pp. 47-54, 2004.

[23] S.C. Pei, H.H. Liu, T.J. Liu and K.H. Liu, “Color image watermarking using SVD,” in Proc. of *International Conference on Multimedia and Expo*, pp. 122-126, July 2010.

[24] M.N. Do and M. Vetterli, “The contourlet transform: An efficient directional multiresolution image representation,” *IEEE Transaction on Image Processing*, vol. 242, pp. 2091-106, 2005.

[25] A.L. Cunha, J. Zhou, and M.N. Do, “The nonsubsampled contourlet transform: theory, design and applications,” *IEEE Transactions on Image Processing*, vol. 15, pp. 3089-3101, 2006.

[26] M.F. Hossain, M.R. Alsharif, and K. Yamashita, “LMMSE-based image denoising in onsubsampled contourlet transform domain,” *Lecture Notes in Computer Science*, vol. 6134, pp. 36-43, 2010.

[27] M. Rastgarpour and J. Shanbehzadeh, “Application of AI techniques in medical image segmentation and novel categorization of available methods and tools,” in Proc. of *International Multi Conference of Engineers and Computer Scientists (IMECS)*, pp. 16-18, Mar. 2011.

[28] H. Hooda, O.P. Verma, and T. Singhal, “Brain tumor segmentation: A performance analysis using K-Means, Fuzzy C-Means and Region growing algorithm” in Proc. of *International Conference on Advanced Communication Control and Computing Technologies (ICACCCT)*, pp. 1621-26, 2014.

[29] V.K. Dehariya, S.K. Shrivastava, and R.C. Jain, “Clustering of image data set using k-means and fuzzy k-means algorithms,” in Proc. of *International Conference on Computational Intelligence and Communication Networks*, pp. 386-391, 2010.

[30] J. MacQueen, “Some methods for classification and analysis of multivariate Observations,” in Proc. of *Symposium on Mathematical Statistics and Probability*, vol. 1, pp.281-97, 1967.

[31] E. Küçükkülahlı, P. Erdoğmuş, and K. Polat, “Histogram-based automatic segmentation of images,” *Neural Computing and Applications*, vol. 27 (5), pp. 1445-50, July 2016.

[32] H. Zhou, G. Schaefer, and C. Shi, “Fuzzy c-means techniques for medical image segmentation,” *Fuzzy Systems in Bioinformatics and Computational Biology*, vol. 242, pp. 257-271, 2009.

[33] H. B. Nandpuru, S.S. Salankar, and V.R. Bora, “MRI barin cancer classification using support vector machine,” in Proc. of *Students’ Conference on Electrical, Electronics and Computer Science (SCEECS)*, Mar. 2014.

[34] Y. Zhang and L. Wu, “An MR brain images classifier via principal component analysis and kernel support vector machine,” *Progress in Electromagnetics*, vol. 130, pp. 369-388, 2012.

[35] S. Chaplot, L.M. Patnaik, and N.R. Jagannathan, “Classification of magnetic resonance brain images using wavelets as input to support vector machine and neural machine,” *Biomedical Signal Processing and Control*, vol. 1, pp.86-92, Jan. 2006.

[36] M.K. Abd-Ellah, A.I. Awad, A.A.M. Khalaf, and H.F.A. Hamed, “Classification of brain tumor MRI brain images using a kernel support vector machine,” *Communications in Computer and Information Science*, vol. 636, pp. 151-160, Sep. 2015.

[37] O.A. Abdalla, M.N. Zakaria, S. Sulaiman, and W.F.W.Ahmad, “A comparison of feed-forward back-propagation and radial basis artificial neural networks: A Monte Carlo study,” *International Symposium in Information Technology,* pp. 994-98, June 2010.

[38] A. A. Konate´, H. Pan, N. Khan, and J. H. Yang, “Generalized regression and feed-forward back propagation neural networks in modeling porosity from geophysical well logs,” *Journal of Petroleum Exploration and Production Technology,* vol. 5 (2), pp. 157-66, June 2015.

[39] D.E. Rumelhart, G.E. Hinton, and R.J. Williams, “Learning internal representations by error propagation,” *Parallel Distributed Processing: Explorations in the Microstructure of Cognition*, vol. 1, pp. 318-62, 1986.

[40] S. Haykin, “Neural Networks – A comprehensive foundation,” 2nd edition, pp. 10-11, Singapore, Pearson Education.

[41] J. Li, M. Huang, H. Zhang, C. Dong, and Y. Bai, “The medical images watermarking using DWT and Arnold,” *in Proc. of International Conference on Computer Science and Automation Engineering (CSAE)*, 2012.

[42] G.A. Sathishkumar, K. B. Bagan, and N. Sriraam, “Image encryption based on diffusion and multiple chaotic maps,” *International Journal of Network Security & Its Applications (IJNSA)*, pp. 1212-15, August 2016.

[43] A. Dalhoum, M. MAhafzah, A. Awwad, I. Aldamari, A. Oterga and M. Alfonseca “Digital image scrambling using 2D cellular automata”, in proc. of *14th IEEE international Symposium on Multimedia*, 10-12 December 2012, Irvine, CA,US.

[44] S.C. Pei, H.H. Liu, T.J. Liu and K.H. Liu,“Color image watermarking using SVD,” in Proc. of *International Conference on Multimedia and Expo*, pp. 122-126, July 2010.

[45] C.C. Chang, P. Tsai, and C.C. Lin, “SVD-based digital image watermarking scheme,” *Pattern Recognition Letters*, vol. 26, pp. 1577-86, 2005.

[46] A.S. Nedooshan, K. Yaghmaie and R.S. Nadooshan, “Medical image watermarking based on SVD-DWT technique,” *International Congress on Informatics, Environment, Energy and Applications (IEEA)*, vol. 38, 2012.

[47] A.M. Joshi, S. Gupta, M. Girdhar, P. Agarwal, and R. Sarker “Combined DWT-DCT-based video watermarking algorithm using arnold transform technique,” *International Conference on Data Engineering and Communication Technology*, vol. 3 (2), pp.181-94, 2011.

CHAPTER III

PROPOSED METHODOLOGIES

3.1 Introduction

This chapter presents proposed methodologies for brain tumor classification and watermarking using nonsubsampled contourlet transform (NSCT). Firstly, NSCT based MRI brain tumor classification using support vector machine (SVM) and artificial neural network (ANN) classifier is proposed. In this scheme, K-means clustering is applied for segmentation of region of interest (ROI) of MRI. NSCT is applied to the ROI of brain image in order to obtain its low and high subband coefficients. Then from the coefficients of NSCT, twelve features are collected from ROI. SVM which incorporates two stages is trained with these twelve features. 1^{st} stage of SVM is able to classify brain image as normal or abnormal and then 2^{nd} stage of SVM classifies grade of tumor as low grade or high grade. The grade of tumor is also classified using the ANN classifier based on feed forward back propagation. Secondly, cellular automata based image watermarking using NSCT and singular value decomposition (SVD) is proposed. Game of life (GOL) cellular automata is used to scramble binary watermark so that no one can recover the watermark without secret scrambling keys. Because of the salient features like multiscale, multidirection and shift invariance of NSCT, 2-level NSCT is applied to magnetic resonance images. Most of the perceptual content of an image focuses on low frequency subband of NSCT and the singular values of low frequency subband have certain stability. So a modest change in the singular values of low frequency subband of NSCT is applicable. In this proposed scheme, each singular value of scrambled binary watermark is embedded in fixed location of singular value matrix of low frequency subbands of NSCT of magnetic resonance image. This watermarking scheme is also applied on RGB color image which is used as a cover image. Thirdly, a hybrid magnetic resonance imaging (MRI) medical images watermarking technique has been proposed using chaotic maps, NSCT and DCT. Multiple chaotic maps are used to enhance the security of proposed MRI watermarking technique. At first, an arranged chaotic sequence which is created by logistic map is used to shuffle the pixel positions of MRI. Patient information, watermark is encrypted by two chaotic maps, like Arnold's Cat map and tent map. Several secret keys are required to extract the patient information from MRI. Then DCT coefficients of encrypted watermark are embedded into the DCT coefficients of approximation band of NSCT of shuffled MRI.

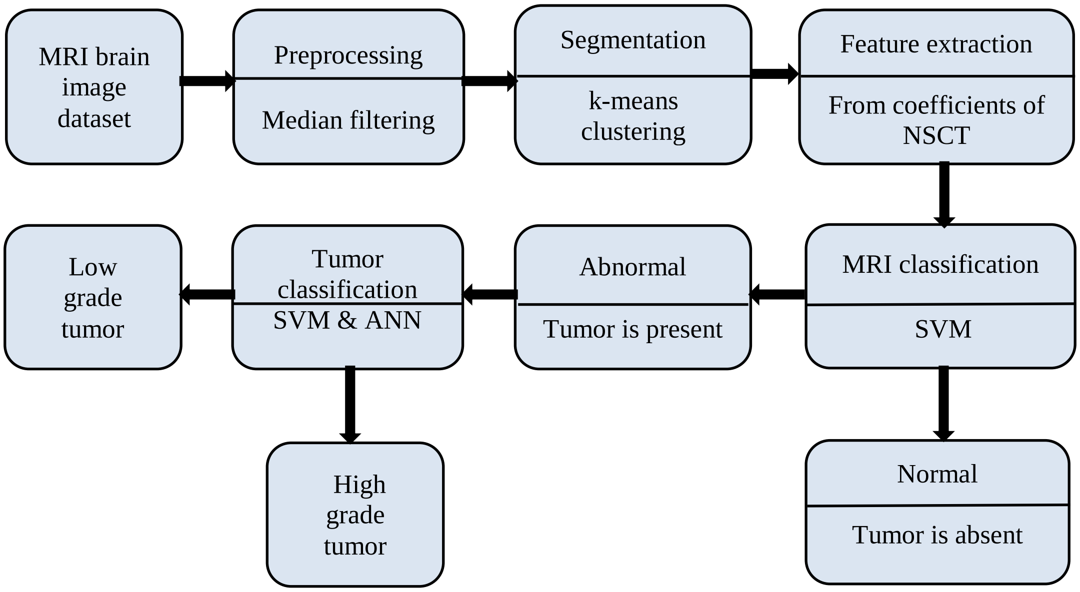

Figure 3.1**:** Block diagram of proposed tumor classification scheme.

3.2 Proposed Hybrid Brain Tumor Classification Scheme

The proposed hybrid brain tumor classification scheme consists of preprocessing, segmentation, feature extraction and classification stage which is shown in Figure 3.1. In preprocessing stage, median filtering is used for reducing the noise levels of MRIs. In segmentation stage, the most emerging clustering technique, K-means clustering has been used in order to extract the region of interest of processed MRIs. Then in features extraction step, 2-level NSCT is applied on the region of interest in order to obtain the high and low subband coefficients. Afterwards, twelve features are extracted from the subband coefficients which are applied in 1st stage of SVM for classification of normal or abnormal MRIs. Then the grades of tumors are classified using both SVM and ANN classifier.

3.2.1 Preprocessing Stage

The most common problems of using MRIs are the noise produced by the MRI scanner, diffusive or missing boundaries [1]. Preprocessing of MRIs is the compulsory stage before segmentation or further classification of MRIs. Preprocessing of MRIs includes the task of diminishing the noise level of MRIs. Several conventional filters such as median, Gaussian, Wiener, mean, anisotropic [2] etc. can be applied for removing noise. But median filtering gives satisfactory performances for removing noise of MRI image by preserving its edge [3]. It works on the overall image by moving a window (model of neighbors) pixel by pixel and a median is computed from the intensities of the pixels of the window. Then it subdues isolated noise of an image by replacing each pixel value with this median value.

3.2.2 Segmentation Stage

In this stage, K-means clustering is employed in order to segment the region of interest of brain image. The details of K-means clustering are described in previous chapter. K-means clustering is one of the prominent examples of unsupervised learning algorithm which has the capability to solve the clustering problem [4] of a given data set with a fixed number of clusters, say K. [5]. The main goal of K-means clustering is to minimize the sum of squared error, which is also called objective function [6]. This function is defined in Eq. 3.1.

$$E = \sum_{b=1}^{K} \sum_{a=1}^{N} \left\| x_a^{(b)} - c_b \right\|^2 \tag{3.1}$$

where, $\left\| x_a^{(b)} - c_b \right\|^2$ is defined as distance between any data point x_a^b and its closest centroid of the cluster c_b. The number of clusters and the number of data points are represented by K and N, respectively.

For minimizing the objective function E [6], following steps should be followed:

i. Initially, place group or cluster centroids K.
ii. Allocate each data point to the cluster with closest centroid.
iii. When all data points are allocated then recalculate the positions of the cluster centroids.
iv. Repeat step 2 and 3, until the positions of the centroids no longer shift.

3.2.3 Features Extraction Stage

In this stage, 2-level NSCT [7] is applied to the segmented image for extracting features from the low and high frequency subband coefficients. NSCT has three salient properties, like multiscale, multidirection and shift invariance and also it has better frequency selectivity and regularity rather than contourlet transform. Besides, it provides provide desirable performance in contour characterization, edge detection, image enhancement, denoising. Due to these reasons, NSCT is used in this stage for extracting features. The structure of NSCT is briefly described in the previous chapter. is As N-level NSCT produces 2^N directional subbands, so in the proposed scheme we have restricted our scope to 2-level NSCT for reducing high frequency subband coefficients and also for reducing computational time. Twelve features are extracted which are contrast, entropy, mean, variance, correlation, standard deviation (SD), root mean square (RMS), energy, skewness, kurtosis, inverse difference moment (IDM) and homogeneity [8] from ROI which are defined by following (3.2-3.14).

a) Contrast: Contrast is a measure of intensity level of a pixel and its neighbor over the image which is defined as following

$$Contrast = \sum_{x=1}^{m}\sum_{y=1}^{n}(x-y)^2 p(x,y) \tag{3.2}$$

where,

$$P(x,y) = |I(x,y)|^2 \Big/ \sqrt{\sum_{x=1}^{m}\sum_{y=1}^{n}[I(x,y)]^2} \tag{3.3}$$

b) Entropy: Entropy is used to characterize the randomness of the textural image which is defined as following

$$Entropy = -\sum_{x=1}^{m}\sum_{y=1}^{n} p(x,y)\cdot\log[p(x,y)] \tag{3.4}$$

c) Mean: Mean is calculated by adding all the pixel values of an image divided by the total number of pixels in that image. It is defined as following

$$Mean = \frac{1}{m*n}\sum_{x=1}^{m}\sum_{y=1}^{n} f(x,y) \tag{3.5}$$

d) Variance: The Variance of an image is defined as following

$$Variance = \frac{1}{m*n}\sum_{x=1}^{m}\sum_{y=1}^{n}(I(x,y)-\bar{I})^2 \tag{3.6}$$

e) Correlation: Correlation feature exhibits the spatial dependencies between pixels and it is defined as following

$$Correlation = \frac{\sum_{x=1}^{m}\sum_{y=1}^{n}(x,y)f(x,y) - M_x M_y}{\sigma_x \sigma_y} \tag{3.7}$$

where, M_x and M_y are the mean in the horizontal or x-direction

f) Standard deviation: It is the second central moment describing the probability distribution of an observed population and can server as a measure inhomogeneity. A higher value indicates the better intensity level and high contrast of edges of an image [8]

$$Standard\ Deviation = \sqrt{\frac{1}{m*n}\sum_{x=1}^{m}\sum_{y=1}^{n}(I(x,y)-\bar{I})^2} \tag{3.8}$$

where,

$$\bar{I} = \frac{1}{m*n}\sum_{x=1}^{m}\sum_{y=1}^{n} I(x,y) \tag{3.9}$$

g) Root mean square (RMS): RMS is the square root of the mean of the squares of the pixel values of an image.

$$RMS = \sqrt{\frac{1}{m*n}\sum_{x=1}^{m}\sum_{y=1}^{n}[f(x,y)]^2} \tag{3.10}$$

h) Energy: It can be referred to as the quantifiable amount of the extent of pixel pair repetitions. Energy is a parameter to measure the similarity of an image. If energy is defined by Haralicks gray level co-occurrences matrix (GLCM) feature, then it is also defined as angular second moment. It is defined as following

$$Energy = \frac{1}{m*n}\sum_{x=1}^{m}\sum_{y=1}^{n}[I(x,y)]^2 \tag{3.11}$$

i) Skewness: It is a measure of symmetry or the lack of symmetry. The skewness is defined as

$$Skewness = \left(\frac{1}{variance^3}\right)\sum_{x=1}^{m}\sum_{y=1}^{n}(I(x,y)-\bar{I})^3 \tag{3.12}$$

j) Kurtosis: The shape of a random variable’s probability distribution is described by the parameter called Kurtosis. It is defined as following

$$kurtosis = \left(\frac{1}{variance^4}\right)\sum_{x=1}^{m}\sum_{y=1}^{n}(I(x,y)-\bar{I})^4 \tag{3.13}$$

k) Inverse difference moment (IDM) or homogeneity: IDM is a measure of the local homogeneity of an image. IDM may have a single or a range of values so as to determine whether the image is textured or non-textured. It is defined as following

$$IDM = \sum_{x=1}^{m}\sum_{y=1}^{n}\frac{1}{1+(x-y)^2}f(x,y) \tag{3.14}$$

3.2.4 Features Classification Stage

Twelve features are extracted in the previous stage. These features are used to train the support vector machine (SVM) for the classification. SVM which consists of two stages is trained with these twelve features. 1st stage of SVM is able to classify brain image as normal or abnormal and then 2nd stage of SVM classifies grade of tumor as low grade or high grade. The grade of tumor is also classified using the ANN classifier based on feed forward back propagation.

SVM is a two class classifier [9] based on supervised learning technique which is used for classification of data and regression analysis. It is a non-probabilistic binary linear classifier which classifies between two classes by forming a hyperplane in feature space and has some advantages like high accuracy, sophisticated mathematical tractability [10]. The SVM classification process normally involves with training and testing data and the training data contains class labels and several attributes or features. In spite of various families of SVM like box constraint, autoscale, kernel [11], the kernel support vector machine has been selected in this proposed scheme due to its advantages like few tunable parameters, convex quadratic optimization for training [10]. Although there is a wide range of kernel functions, linear, polynomial, Gaussian radial basis function (GRB) are used in this classification stage.

ANN is a set of biologically revitalized computing system which copies the neural architecture of human brain [12]. It is described as a group of interconnected artificial neurons that are organized in parallel layers. ANN is widely used in the areas of classification, pattern recognition, pattern completion, optimization, control, function approximation, data mining etc. In our proposed scheme feed forward back propagation based ANN classifier is used. The overview of feed forward back propagation ANN is briefly described in previous section. The features of glioma images that are applied for training and testing of SVM are also used here for the classification of low and high grade tumors.

3.3 Proposed Cellular Automata Based Watermarking Using NSCT and SVD

Here, game of life cellular automata based watermarking using NSCT and SVD is proposed. Cellular automata are widely used in various fields of applications, like random number generation, pattern recognition, games etc. Game of life cellular automata is used here for shuffling pixels of an image that ensures the security of the watermarking scheme. A brief description of cellular automata is provided in chapter 2. The summary of game of life rules are given in the following table 3.1.

Game of life has four rules [13]: birth, death by overcrowding, death by exposure and survival. In an image, dead cell and alive cell are represented by 0 and 1, respectively. Watermark scrambling algorithm using these four rules is described in the next section. Figure 3.2 described watermarking scrambling process using game of life cellular automata. Figure 3.2 (a) depicts a matrix which is obtained after 1st generation of game of life and nine alive (1) cells. Figure 3.2 (b) demonstrates the original image pixel values. The positions of first nine pixels of the original image are shuffled according the 1st generation matrix. The scrambled image using 1st generation of GOL is shown in Figure 3.2 (b).

The low frequency subband of NSCT contains most of the perceptual content of an image and a modest change in the singular values of low frequency subband of NSCT does not affect the image quality after reconstruction. In addition, NSCT along with SVD provides the required robustness of watermarking against various image processing and geometric attacks. The scheme will offer security, imperceptibility and robustness against various image processing and geometric attacks like Gaussian white noise, salt and pepper noise, median filtering, JPEG compression, cropping and rotation

Table 3.1 Summary of game of life cellular automata rules

Rules	**Cell state at time-t**	**Cell state at time-t+1**	**States of neighbors at time-t**
Birth	Dead (0)	Alive (1)	Exactly 3 neighbors are alive
Death by over-crowding	Alive (1)	Dead (0)	Four or more neighbors are alive
Death by exposure	Alive (1)	Dead (0)	One or none neighbor are alive
Survival	Alive (1)	Alive (1)	Two neighbors are alive

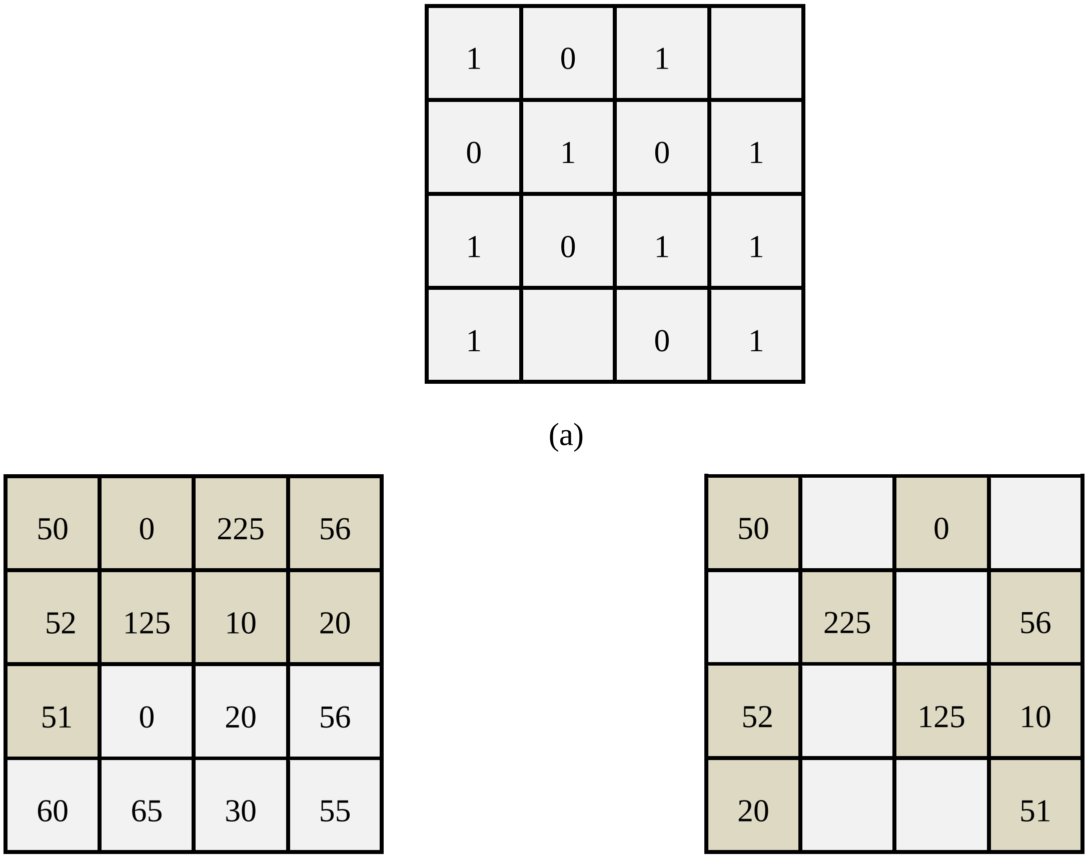

1	0	1	
0	1	0	1
1	0	1	1
1		0	1

(a)

50	0	225	56
52	125	10	20
51	0	20	56
60	65	30	55

(b)

50		0	
	225		56
52		125	10
20			51

(c)

Figure 3.2: Watermark scrambling process using game of life cellular automata: (a) 1st generation of game of life (GOL); (b) original image pixel values; (c) scrambled image using 1st generation of GOL.

3.3.1 Watermark Scrambling and Embedding Algorithm

A MRI of size *M×N×3* is considered as a cover image and a of size *M/3×N/3* is considered as watermark. Figure 3.3 shows the block diagram of proposed watermark embedding scheme. The proposed watermark scrambling and embedding procedures are described as follows:

1) A logistic map (considered as primary matrix G_0) of size M/3×N/3 is generated following (4.1).

$$G_{i+1} = \mu G_i(1 - G_i) \tag{3.15}$$

where, μ and G_1 are the initial parameters of logistic map and their values are taken as 3.91 and 0.4346, respectively in the proposed scheme. The values of μ and G_1 are considered as secret key $K_{1.}$

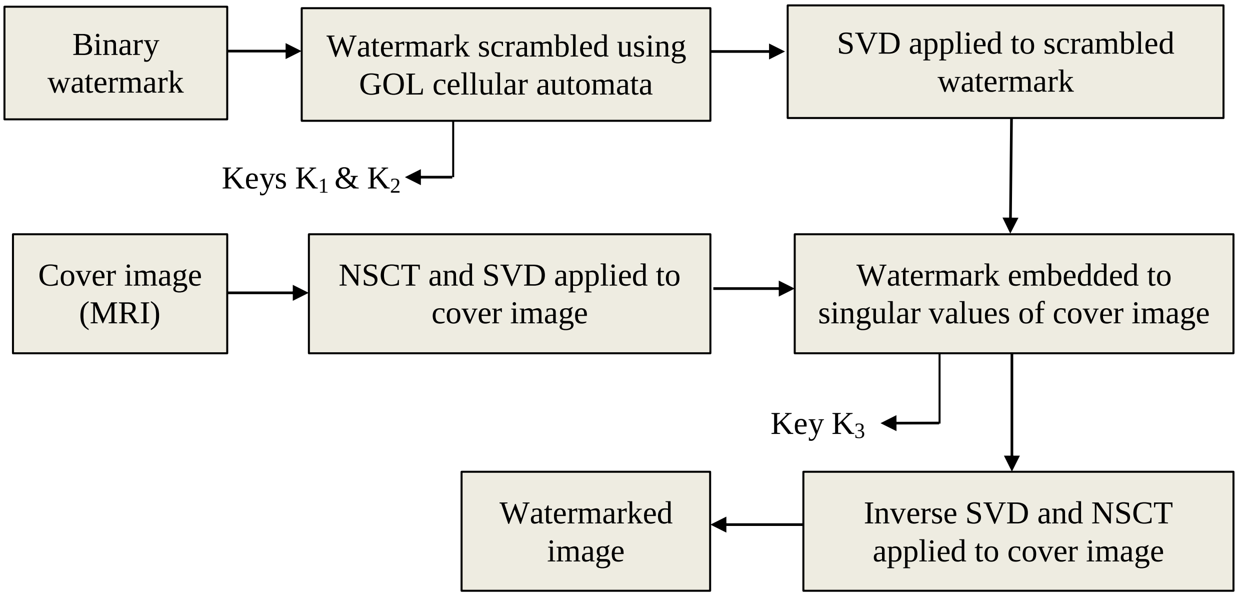

Figure 3.3: Block diagram of proposed watermark embedding scheme

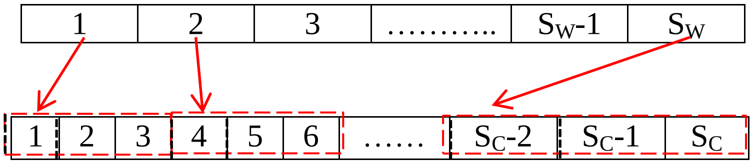

Figure 3.4: Watermark embedding process in singular value matrix of cover image.

2) GOL rules are applied to G_0 in order to produce 1st generation G_1, then the rules are applied to G_1 in order to produce 2nd generation G_2; thus this process is run for K_2 times to produce K_2 (another key) generations.

3) The pixels of watermark are scrambled in accordance with G_1 (x, y) = 1, where x=1, 2, 3………M/3 and y=1, 2. 3………N/3.

4) The pixels of watermark that are not scrambled in 1st generations are scrambled in accordance with G_2 (x, y) =1 and G_1 (x, y) = 0. This process is reoccurred until K_2 generation is achieved.

5) At last the remaining pixels, if any after K_2 generation, that are scrambled in accordance with G_{K2} (x, y) = 0. In the proposed scheme, 7th generation (K_2=7) of GOL is considered.

6) MRI is converted to gray-scale image.

7) 2-level NSCT is applied to the gray-scale of MRI in order to obtain low frequency subband of NSCT.

8) Then SVD is applied to the low frequency subband of NSCT in order to obtain singular value matrix.

9) On the other hand, in order to obtain singular value matrix of watermark, SVD is applied to the scrambled binary watermark.

10) Each singular value matrix MRI is partitioned into blocks and the number of blocks is equal to M/3 or N/3.

11) Each singular value of scrambled watermark is embedded to 1st singular value of each block of singular value matrix of MRI using following (4.2). This process is demonstrated in Figure 3.4.

$$S_{WM} = S_c + \sigma S_w \tag{3.16}$$

where, σ is scaling factor

12) This value of embedding locations is used as embedding secret key array K_3.

13) Watermarked image obtained by employing inverse SVD and NSCT.

3.3.2 Watermark Extracting and Descrambling Algorithm

In the previous section, three secret keys (K_1, K_2, K_3) are used for scrambling and embedding watermark and no one can extract the watermark if one of the keys is wrong. So these three keys of our proposed scheme are very crucial for extracting and descrambling the watermark. Figure 3.5 shows the proposed watermark descrambling and extracting scheme and procedures involved in the scheme are described as follows:

1) Firstly, 2-level NSCT is applied to the watermarkd MRI in order to obtain low frequency subband.

2) The SVD is applied to the low frequecy subband of NSCT in order to obtain singular value matrix.

3) The key K_3 is used to extract the sigular values of scrambled watermark from singular value matrix of watermarked MRI following (4.3).

$$S_w^* = (S_{WM}^* - S_c)/\sigma \tag{3.17}$$

4) Inverse SVD is applied separately in order to get scrambled watermark.

5) After obtaining scrambled watermark from watermarked MRI, final descrambled watermark is achieved by following steps 6-9.

6) Key K_1 is used to generate initial matrix G_0 using logistic map.

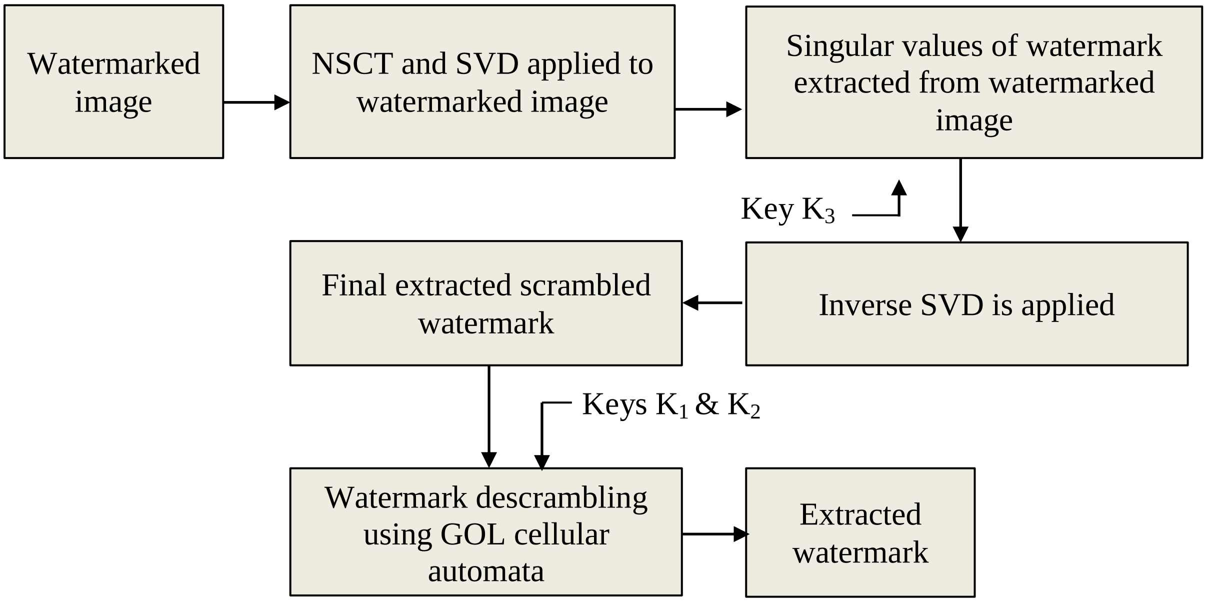

Figure 3.5: Block diagram of proposed watermark extracting scheme

7) GOL rules are applied to G_0 in order to produce 1st generation G_1, then watermark is extracted following $W_{ext}(a,b) = W_{scr}(x,y)$ if $G_1(x, y) = 1$ where, $W_{ext}(a,b)$ commencing from $a=b=1$.

8) Rules are applied to G_1 in order to produce 2nd generation G_2, then watermark is extracted following $W_{ext}(a,b)= W_{scr}(x,y)$ if $G_2(x, y) = 1$and $G_1(x, y) = 0$. This process is repeated until K_2 geneartion is achieved.

9) The remainig pixels, if any after K_2 generation, that are extracted following $W_{ext}(a,b)= W_{scr}(x,y)$ if $G_{K2}(x, y) = 0$ and finally the extracted watermark W_{ext} is obtained.

3.4 Proposed Multiple Chaotic Maps Based Watermarking Using NSCT and DCT

In this scheme, multiple chaotic maps are used to enhance the security of MRI watermarking technique. Here, both MRI and watermark are encrypted using multiple chaotic maps. An arranged chaotic sequence which is created by logistic map is used to shuffle the pixel positions of MRI. Patient information, watermark is encrypted by two chaotic maps, like Arnold's Cat map and tent map. Afterwards, NSCT is applied on shuffled MRI for getting approximation band of NSCT and then DCT is applied on this approximation band. DCT is also applied on watermark and its DCT coefficients are embedded into the DCT coefficients of approximation band of shuffled MRI. Fig. 3.6 illustrates the proposed embedding and extracting algorithm of MRI medical images watermarking scheme, respectively. In the embedding phase, 4 secret keys are engaged that are required for recovering watermark in the extracting phase.

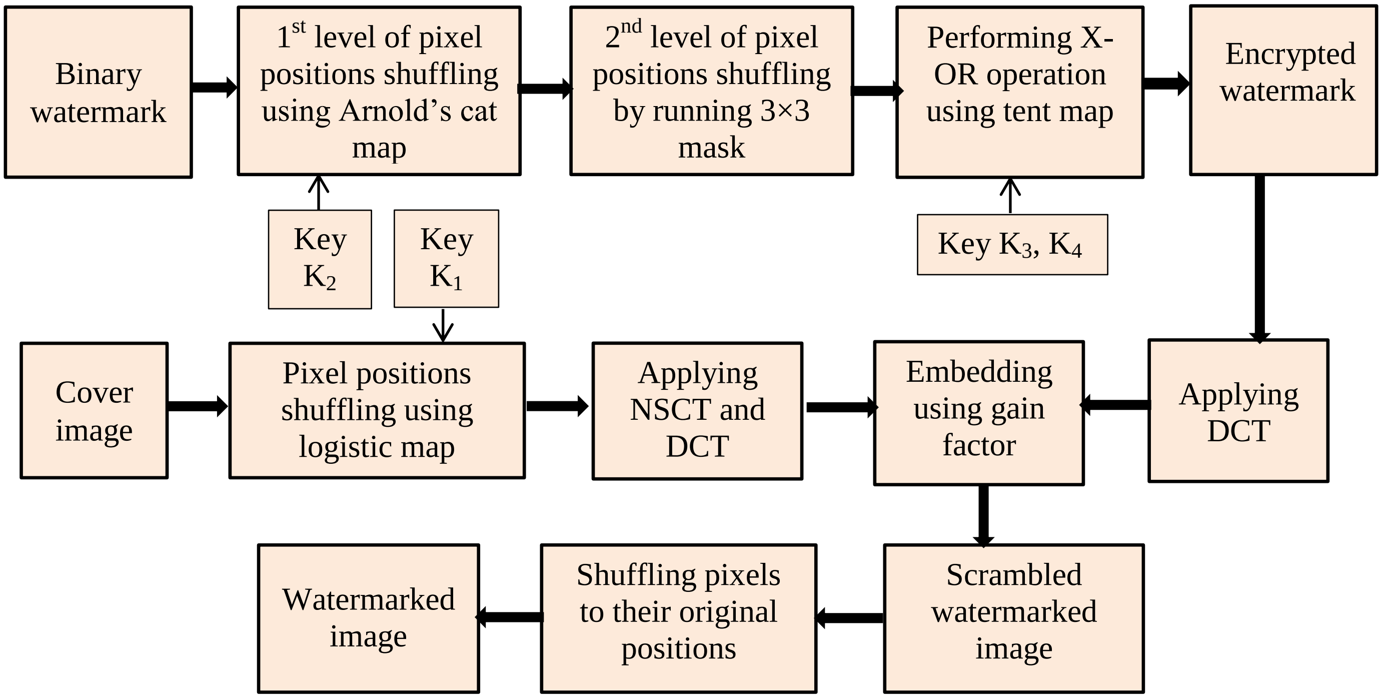

Figure 3.6: Proposed watermark embedding technique

3.4.1 Embedding Algorithm

1) A MRI image of size $M \times N$ is taken as cover image, C

2) The pixels of cover image are shuffled by logistic map. At first a chaotic sequence of size 1× MN is produced following (1), where $\mu = 3.9$ and $x(1) = 0.5$ are considered as confidential key K_1.

3) Then the sequence is arranged in ascending or descending order. The positions of the pixels of cover image, C are shuffled in accordance with the positions of arranged sequence of logistic map [4] to get C_S. This shuffling process for a portion of cover image of size 3×3 is depicted in Fig. 3.7. The scrambled brain MRI using this shuffling process is demonstrated in Fig. 3.8.

4) NSCT is applied on the shuffled cover image, C_S for getting the low pass subband, C_{SL} and then DCT is applied on C_{SL} band in order to obtain DCT coefficients, C_{SLDCT}.

5) In 1st level of shuffling of watermark, a binary watermark, W of size $(M/3, N/3)$ is shuffled by Arnold's cat map to get W_A. The number of iterations of watermark can be used as key K_2. Then a 3×3 mask is run over the scrambled watermark, W_A for 2nd level of shuffling. For each 3×3 mask of watermark W_A, this shuffling technique is demonstrated in Fig. 3.9.

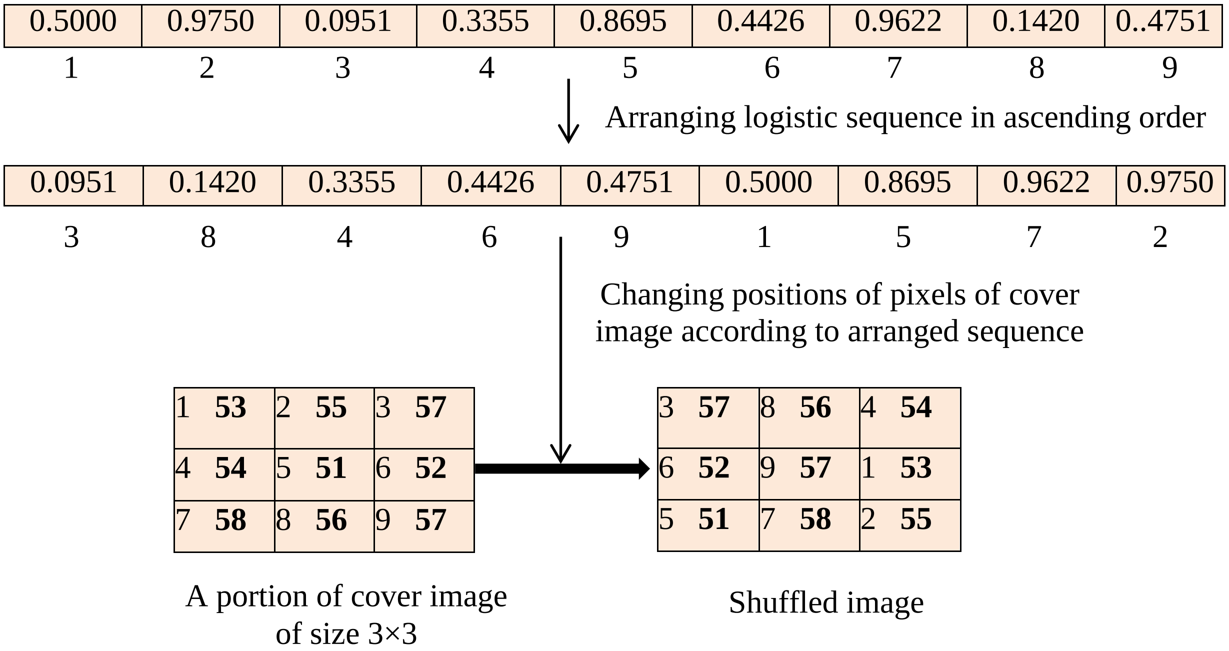

0.5000	0.9750	0.0951	0.3355	0.8695	0.4426	0.9622	0.1420	0..4751
1	2	3	4	5	6	7	8	9

0.0951	0.1420	0.3355	0.4426	0.4751	0.5000	0.8695	0.9622	0.9750
3	8	4	6	9	1	5	7	2

1 **53**	2 **55**	3 **57**
4 **54**	5 **51**	6 **52**
7 **58**	8 **56**	9 **57**

3 **57**	8 **56**	4 **54**
6 **52**	9 **57**	1 **53**
5 **51**	7 **58**	2 **55**

Figure 3.7: Cover image shuffling process using logistic map

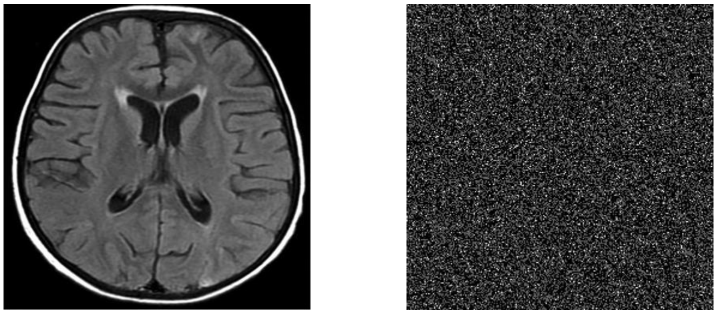
(a) (b)

Figure 3.8: (a) Brain MRI; (b) Scrambled MRI using logistic map pixel shuffling process

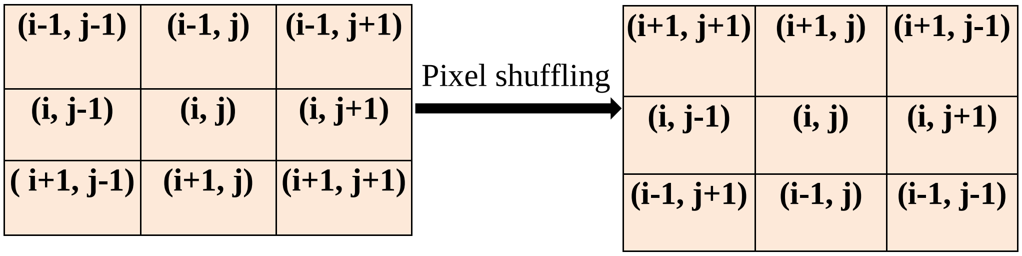

(i-1, j-1)	**(i-1, j)**	**(i-1, j+1)**
(i, j-1)	**(i, j)**	**(i, j+1)**
(i+1, j-1)	**(i+1, j)**	**(i+1, j+1)**

(i+1, j+1)	**(i+1, j)**	**(i+1, j-1)**
(i, j-1)	**(i, j)**	**(i, j+1)**
(i-1, j+1)	**(i-1, j)**	**(i-1, j-1)**

Figure 3.9: 2^{nd} level of pixel shuffling of watermark

6) The two chaotic sequences of each size 1× M/6×N/3 are generated following (3) of tent map. Then the two sequences are rounded to binary numbers. The initial assumed values of two chaotic sequences are considered as keys K_3 and K_4 for tent map.

7) The two binary sequences are reshaped to two matrices of each size $(M/6, N/3)$. The 1st binary matrix of tent map is X-ORed with the scrambled watermark, $W_{A(i,j)}$, where, $i = 1 \dots \dots \dots M/6$ and $j = 1 \dots \dots \dots N/3$.

8) Then X-OR operation is performed between the 2nd binary matrix of tent map and the remaining pixels of $W_{A(i,j)}$, where, $i = M/6 + 1 \dots \dots \dots M/3$ and $j = 1 \dots \dots \dots N/3$.

9) Finally, the encrypted watermark is achieved and DCT is performed on it. Then the DCT coefficients of encrypted watermark, W_{DCT} are embedded into the DCT coefficients of cover image following (5) to get coefficients of scrambled watermarked image, $WM_{C.}$

$$WM_C = C_{SLDCT} + \gamma W_{DCT} \tag{3.18}$$

where, $\gamma =$ gain factor [12]

10) Inverse DCT is applied on WM_C and then inverse NSCT are applied for getting scrambled watermarked image, *WM*. Then *WM* is descrambled following the inverse process which is described in step 1 and 2. After descrambling, final watermarked image is acquired.

3.4.2 Extracting Algorithm

In extracting phase, four keys are required for extracting watermark from watermarked image and this extracting technique is demonstrated in Fig. 3.10.

1) The pixels of the watermarked MRI, *WM* are shuffled to their shuffled positions. Here key K_1 is used for generating chaotic sequence and using this sequence the pixels are shuffled according to step 2 and 3 in embedding algorithm.

2) The NSCT is applied on the shuffled watermarked MRI for achieving low pass subband and then DCT is applied on this band to get WM_C

3) Then DCT coefficients of watermark, W_{EDCT} are extracted by following (6). Inverse DCT is applied on W_{EDCT} to obtain encrypted watermark, W_E.

$$W_{EDCT} = (WM_C - C_{SLDCT})/\gamma \tag{3.19}$$

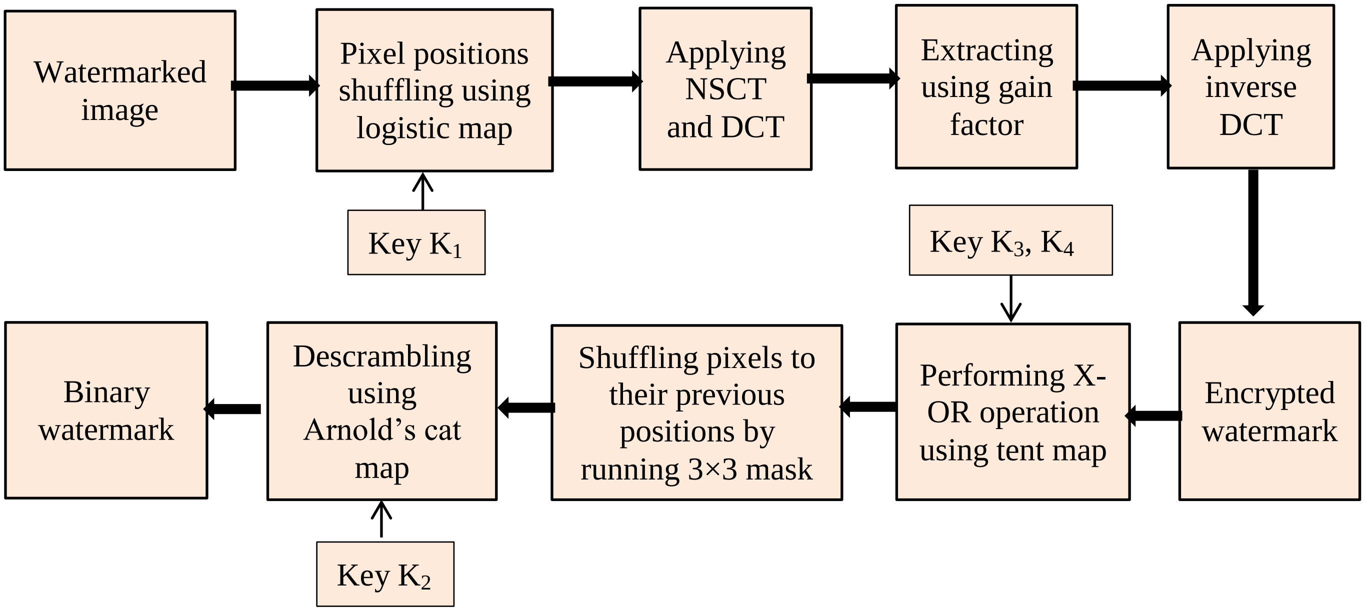

Figure 3.10: Proposed watermark extracting technique

4) Keys K_3 and K_4 are used to generate the same chaotic sequences using tent map. Then the same procedures which are described in step 6-8 of embedding algorithm are followed to get scrambled watermark, W_{EA}.
5) Then the pixels of scrambled watermark W_{EA}, are shuffled to their original positions for each 3×3 mask and then Arnold's cat map using K_4 is used to get the descrambled watermark, W_E.

3.5 Summary

A hybrid scheme for classification of brain MRI and tumor is proposed. For segmentation of MRI image, K-means clustering is used in this proposed scheme. Instead of DWT, NSCT is used for extracting twelve features from segmented image. Using these features, SVM and ANN are used for desired classification. Then cellular automata based image watermarking using NSCT and SVD has been proposed. GOL cellular automata are used to scramble binary watermark and two keys are involved in the scrambling process. This scrambled watermark is embedded into MRI using NSCT and SVD. Cellular automata keys and the embedding key array improve the security of proposed scheme because without these secret keys, no one can extract and descramble the watermark. At last, a hybrid MRI medical images watermarking technique has been proposed using chaotic maps, NSCT and DCT. Three chaotic maps are incorporated in this watermarking technique and they are used in different ways to ameliorate the security of the scheme. Four secret keys that obtained from three chaotic maps are required to extract the watermark or patient information from MRI. Combination of NSCT and DCT also enhances the robustness and imperceptibility of MRI watermarking scheme. NSCT is used in both brain tumor classification and watermarking techniques.

References

[1] M. Havaei, P.M. Jodoin, and H. Larochelle, “Efficient interactive brain tumor segmentation within-brain KNN classification,” in Proc. of *22nd International Conference on Pattern Recognition (ICPR)*, pp.556-561, Aug. 2015.

[2] S.R. Anisha and J.V. Krishnan, “Comparison of various filters for noise removal in MRI brain image,” in Proc. *International Conference on Futuristic Trends in Computing and Communication (ICFTCC),* pp.68-73, 2015.

[3] E.A. Castro and D.L. Donoho, “Does median filtering truly preserve edges better than linear filtering,” *The Annals of Statistics*, vol. 37, pp. 1172-1206, 2009.

[4] V.K. Dehariya, S.K. Shrivastava, and R.C. Jain, “Clustering of image data set using k-means and fuzzy k-means algorithms,” in Proc. of *International Conference on Computational Intelligence and Communication Networks*, pp. 386-391, 2010.

[5] M.K. Abd-Ellah, A.I. Awad, A.A.M. Khalaf and H.F.A. Hamed, “Classification of brain tumor MRI brain images using a kernel support vector machine,” *Communications in Computer and Information Science,* vol. 636, pp.151-160, September 2016.

[6] H. Zhou, G. Schaefer, and C. Shi, “Fuzzy c-means techniques for medical image segmentation,” *Fuzzy Systems in Bioinformatics and Computational Biology*, vol. 242, pp. 257-271, 2009.

[7] A.L. Cunha, J. Zhou, and M.N. Do, “The nonsubsampled contourlet transform: theory, design and applications,” *IEEE Transactions on Image Processing*, vol. 15, pp. 3089-3101, 2006.

[8] N.B. Bahadure, A.K. Ray, and H.P. Thethi, “Image analysis for MRI brain tumor detection and feature extraction using biologically inspired BWT and SVM,” *International Journal of Biomedical Imaging*, vol. 2017, pp.1-12, 2017.

[9] K. Machhale, H.B. Nandpuru, V. Kapur and L. Kosta, “MRI brain cancer classiifcation using hybrid classifier (SVM-KNN),” in Proc. of International Conference on Industrial Instrumentation and Control (ICIC), pp.60-65, May 2015.

[10] Y. Zhang and L. Wu, “An MR brain images classifier via principal component analysis and kernel support vector machine,” Progress in Electromagnetics, vol. 130, pp. 369-388, 2012.

[11] M.K. Abd-Ellah, A.I. Awad, A.A.M. Khalaf and H.F.A. Hamed, “Classification of brain tumor MRI brain images using a kernel support vector machine,”Communications in Computer and Information Science, vol. 636, pp.151-160, September 2016.

[12] O.A. Abdalla, M.N. Zakaria, S. Sulaiman, and W.F.W.Ahmad, “A comparison of feed-forward back-propagation and radial basis artificial neural networks: A Monte Carlo study,” *International Symposium in Information Technology*, pp. 994-98, June 2010.

[13] A. Dalhoum, M. MAhafzah, A. Awwad, I. Aldamari, A. Oterga and M. Alfonseca “Digital image scrambling using 2D cellular automata”, in proc. of *14th IEEE international Symposium on Multimedia*, 10-12 December 2012, Irvine, CA,US.

CHAPTER IV

RESULTS AND DISCUSSION

4.1 Introduction

This chapter outlines the results and discussion of the three previous proposed schemes. In brain tumor classification scheme, 1st stage of SVM is able to classify brain image as normal or abnormal and then 2nd stage of SVM classifies grade of tumor as low grade or high grade. The grade of tumor is also classified using the ANN classifier based on feed forward back propagation. For SVM classifier, the classification accuracy of normal or abnormal brain image is 98.15%. SVM classifier provides low or high grade tumor classification accuracy 81.63%, whereas feed forward back propagation based ANN classifier provides 85.71%. Two proposed watermarking schemes offer security, imperceptibility and robustness against various image processing and geometric attacks like Gaussian white noise, salt and pepper noise, median filtering, JPEG compression, cropping and rotation. The proposed schemes are compared with existing watermarking schemes in terms of Mean Square Error (MSE), Peak Signal to Noise ratio (PSNR), Normalized Correlation (NC) and provides satisfactory performance than other schemes.

4.2 Results and Discussions of Hybrid Brain Tumor Classification Scheme

The proposed scheme is tested in MATLAB 2014a software platform. Computer with core i7/3.60 GHz and 8 GB RAM is used for evaluation. Tumor images which are obtained from BRATS 2015 database [1]. BRATS database [2-3] consists of four types of 3D MRI brain tumor (glioma) images (T1, T2, FLAIR and T1C) in .mha format and we collected FLAIR images from this dataset. These .mha files of MRI brain tumor images were converted to .png formats before preprocessing stage of the proposed scheme. Three important parameters namely sensitivity, specificity and accuracy are chosen for performance evaluation which are defined by following

$$Sensitivity = \frac{TP}{TP + FN} \times 100\% \tag{4.1}$$

$$\text{Specificity} = \frac{TN}{TN + FP} \times 100\% \tag{4.2}$$

$$\text{Accuracy} = \frac{TP + TN}{TP + TN + FP + FN} \times 100\% \tag{4.3}$$

where,

True Positive (TP) = correctly classified positives.

True Negative (TN) = correctly classified negatives.

False Positive (FP) = incorrectly classified positives.

False Negative (FN) = incorrectly classified negatives.

Table 4.1: Number of brain images for training and testing of SVM

Total Number of brain images	**Number of brain images for training of SVM**		**Number of brain images for testing of SVM**	
	Normal	Abnormal	Normal	Abnormal
99	10	35	10	44

Table 4.2: Normal and abnormal brain images classification results with respect to sensitivity, specificity and accuracy for linear, polynomial and RBF kernel based SVM

Kernel Functions	**Performance Evaluation Parameters**						
	TP	***TN***	***FP***	***FN***	***Sensitivity (%)***	***Specificity (%)***	***Accuracy (%)***
Linear	70	15	5	9	88.61	75	85.85
Polynomial	75	18	2	4	94.94	90	93.93
GRB	78	20	0	1	98.73	100	98.98

4.2.1 Classification of Normal and Abnormal Brain Images Using SVM

Table 4.1 shows the number of the normal or abnormal brain images which are used to test and train the SVM. Total 99 MRI brain images are used in our proposed scheme. In order to train the 1st stage of SVM, the features which are extracted from the segmented regions of 45 images (10 normal and 35 abnormal) are used. Then 54 images (10 normal and 44 abnormal) are applied to the 1st stage of SVM classifier for testing. Table 4.2 demonstrates the results of classification results of normal or abnormal brain images for three SVM kernels. For linear kernel, we got sensitivity 88.61%, specificity 75% and accuracy 85.85%, while Polynomial kernel based SVM provides sensitivity 94.94%, specificity 90% and accuracy 93.93%. GRB kernel based SVM ensures better performance than linear and polynomial kernel which provides sensitivity 97.73%, specificity 100% and accuracy 98.15%.

Table 4.3: Number of low and high grade glioma images for training and testing of SVM.

Total Number of glioma images	**Number of glioma images for training of SVM**		**Number of glioma images for testing of SVM**	
	Low grade	High grade	Low grade	High grade
79	10	20	8	41

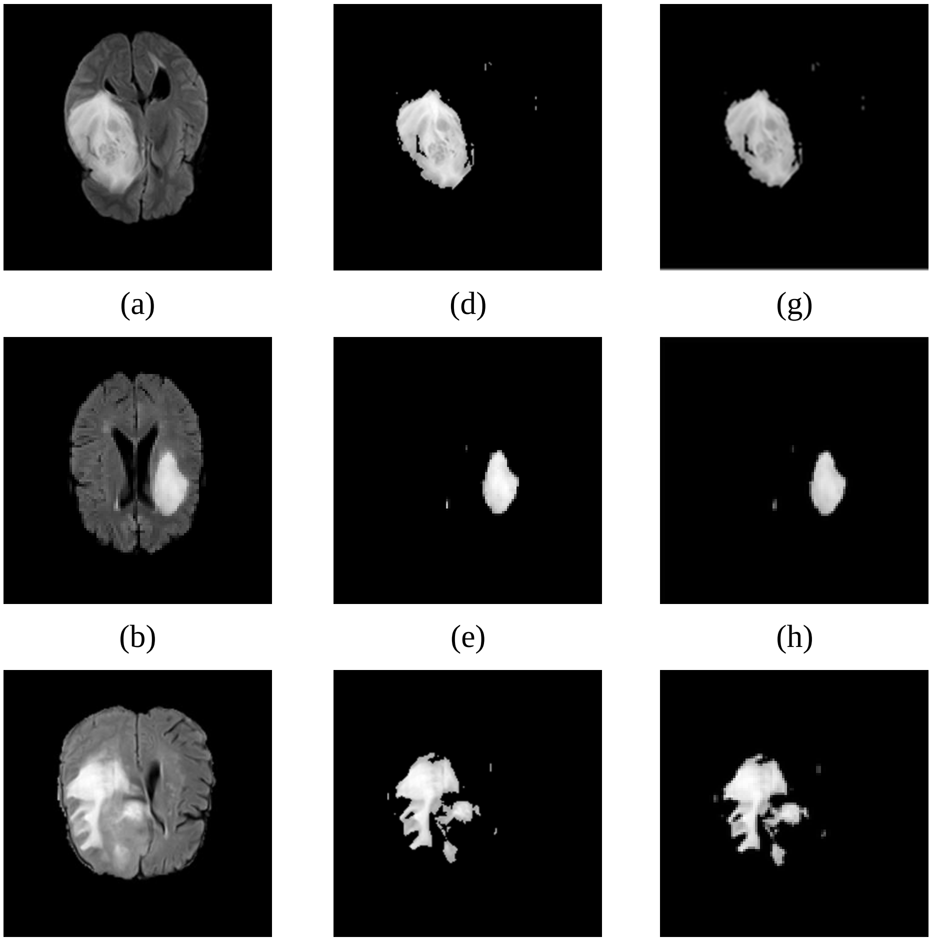

(a) (d) (g)

(b) (e) (h)

(c) (f) (i)

Figure 4.2: (a-d) High grade glioma images; (e-h) their corresponding segmented tumour region; (i-l) low pass subband images in NSCT domain

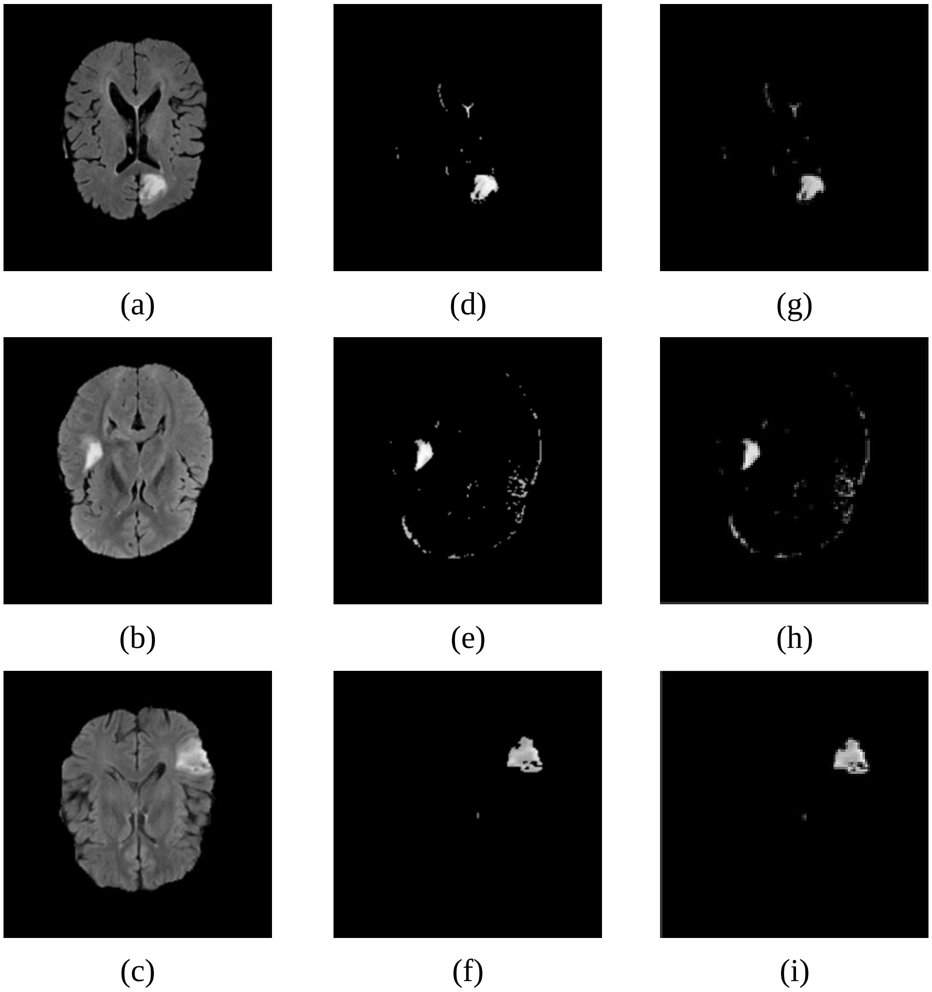

Figure 4.3: (a-c) Low grade glioma images; (d-f) their corresponding segmented tumour region; (g-i) low pass subband images in NSCT domain

4.2.2 Classification of Brain Tumor Using SVM

Table 4.3 shows the number of glioma images which are used to test and train the 2nd stage of SVM. Total 79 glioma images are used for this purpose. In order to train the 2nd stage of SVM, 30 glioma images (10 low grade and 20 high grade) are applied. Then 49 glioma images (8 low grade and 41 high grade) are applied to the 1st stage of SVM classifier for testing. Figure 4.2 (a-c), Figure 4.2 (d-f) and Figure 4.2 (g-i) demonstrates high grade glioma images, their respective segmented tumor region after K-means clustering and the low pass subband image of segmented tumor region in NSCT domain, respectively. Similarly, Figure 4.3 demonstrates the same scenario for low grade glioma images. Twelve features, like contrast, entropy, mean, variance, correlation, standard deviation (SD), root mean square (RMS), energy, skewness, kurtosis, inverse difference moment (IDM) and homogeneity from NSCT subband coefficients of tumor region. These features for six sample high grade and low glioma images are demonstrated in Table 4.4 and Table 4.5, respectively. From the both tables, it is observed that variations among the features are very small. Table 4.6 shows the high grade and low grade glioma classification results for three SVM kernels. Sensitivity 68.29%, specificity 33.33% and accuracy 61.22% are obtained in linear kernel SVM, whereas Polynomial kernel based SVM provides sensitivity 80.48%, specificity 37.5% and accuracy 73.47%. GRB kernel based SVM provides sensitivity 85.36%, specificity 62.5% and accuracy 81.63%, that are higher than other kernels. Although we got poor classification results for low grade tumor, overall accuracy is satisfactory.

Table 4.4: Extracted twelve features from NSCT subband coefficients of tumor region for six high grade glioma images

Features	**Image 1**	**Image 2**	**Image 3**	**Image 4**	**Image 5**	**Image 6**
Contrast	1.6210	1.0663	0.9055	1.4303	1.7223	1.7012
Correlation	0.6866	0.7409	0.7810	0.7237	0.6558	0.6433
Energy	0.7936	0.8436	0.8520	0.8101	0.8087	0.8119
Mean	1.2019	0.8478	1.1327	1.4670	1.2721	1.4313
Variance	192.6959	145.3572	189.7680	218.9057	200.1657	194.7720
RMS	8.7627	7.3279	7.6439	9.0866	7.6873	7.7912
SD	15.9517	12.4665	14.5369	17.1197	15.7240	17.6550
Entropy	1.1420	0.8958	0.8130	0.9679	1.0357	0.9448
Homogeneity	0.9757	0.9709	0.9757	0.9627	0.9546	0.9574
Skewness	10.4036	12.2116	11.4925	9.5929	11.0321	10.2459
Kurtosis	133.3436	181.5880	153.6138	111.8887	138.6379	124.6958
IDM	1.4043E+03	3.7882E+03	2.8295E+03	1.2727E+03	2.9634E+03	1.2788E+03

Table 4.5: Extracted twelve features from NSCT subband coefficients of tumor region for six low grade glioma images

Features	**Image 1**	**Image 2**	**Image 3**	**Image 4**	**Image 5**	**Image 6**
Contrast	5.9846	3.4128	2.8275	2.6497	3.1031	2.6758
Correlation	0.4029	0.5652	0.5083	0.4696	0.5856	0.6366
Energy	0.5751	0.6562	0.7637	0.7791	0.7115	0.7506
Mean	1.5277	0.9460	1.5032	0.8314	1.9725	2.0616
Variance	157.7623	120.9439	175.6028	116.2335	209.2397	210.6177
RMS	6.7980	8.2056	4.9443	4.1585	8.4706	8.3375
SD	15.7874	13.0840	15.5285	11.4933	17.5195	16.9044
Entropy	1.8501	1.8586	1.2127	1.1071	1.4442	1.0955
Homogeneity	0.8491	0.9036	0.9256	0.9287	0.9206	0.9374
Skewness	7.9564	9.4908	9.5131	12.5152	7.5856	7.6068
Kurtosis	82.7797	129.5264	100.9678	182.3024	66.9889	66.9174
IDM	2.5442E+03	1.9211E+03	1.2493E+03	1.0319E+04	1.1443E+04	1.7010E+04

Table 4.6: Low grade and high grade glioma classification for kernel SVM classifier

Kernels	***TP***	***TN***	***FP***	***FN***	***Sensitivity (%)***	***Specificity (%)***	***Accuracy (%)***
Linear	28	2	6	13	68.29	33.33	61.22
Polynomial	33	3	5	8	80.48	37.5	73.47
GRB	35	5	3	6	85.36	62.5	81.63

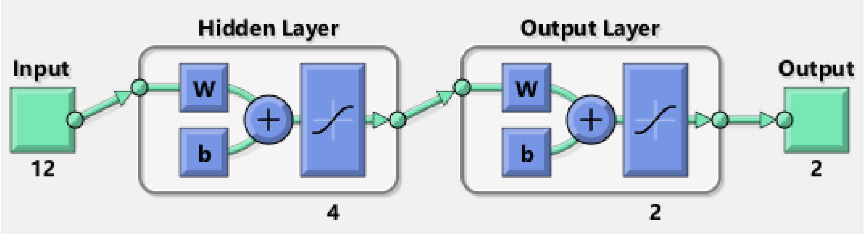

Figure 4.4: Neural network structure for our proposed classification scheme

4.2.3 Classification of Brain Tumor Using ANN

The neural network used in this proposed classification technique is feed forward neural network and scaled conjugate gradient back propagation algorithm is used for training of this network. For building ANN, neural pattern recognition app of MATLAB is used. Figure 4.4 exhibits the architecture of neural network. The network is composed of three layers: one input layer with twelve nodes which are equal to the input features of each segmented tumor region, one hidden layer with four hidden nodes and one output layer with two nodes corresponding to two classes, namely low grade or high grade. The performance curve of the brain tumor classification scheme using ANN is demonstrated in Figure 4.5. This graph represents the mean square error (MSE) values for training; validating and testing samples based different epoch values. MSE is used to measure the incongruity between two distributions. A classifier with small MSE is considered as a good classifier. So, lower value of MSE assures good performance [4] and for epoch 3, the best performance of validation is 9.8591E-05. The network takes 9 iterations to achieve its least MSE value. The regression of ANN classifier in the phases of training, validation and testing is demonstrated in Figure 4.6. The regression for training, validation, testing and overall is 0.92429, 0.99991, 0.9874 and 0.94769, respectively. This regression analysis illustrates fitting of data points to ideal regression line.

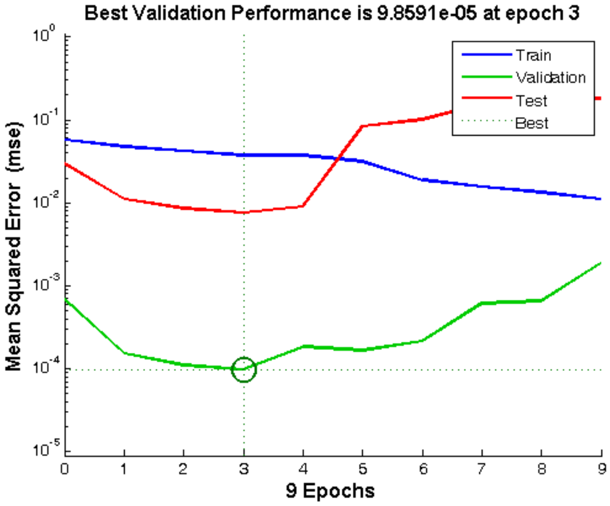

Figure 4.5: Performance curve of the proposed ANN based brain tumor classification scheme after training

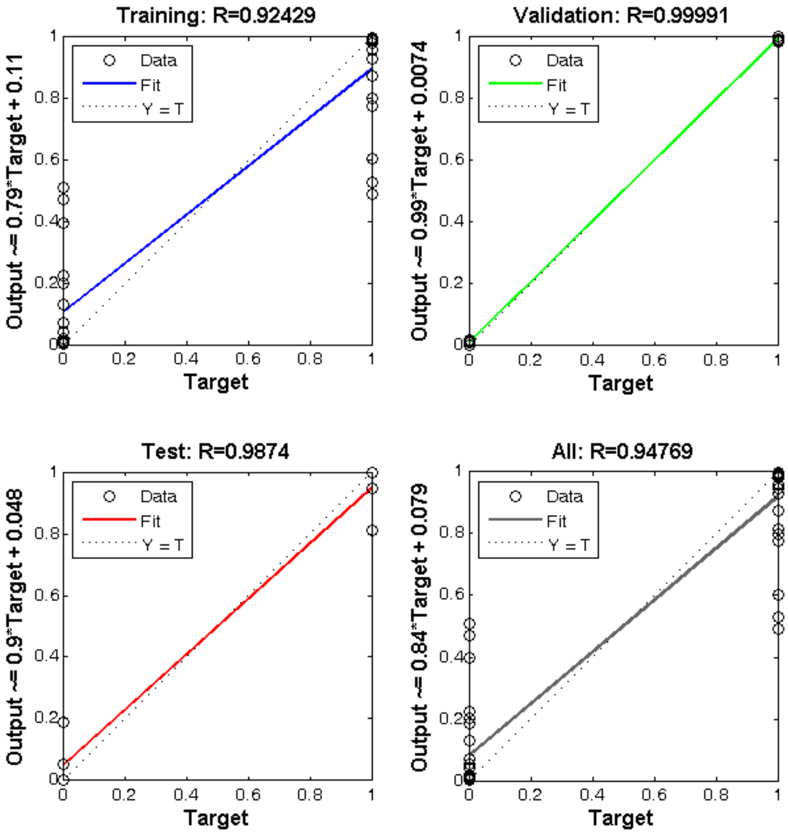

Figure 4.6: The regression process of the network

Table 4.7: Brain images classification comparison of proposed scheme with other schemes

Evaluating Parameters	**Scheme [5]**	**Scheme [6]**	**Scheme [7]**	**Scheme [8]**	**Proposed Scheme**
Sensitivity (%)	100	98.3	100	95	97.73
Specificity (%)	90	90	50	90	100
Accuracy (%)	98.7	97	84	94	98.15

Table 4.8: Performance comparison between SVM and ANN for tumor grade classification

Evaluating Parameters	**Linear kernel SVM**	**Polynomial kernel SVM**	**GRB kernel SVM**	**ANN**
Sensitivity (%)	68.29	80.48	85.36	90.24
Specificity (%)	33.33	37.5	62.5	62.5
Accuracy (%)	61.22	73.47	81.63	85.71

We also evaluate the testing performance of ANN classifier using 49 glioma images which are used for testing of SVM. After testing of neural network, we have obtain TP=37, TN=5, FP=3, FN=4. From the equation (5-7), we calculated sensitivity 90.24%, specificity 62.5% and accuracy 85.71% for Feed forward back propagation based ANN. Table 4.7 shows the performance comparison of normal or abnormal brain images classification results of proposed scheme with schemes [5], [6], [7], [8]. The normal and abnormal brain images classification sensitivity, specificity and accuracy of the proposed scheme are 97.73%, 100% and 98.15%, respectively. The overall classification accuracy is higher than other existing schemes. Table 4.8 demonstrates the performance comparison between SVM and ANN for tumor grade classification. The sensitivity, specificity and accuracy of linear kernel SVM is 68.29%, 33.33% and 61.22%, respectively. The classification accuracy of polynomial and GRB kernel SVM is 73.47% and 81.63%, respectively. But feed forward back propagation based ANN provides accuracy 85.71% which is greater than kernel based SVM.

4.3 Results and Discussions of Cellular Automata Based Watermarking Using NSCT and SVD

4.3.1 Platform and Performance Evaluating Parameters

MATLAB 2014a (32 bit) software is used to implement and evaluate the effectiveness of watermarking scheme. In order to estimate the performance of our scheme three popular performance evaluating parameters like Mean Square Error (MSE), Peak Signal to Noise Ratio (PSNR) and Normalized Correlation (NC) are used in watermarking area. MSE is an important parameter to find out the error between the cover image f_h and watermarked image f_w which is defined by following (4.4). PSNR is a well-known performance evaluating parameter which is used to estimate the imperceptibility [9] by finding out the resemblance between the cover image f_h and watermarked image f_w and is calculated from (4.5)

$$MSE = \frac{1}{MN}\sum_{i=1}^{M}\sum_{j=1}^{N}[f_h(i,j) - f_w(i,j)]^2 \tag{4.4}$$

$$PSNR = 10log_{10}\left[\frac{max^2}{MSE}\right] \tag{4.5}$$

where, *max* = maximum gray level value of the image.

Additionally, NC is a well-known parameter in the watermarking area for examining the uniformity between the original watermark W and extracted or recovered watermark W_e and is calculated from (4.6)

$$NC = \frac{\sum_{i=1}^{M}\sum_{j=1}^{N}(W(i,j) \times W_e(i,j))}{\sum_{i=1}^{M}\sum_{j=1}^{N}W(i,j)^2} \quad (4.6)$$

4.3.2 Imperceptibility Test

In experimental results section, we have experimented with different types of MRIs. Here we present our results for some of MRIs namely, brain MRI (Axial), brain MRI (Sagittal), thorax MRI and abdomen MRI which are collected form [10]. These MRIs are used as cover images and a binary watermark is embedded in these MRIs. Figure 4.7 demostrates the scrambled watermark using 1st, 2nd, 3rd, 4th, 5th, 6th and 7th generations of game of life. Figure 4.8 (a-d) demonstrates brain MRI (Axial), brain MRI (Sagittal), thorax MRI and abdomen MRI. Figure 4.8 (e) depicts the binary watermark. Figure 4.8 (f) shows the scrambled binary watermark using 7th generation of GOL. Figure 4.8 (g-j) shows the corresponding watermarked images. Figure 4.8 (k) shows the extracted watermark using correct secret keys and Figure 4.8 (l-n) demonstrates the extracted watermark using wrong secret keys.

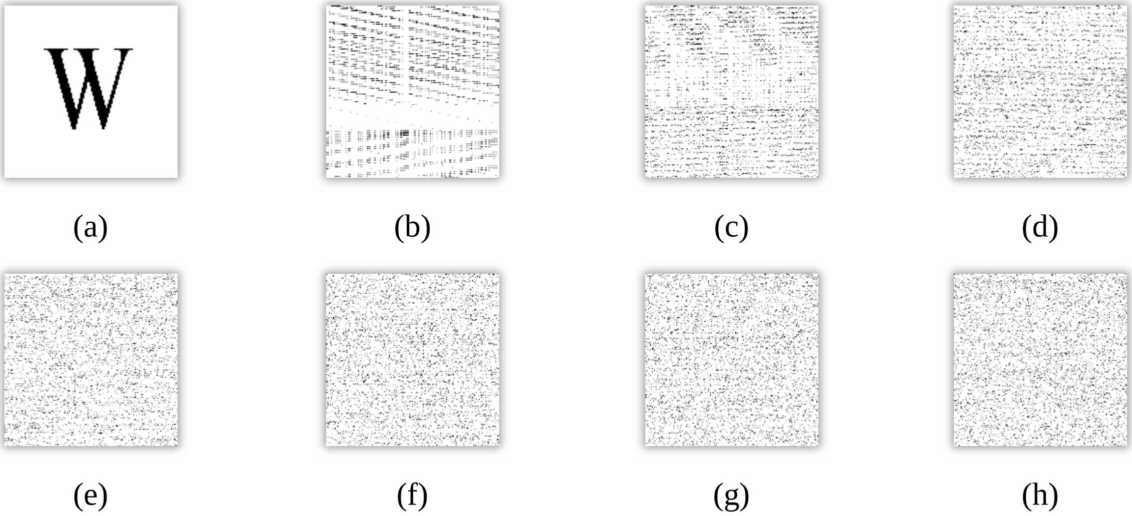
(a) (b) (c) (d)
(e) (f) (g) (h)

Figure 4.7: Watermark scrambling using game of life rules: (a) watermark; (b-h) watermark scrambling using 1st, 2nd, 3rd, 4th, 5th, 6th and 7th generation of game of life, respectively.

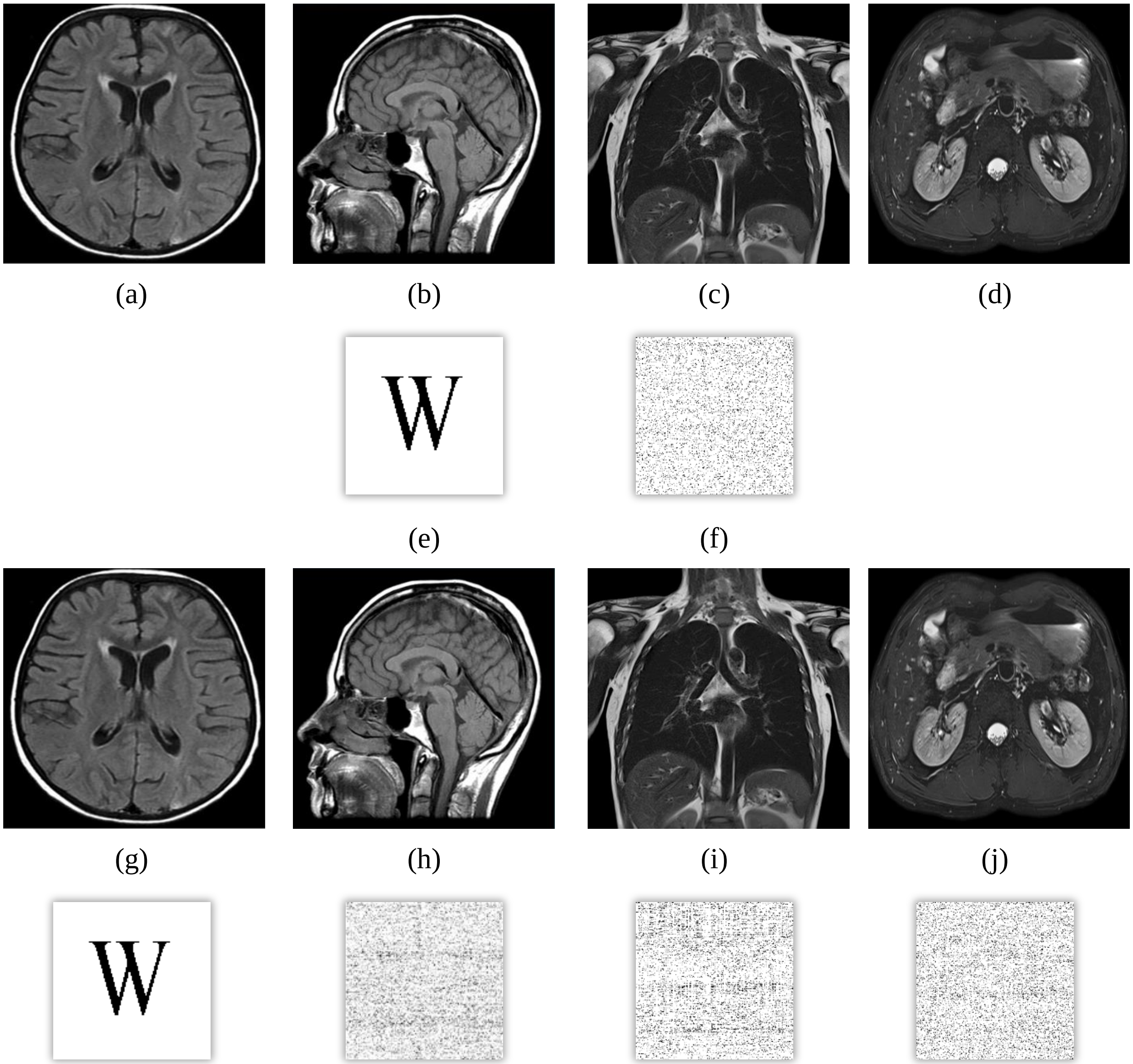

(a) (b) (c) (d)

(e) (f)

(g) (h) (i) (j)

(k) (l) (m) (n)

Figure 4.8: Cover image: (a) Brain MRI (Axial), (b) Brain MRI (Sagittal), (c) Thorax MRI, (d) Abdomen MRI; (e) binary watermark; (f) scrambled watermark after 7th generation of GOL; (g-j) Corresponding watermarked image; (k) extracted watermark using correct secret keys; (l-n) extracted watermark for wrong secret keys.

Table 4.9: MSE and PSNR values of watermarked images & NC of extracted watermark for various values of scaling factor, σ

Scaling Factor (σ)	**Brain MRI (Axial)**			**Brain MRI (Sagittal)**			**Thorax MRI**			**Abdomen MRI**		
	MSE	PSNR	NC	MSE	PSNR	NC	MSE	PSNR	NC	MSE	PSNR	NC
2	0.4146	52.0881	0.9938	0.4146	52.0653	0.9956	0.4145	51.0978	0.9995	0.4145	52.1596	0.9999
2.5	0.6479	50.1831	0.9959	0.6477	50.1544	0.9963	0.6477	49.1598	1.0000	0.6476	50.2716	1.0000
3	0.9329	48.6325	0.9968	0.9328	48.5981	0.9974	0.9326	47.5764	1.0000	0.9326	48.7379	1.0000
3.5	1.2698	47.3265	0.9972	1.2696	47.2863	0.9975	1.2694	46.2377	1.0000	1.2693	47.4486	1.0000
4	1.6586	46.1995	0.9973	1.6582	46.1536	0.9976	1.6580	45.0781	1.0000	1.6579	46.3381	1.0000
4.5	2.0991	45.2091	0.9973	2.0987	45.1576	0.9977	2.0984	44.0552	1.0000	2.0982	45.3641	1.0000
5	2.5915	44.3265	0.9974	2.5910	44.2694	0.9980	2.5907	43.1403	1.0000	2.5904	44.4977	1.0000
5.5	3.1357	43.5311	0.9978	3.1351	43.4684	0.9982	3.1347	42.3127	1.0000	3.1344	43.7184	1.0000
6	3.7318	42.8076	0.9983	3.7310	42.7394	0.9988	3.7305	41.5571	1.0000	3.7302	43.0108	1.0000

Scaling factor, σ is a pivotal factor in watermark embedding and extracting procedure. The range of scaling factor, σ is chosen so that the PSNR of watermarked image remains in accepted level. Table 4.9 demonstrates the MSE and PSNR values of watermarked images and NC of extracted watermark for various values of scaling factor σ. From the Table 4.9, it is observed that the value of MSE is increasing with increasing the value of σ, but the value of PSNR is decreasing with increasing the value of σ. The minimum value of PSNR is 38 dB which is accepted in the field of watermarking [9] but in our proposed method the PSNR value is greater than 50 dB when the value of σ is in the range of 2-2.5 for four MRIs. The value of NC of extracted watermark is increasing with increasing the value of σ. The value of NC is high when σ = 6 for two brain MRIs. In case of thorax and abdomen MRI, the value of NC is 1.0000 (ideal value) over the range σ = 2.5-6. But when the value of NC is high, the PSNR value of watermarked image is lowest that sometimes fails to satisfy the imperceptibility of watermarking. So, we choose the range of scaling factor, σ = 2.5-4 in our proposed watermarking scheme.

Figure 4.9 (a-d) and Figure 4.9 (e-h) demonstrate the watermarked images and their corresponding extracted watermark for scaling factor σ = 2, respectively. Similarly, Figure4.10, Figure 4.11 and Figure 4.12 demonstrate the watermarked images and their corresponding extracted watermark for scaling factor σ = 2, 3 and 4, respectively.

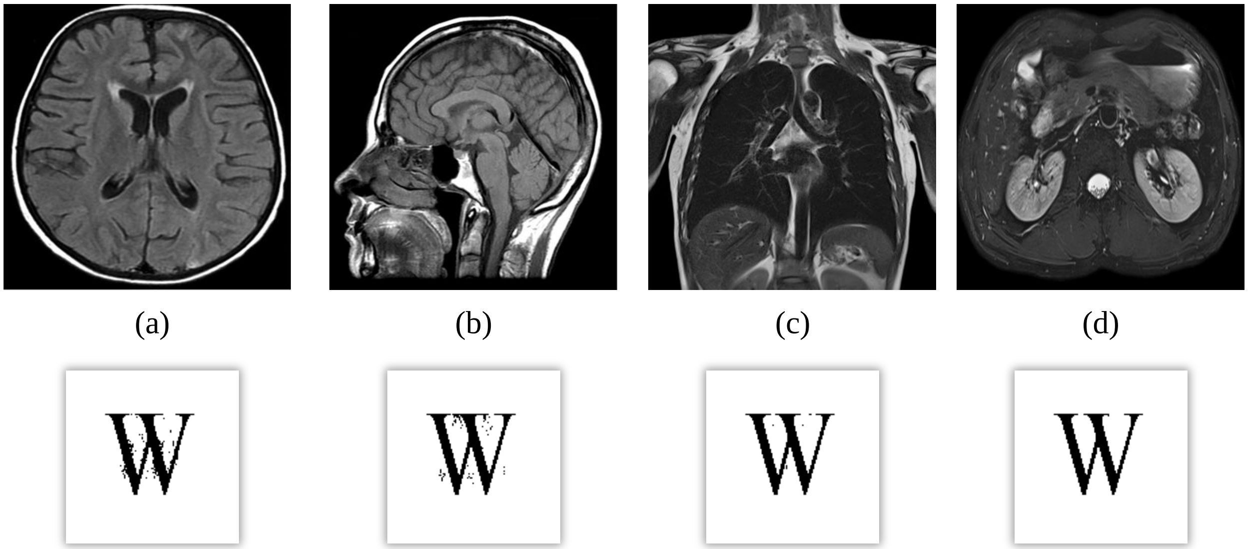

(a) (b) (c) (d)

(e) (f) (g) (h)

Figure 4.9: Watermarked images and their corresponding extracted watermark for scaling factor, σ = 2

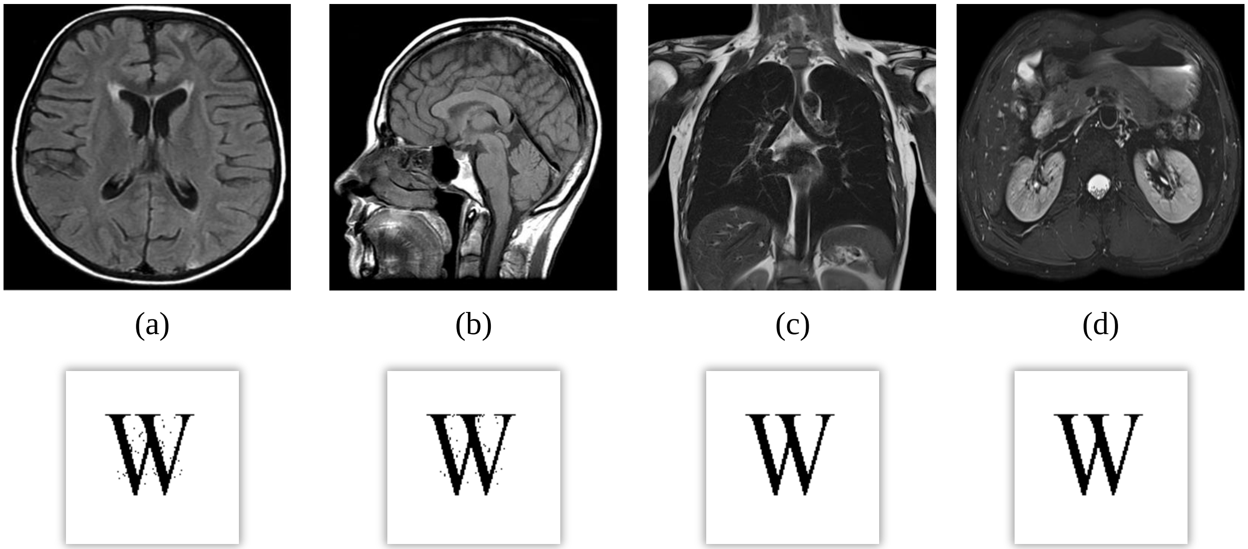

(a) (b) (c) (d)

(e) (f) (g) (h)

Figure 4.10: Watermarked images and their corresponding extracted watermark for scaling factor, σ = 3

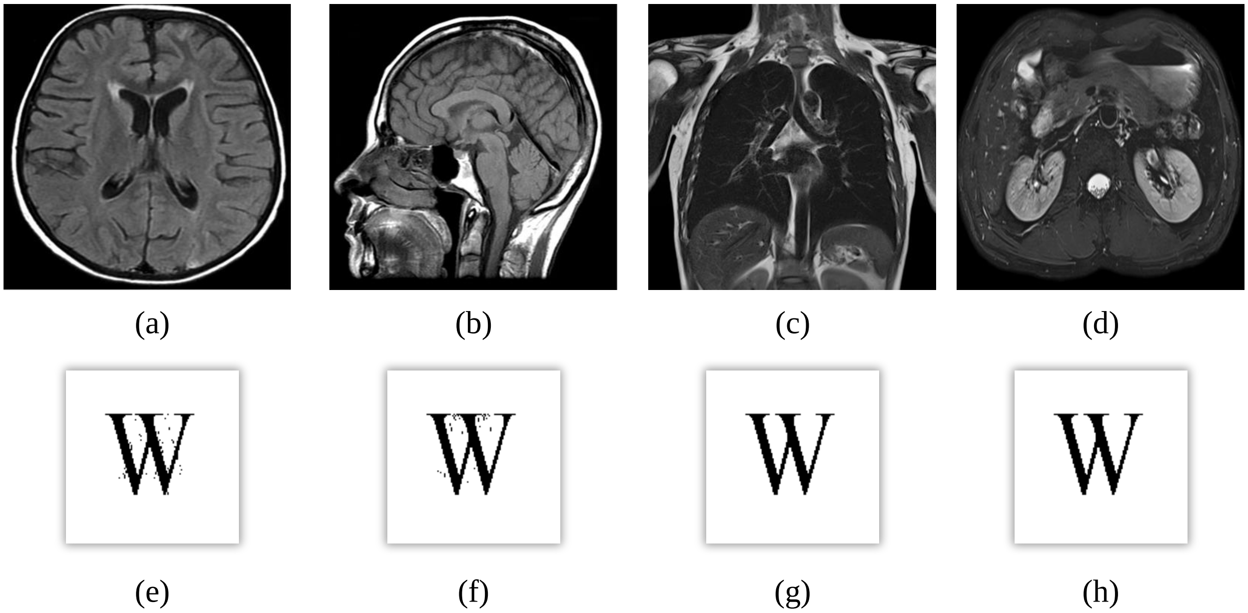
(a) (b) (c) (d)

(e) (f) (g) (h)

Figure 4.11: Watermarked images and their corresponding extracted watermark for scaling factor, σ = 4

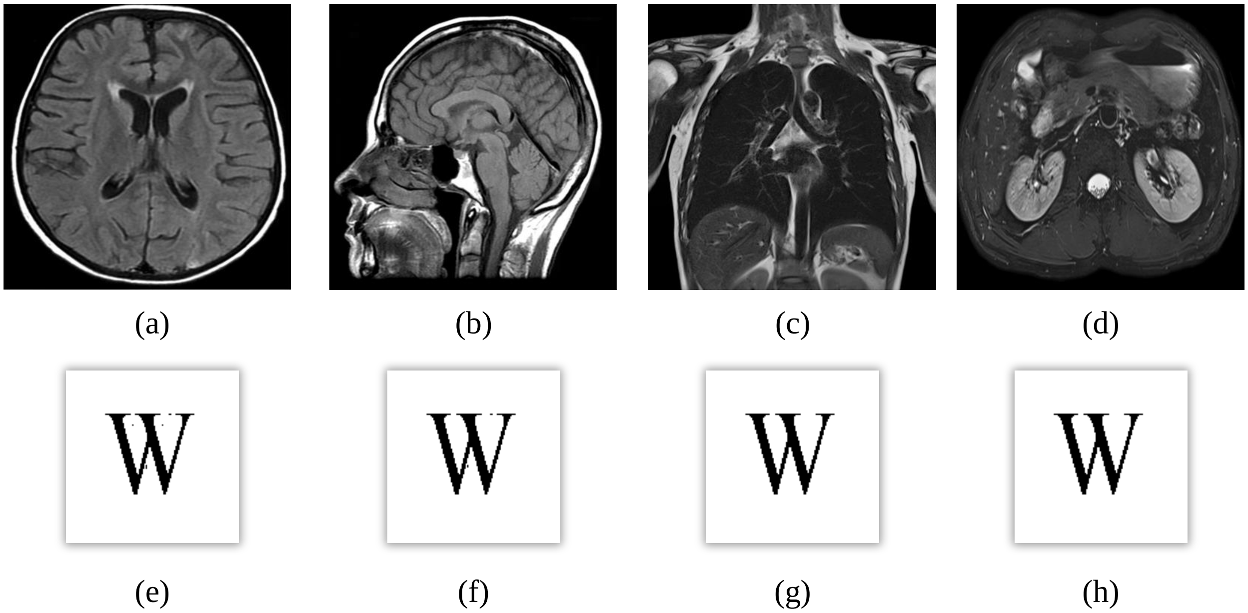
(a) (b) (c) (d)

(e) (f) (g) (h)

Figure 4.12: Watermarked images and their corresponding extracted watermark for scaling factor, σ = 5

4.3.3 Robustness Test & Comparison

For testing the robustness, various image processing and geometric attacks like Gaussian white noise, salt and pepper noise, median filtering, JPEG compression, cropping and rotation are used. At the receiver side, if the embedded watermark is extracted from the corrupted watermarked image, then the watermark would be robust and secure. Table 4.10 demonstrates the values of NC of extracted watermark from watermarked image under salt & pepper noise, Gaussian noise and speckle Noise attacks. From the Table 4.10, it is observed that the value of NC reduces with increasing the variance of noise. Our scheme provides satisfactory performance against Salt & Pepper Noise, Gaussian Noise and speckle noise with variance 0.001.

Table 4.10: NC of extracted watermark under noise addition attacks

Noise	**Brain MRI (Axial)**	**Brain MRI (Sagittal)**	**Thorax MRI**	**Abdomen MRI**
Salt & Pepper Noise (Variance=0.001)	0.9010	0.9453	0.9531	0.9909
Salt & Pepper Noise (Variance=0.003)	0.8235	0.8900	0.9571	0.9045
Salt & Pepper Noise (Variance=0.005)	0.4579	0.5667	0.8029	0.7002
Gaussian Noise (Variance=0.001)	0.8005	0.7006	0.7503	0.7212
Speckle Noise (Variance=0.001)	0.8107	0.7210	0.9998	0.9028

Table 4.11: NC of extracted watermark under JPEG compression attacks with different Q

JPEG Compression Attack (%)	**Brain MRI (Axial)**	**Brain MRI (Sagittal)**	**Thorax MRI**	**Abdomen MRI**
Q=90	0.9849	0.9568	0.9998	0.9885
Q=80	0.9527	0.9290	0.9987	0.9546
Q=70	0.8728	0.7828	0.8970	0.8526
Q=60	0.8612	0.7722	0.8790	0.8011
Q=50	0.8228	0.6050	0.8245	0.7321

Table 4.12: NC of extracted watermark under median filtering attacks

Median filtering Attack	**Brain MRI (Axial)**	**Brain MRI (Sagittal)**	**Thorax MRI**	**Abdomen MRI**
Median Filtering (2×2)	0.9297	0.9036	0.9456	0.9345
Median Filtering (3×3)	0.8292	0.7236	0.8423	0.8124
Median Filtering (5×5)	0.5356	0.4636	0.6057	0.5535

Table 4.13: NC of extracted watermark under geometric attacks

Median filtering Attack	**Brain MRI (Axial)**	**Brain MRI (Sagittal)**	**Thorax MRI**	**Abdomen MRI**
Rotation (angle 5)	0.9556	0.9145	0.9323	0.9278
Rotation (angle 10)	0.9023	0.8745	0.9078	0.8623
Cropping (Middle)	0.8945	0.8523	0.9089	0.9003

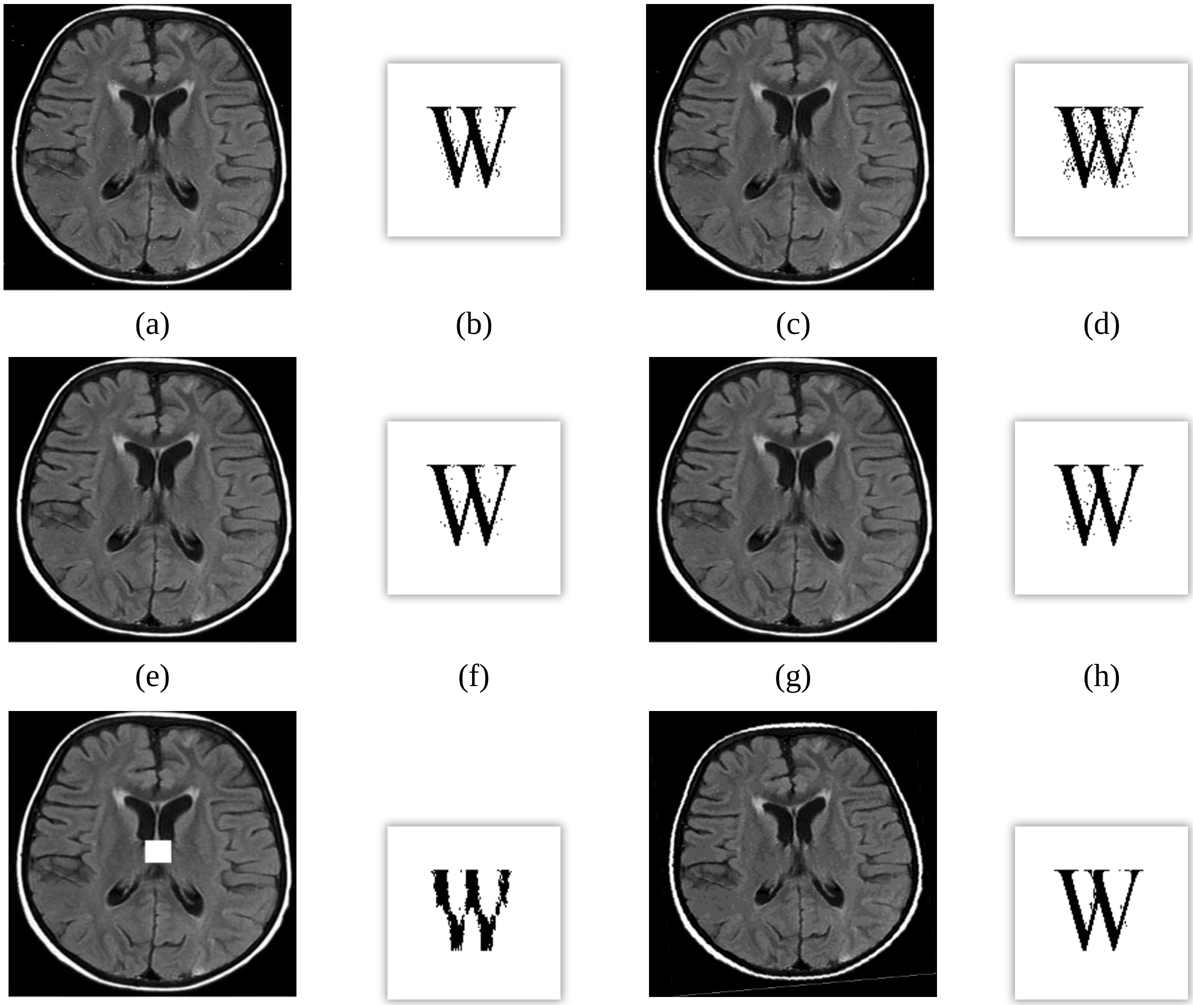

(a) (b) (c) (d)

(e) (f) (g) (h)

(i) (j) (k) (l)

Figure 4.13: Extraction of descrambled watermark from the watermarked brain MRI (axial): (a, b) Salt & pepper noise (0.001) attack, (c, d) speckle noise (0.001) attack, (e, f) JPEG compression (Q=90) attack, (g, h) JPEG compression (Q=80), (i, j) Cropping (middle), (k, l) Rotation (angle 5).

JPEG compression compresses an image in such a way that the visual quality of a compressed image is same as the original image. JEG compression with various quality factors is applied on watermarked brain MRI (Axial), brain MRI (Sagittal), thorax MRI and abdomen MRI. Table 4.11 demonstrates the values of NC of extracted watermark from watermarked image under JPEG compression attacks with different Q. High value of quality factor Q of JPEG compression means that the compressed image has higher image quality. So the higher value of Q results in lower compressed watermarked image. We got higher values of NC for thorax MRI Form the Table 4.11, it is observed that this scheme provides satisfactory performance under JPEG compression attacks. Table 4.12 demonstrates the values of NC of extracted watermark from watermarked image under median filtering attacks. The values of NC are decreasing with increasing the mask size of median filtering. For median filtering of 2×2, the NC values of extracted watermarks from Brain MRI (axial), Brain MRI (sagittal), Thorax MRI and Abdomen MRI are 0.9297, 0.9036, 0.9456 and 0.9345, respectively. For median filtering of 3×3, the values NC of watermarks are satisfactory, but in case of median filtering of 3×3, NC values are not in the accepted range. Table 4.13 summarizes the values of NC of extracted watermark under geometric attacks like rotation and cropping. The values of NC of extracted watermarks from four watermarked images are dependent on the angle of rotation and amount of cropping. NC values of extracted watermarks from four watermarked images are 0.9556, .09145, 0.9323 and 0.9278, respectively for rotation of angle 5. The values are reduced after increasing rotation angle from 5 to 10. A small portion is cropped from the middle of four watermarked images and we got NC values, 0.8945, 0.8523, 0.9089 and 0.9003. Figure 4.13 demonstrates some of descrambled watermark from watermarked brain MRI (axial) under salt & pepper noise, speckle noise, JPEG compression, cropping and rotation attacks. From the results it is observed that this scheme provides satisfactory performances against geometric attacks.

Figure 4.14 demonstrates the performance comparison of our proposed MRI watermarking scheme with scheme [11] in terms of NC under JPEG compression attacks with various values of quality factor, Q. Here The values of NC of our proposed scheme are higher than that of scheme [11] over the range of quality factor, Q= 50 to 90%. Figure 4.15 demonstrates the performance comparison of our proposed scheme with existing scheme [11], [12] and [13] in terms of PSNR. In our scheme, we got PNSR 52 dB which is higher than other schemes. From the chart it is observed that our proposed scheme has higher PSNR value than other existing schemes.

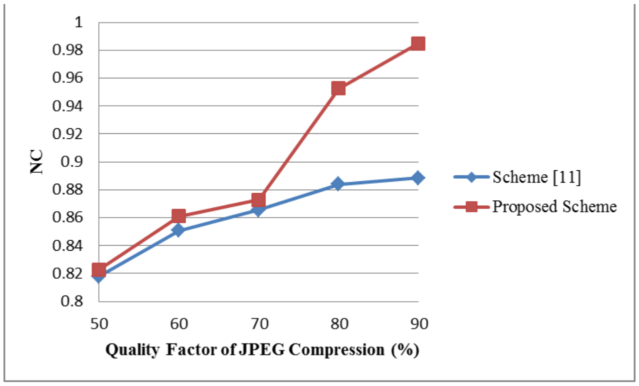

Figure 4.14: Performance comparison with scheme [11] in terms of NC under JPEG compression attacks with different quality factor, Q

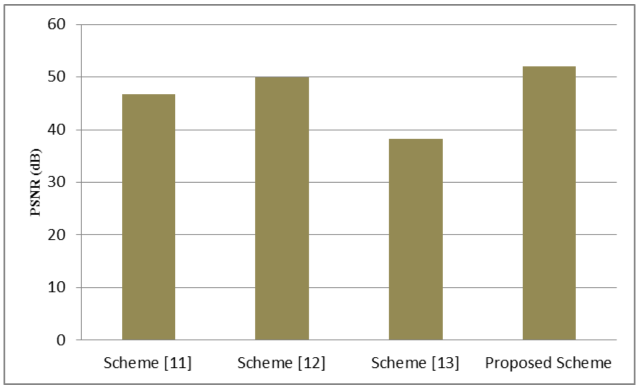

Figure 4.15: Performance comparison with schemes [11], [12] and [13] in terms of PSNR

4.3.4 Results Extension Using RGB Color Images

We also expand our result analysis section by applying our watermarking scheme in case of RGB color images. Here, we have used same watermark scrambling, embedding, extracting and descrambling algorithm that were described in section 3.3, but we have changed the cover image from MRI to color image. But in this case, the singular values of scrambled watermark are embedded to R, G and B plane of RGB color image separately. We have experimented with different types of color images. Here we present our results for some of color images namely, Lena ($384\times384\times3$, PNG), Peppers ($384\times384\times3$, TIFF) and Baboon ($384\times384\times3$, PNG). Binary watermark of size 128×128 is embedded in the red, green and blue components of those color images. The original color images, red, green, blue component of color Lena image, binary watermark image, scrambled watermark after 7th generation of game of life cellular automata, watermarked image and final extracted watermark after descrambling are shown in Figure 4.16 (a-h), respectively. Table 4.14 demonstrates the PSNR of watermarked images (Lena, Peppers and Baboon) and NC of extracted watermark for various values of scaling factor σ. We observed that the value of PSNR is decreasing with increasing the value of σ. The

(a) (b) (c) (d)

(e) (f) (g) (h)

Figure 4.16: (a) Cover Lena image; (b) red, (c) green, (d) blue component; (e) binary watermark; (f) scrambled watermark after 7th generation of GOL; (g) watermarked image; (h) extracted descrambled watermark

Table 4.14: PSNR of watermarked images (Lena, Peppers & Baboon) & NC of extracted watermark for various values of scaling factor

(σ)	**Lena**				**Peppers**				**Baboon**			
	PSNR			***NC***	***PSNR***			***NC***	***PSNR***			***NC***
	R	***G***	***B***		***R***	***G***	***B***		***R***	***G***	***B***	
0.2	71.73	70.58	71.99	0.999	72.05	71.97	72.07	0.998	71.53	70.46	71.72	0.998
0.4	65.72	64.56	65.97	1	65.98	65.96	66.05	1	65.51	64.45	65.70	1
0.6	62.20	61.80	62.45	1	62.47	62.45	62.53	1	61.99	60.92	62.18	1
0.8	59.70	58.55	59.95	1	59.99	59.96	60.03	1	59.68	58.42	59.49	1
1.0	58.01	57.76	57.46	1	58.09	58.03	58.07	1	57.74	56.48	57.55	1
1.2	56.43	56.18	55.03	1	56.51	56.46	56.50	1	56.16	54.90	55.96	1
1.4	55.09	54.84	53.69	1	55.18	55.13	55.17	1	54.82	53.56	54.62	1
1.6	53.93	53.68	52.54	1	54.02	53.98	54.03	1	53.67	52.40	53.46	1
1.8	52.91	52.66	51.52	1	53.00	52.97	53.03	1	52.64	51.38	52.44	1
2.0	52.00	51.75	50.60	1	52.08	52.06	52.13	1	51.73	50.46	51.53	1

Table 4.15: Performance of watermarking scheme against various image processing and geometric attacks

Type of Attack	**Lena**	**Peppers**	**Baboon**
	NC	***NC***	***NC***
No attack	1.0000	1.0000	1.0000
Salt & pepper (0.01)	0.9855	0.9815	0.9875
Salt & pepper (0.005)	0.9932	0.9920	0.9945
Gaussian noise (0.005)	0.9869	0.9853	0.9882
Speckle Noise (0.01)	0.9944	0.9919	0.9968
Median filtering (2,2)	0.9840	0.9829	0.9787
Cropping (upper left corner 5%)	0.8968	0.8912	0.9054
Cropping (middle 5%)	0.8723	0.8652	0.8839
Rotation (angle 10)	0.9657	0.9627	0.9689
Rotation (angle 15)	0.9052	0.9011	0.9116
JPEG compression (Q=50)	0.9745	0.9791	0.9753

minimum value of PSNR is 38 dB which is accepted in the field of watermarking [9] but in our proposed method the PSNR value is greater than 60 dB when the value of σ is in the range of 0.4-0.6. The value of NC is 1 for all values (0.4-2.0) of σ, except 0.2.

Table 4.15 demonstrates the performance our proposed watermarking scheme against different kinds of image processing and geometric attacks. The values of NC of extracted watermark from three watermarked images are 1, when no attack is applied. The NC values of watermarked for three noise attacks (salt & pepper, Gaussian and speckle) are in the accepted range. The extracted watermark provides NC values against median filtering of mask 2× 2, cropping (middle 5%), rotation (angle 10), JPEG compression are 0.9840, 0.8723, 0.9657 and 0.9745, respectively for Lena image. Extracted descrambled watermark from the watermarked image Lena after different distortion attacks, like salt & pepper noise (0.005), Gaussian noise (0.005), speckle Noise (0.01), median filtering (2,2), cropping (upper left corner 5%), cropping (middle 5%), image rotation (angle 10, 15) and JPEG compression (Q=40, 50) is demonstrated in Figure 4.17. The proposed scheme provides satisfactory performance against distortion attacks, which means that our scheme exhibits robustness against attacks as well as our scheme, provides imperceptibility and security.

Table 4.16 demonstrates the performance comparison of the proposed scheme for Lena image in terms of PSNR with three color image watermarking methods in different color spaces [14], [15], [16]. Table 4.17 demonstrates the performance comparison of the proposed scheme for Lena image in terms of NC with two color image watermarking schemes [14], [16]. Compared to other schemes, our proposed watermarking scheme provides better performance with respect to PSNR and NC.

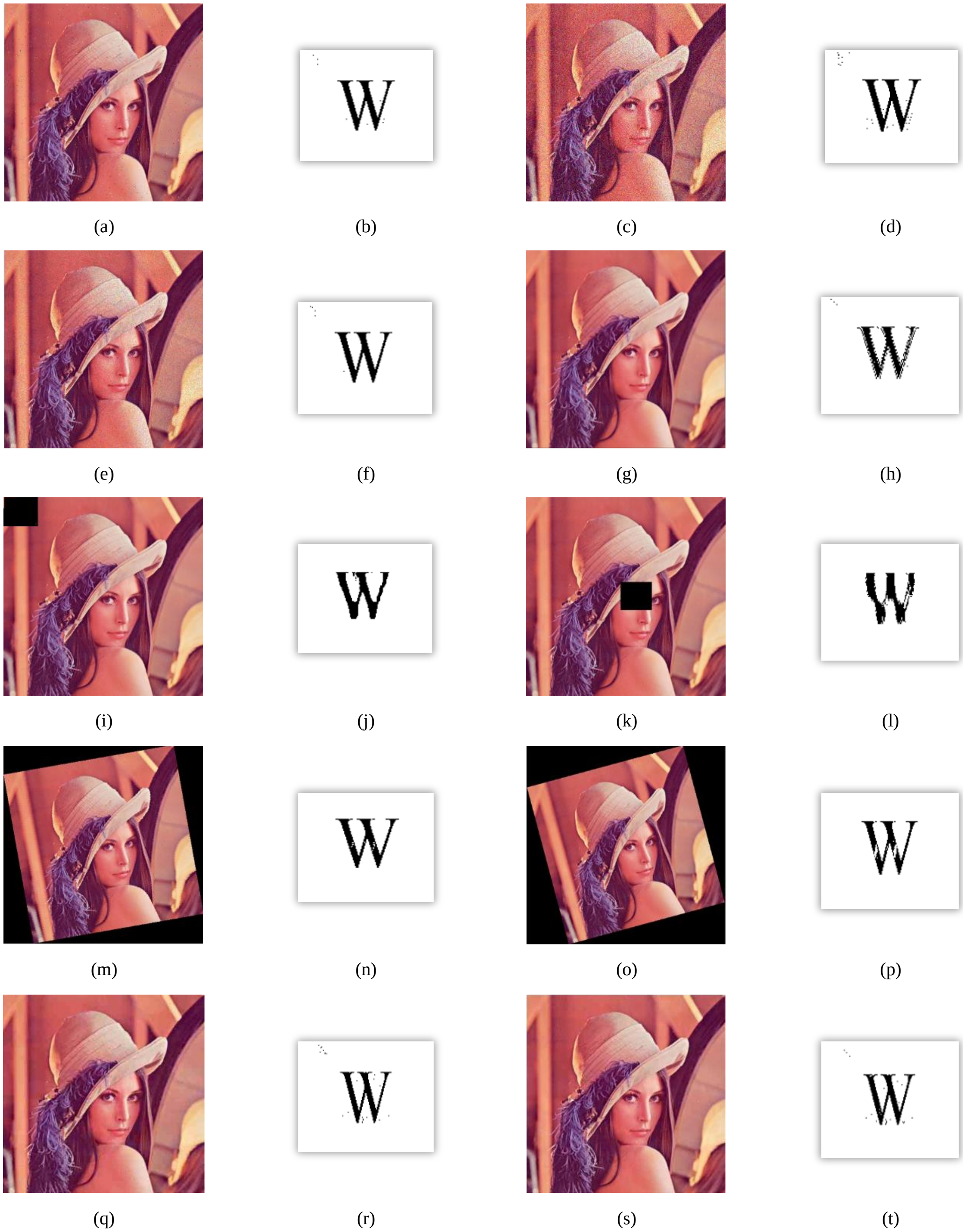

Figure 4.17: Extraction of descrambled watermark from the watermarked Lena image : (a, b) Salt & pepper noise (0.005) attack, (c, d) Gaussian noise (0.005) attack, (e, f) Speckle Noise (0.01) attack, (g, h) Median filtering (2,2), (i, j) Cropping (upper left corner 5%), (k, l) Cropping (middle 5%), (m, n) Image rotation (angle 10), (o, p) Image rotation (angle 15), (q, r) JPEG compression (Q=40) and (s, t) JPEG compression (Q=50)

Table 4.16: Performance comparison with other schemes in terms of PSNR

Scheme [14]		**Scheme [15]**		**Scheme [16]**		**Proposed Scheme**	
YUV	***PSNR***	***RGB***	***PSNR***	***YIQ***	***PSNR***	***RGB***	***PSNR***
Y	36.61	R	48.33	Y	52.28	R	65.72
U	33.95	G	48.20	I	47.39	G	64.56
V	30.26	B	48.63	Q	49.87	B	65.97

Table 4.17: Comparison results in terms of Normalized Correlation (NC)

Scheme [14]		**Scheme [16]**		**Proposed Scheme**	
YUV	***NC***	***YIQ***	***NC***	***RGB***	***NC***
Y	0.9980	Y	0.9988	R	1.000
U	0.9994	I	0.9990	G	1.000
V	0.9498	Q	0.9995	B	1.000

4.4 Results and Discussions of Multiple Chaotic Maps Based Watermarking Using NSCT and DCT

4.4.1 Imperceptibility Test

This MRI watermarking scheme is executed on MATLAB 2014a (32 bit) platform for three MRIs: brain axial MRI (*384×384×3*, TIFF), thorax MRI (384×384×3), TIFF, brain sagittal MRI (*384×384×3*, PNG). Among three watermarks, two watermarks include patient's confidential information. Three watermarks embedded into the corresponding cover images after encryption. Figure 4.18 (a-c), Figure 4.18 (d-f) and Figure 4.18 (g-i) demonstrates MRIs, watermarks and watermarked MRI, respectively. Figure 4.18 (j-l) depicts the significance of four secret keys. If any of the keys is wrong, then the watermark can't be recovered correctly. This scheme is also evaluated using PSNR and NC.

Table 18 exhibits PSNR values of the proposed MRI watermarking scheme for gain factor $\gamma = 1$ to 5. The changes of PSNR are demonstrated for brain axial MRI, thorax MRI and brain sagittal MRI. We observed that the value of PSNR is decreasing with increasing the value of σ. The minimum value of PSNR is 38 dB which is accepted in the field of watermarking [2] but in our proposed method the PSNR value is greater than 58 dB when the value of gain factor is in the range of 1-2. Three watermarks are embedded in three MRIs (brain axial, thorax, brain sagittal) individually and then PSNR is calculated. The values of PSNR for three MRIs are in the range from 58 to 44dB for gain factor 1-5.

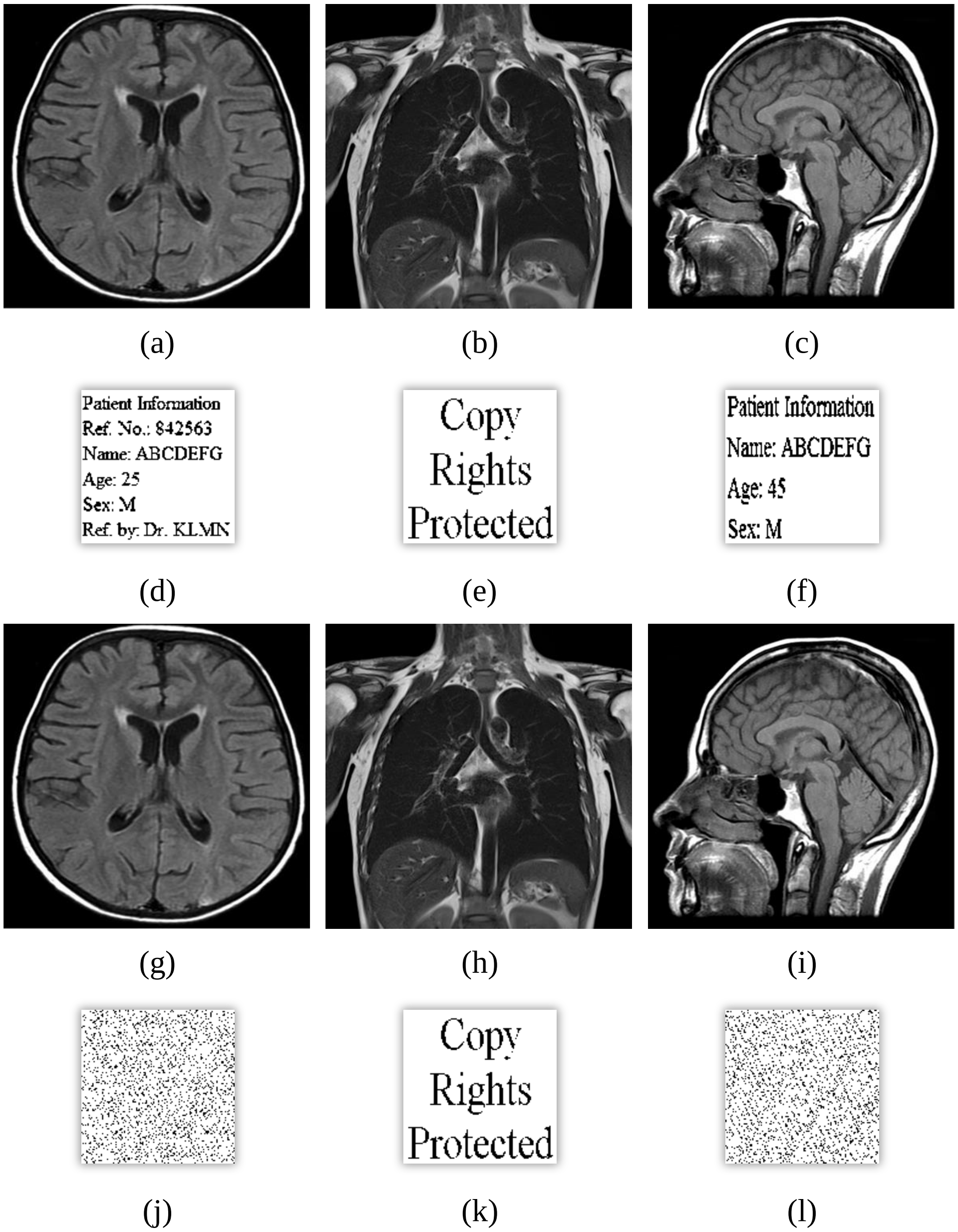

Figure 4.18: Cover image: (a) Brain MRI (sxial), (b) Thorax MRI, (c) Brain MRI (sagittal); (d-f) watermarks; (g-i) respective watermarked images; (f) unrecovered watermark for incorrect keys; (g) recovered watermark; (h) unrecovered watermark

Table 4.18: PSNR values of proposed watermarking scheme for various values of gain factor

Gain factor, γ	***PSNR (dB)***			
	Cover Image	***Watermark 1***	***Watermark 2***	***Watermark 3***
1	Brain MRI (Axial)	58.3265	58.2232	58.2759
	Thorax MRI	57.4640	57.3642	57.4153
	Brain MRI (Sagittal)	58.3273	58.2252	58.2787
2	Brain MRI (Axial)	52.3224	52.2170	52.2698
	Thorax MRI	51.4559	51.3575	51.4072
	Brain MRI (Sagittal)	52.3239	52.2209	52.2754
3	Brain MRI (Axial)	48.8170	48.7095	48.7624
	Thorax MRI	47.9466	47.8495	47.8979
	Brain MRI (Sagittal)	48.8192	48.7153	48.7709
4	Brain MRI (Axial)	46.3346	46.2250	46.2780
	Thorax MRI	45.4603	45.3646	45.4116
	Brain MRI (Sagittal)	46.3376	46.2328	46.2894
5	Brain MRI (Axial)	44.4128	44.3011	44.3543
	Thorax MRI	43.5345	43.4402	43.4859
	Brain MRI (Sagittal)	44.4165	44.3108	44.3684

4.4.2 Robustness Test & Comparison

Table 4.19: Performance of watermarking scheme against various image processing and geometric attacks

Noises	**Brain MRI (Axial)**	**Thorax MRI**	**Brain MRI (Sagittal)**
	NC	***NC***	***NC***
Salt & pepper (0.0001)	0.9952	0.9966	0.9947
Speckle (0.0002)	0.9934	0.9923	0.9912
Speckle (0.0001)	0.9945	0.9941	0.9934
Gaussian (0.0001)	0.9576	0.9425	0.9221
JPEG Compression (Q =90%)	0.9845	0.9981	0.9593
JPEG Compression (Q =70%)	0.9601	0.9845	0.9482
JPEG Compression (Q =50%)	0.9495	0.9709	0.9439
Rotation (angle 5°)	0.9256	0.9023	0.9156
Rotation (angle 7°)	0.8763	0.8545	0.8888
Cropping (5%)	0.9423	0.9379	0.9112

Table 4.19 depicts the NC values of recovered watermark by considering salt & pepper, speckle and Gaussian noise with different variances, JPEG compression, and geometric attacks. It has been observed that this MRI watermarking scheme ensures high values NC against noise addition attacks. But the proposed watermarking gives better performance under salt & pepper noise and speckle noise attacks rather than Gaussian noise attacks. JEG compression with various quality factors (Q=90%, 70%, and 50%) is applied on watermarked brain MRI (Axial), brain MRI (Sagittal), thorax MRI. The values of NC are reducing with decreasing of Q of JPEG compression. We got higher values of NC of watermark that is extracted from thorax MRI. The performance of MRI watermarking scheme under two

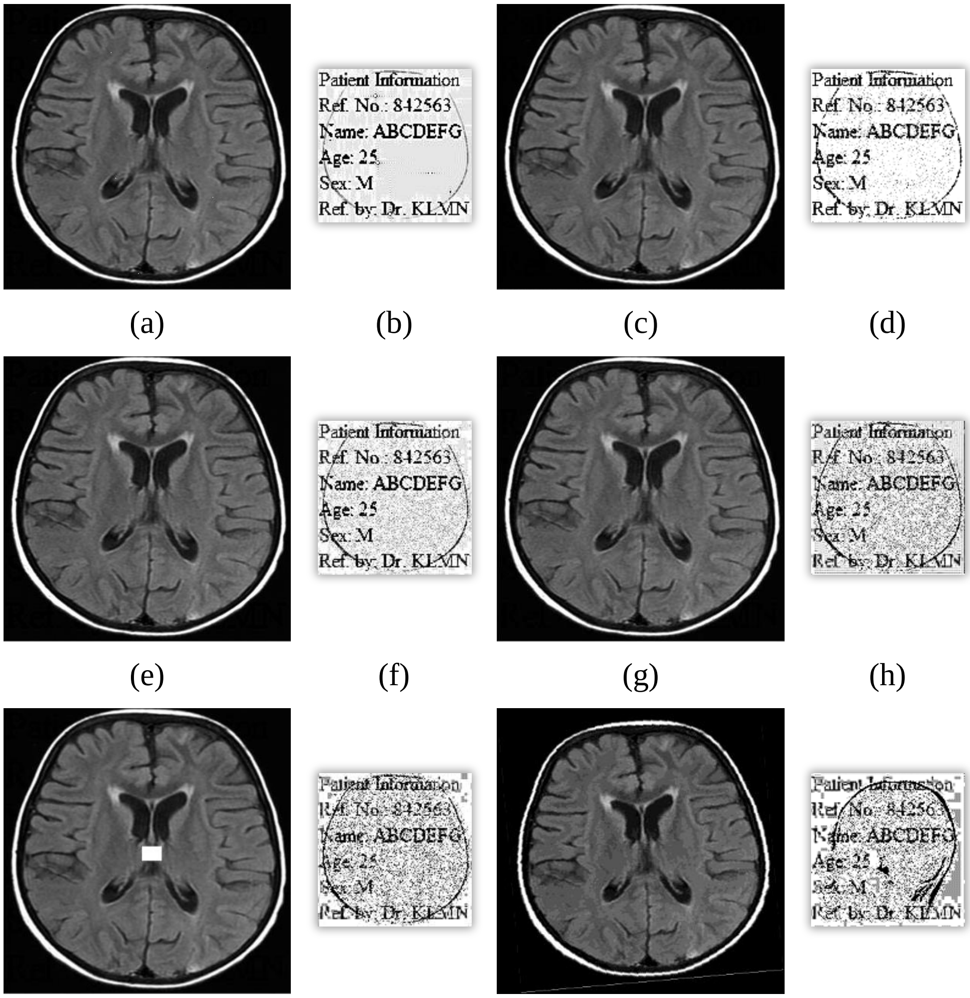

(a) (b) (c) (d)

(e) (f) (g) (h)

(i) (j) (k) (l)

Figure 4.19: Robustness test of the scheme : (a, b) Salt & pepper (0.0001) noise, (c, d), (c, d) Speckle (0.0001) noise, (e, f) Compression attacks (Q=80) (g, h) Compression attacks (Q=60), (i, j) Cropping (5%), (k, l) Rotation (5°)

geometric attacks like rotation and cropping is shown in Table 4.19. The quality of extracted watermark is not satisfactory under rotation attacks. Figure 4.19 exhibits the watermarked images and their corresponding extracted watermarks under various attacks. The quality of extracted patient record information is satisfactory under salt & pepper and speckle noise attacks with small variance. But the quality of extracted information degrades for JPEG compression with Q=60%, cropping and rotation attacks.

Fig. 4.20 and Fig. 4.21 demonstrates the comparison of MRI watermarking technique with other schemes [11], [12] with respect to JPEG compression and NC, respectively. Our scheme gives better performance than scheme [11] under JPEG compression attacks and also provides better PSNR compared with schemes [11], [12].

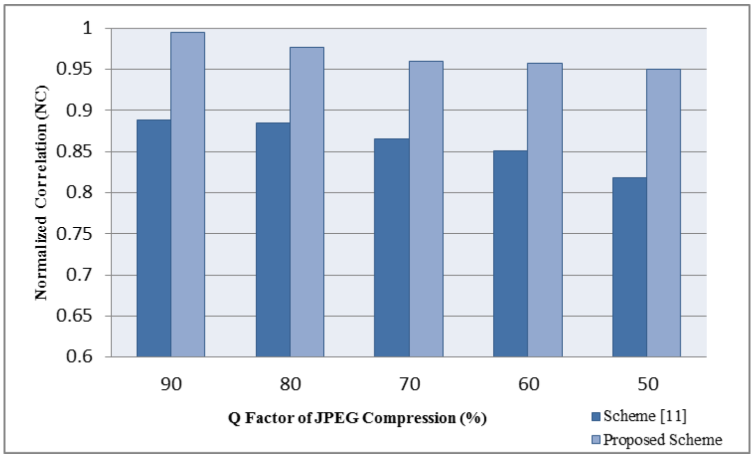

Figure 4.20: Performance comparison with scheme [11] in terms of NC under JPEG compression attacks.

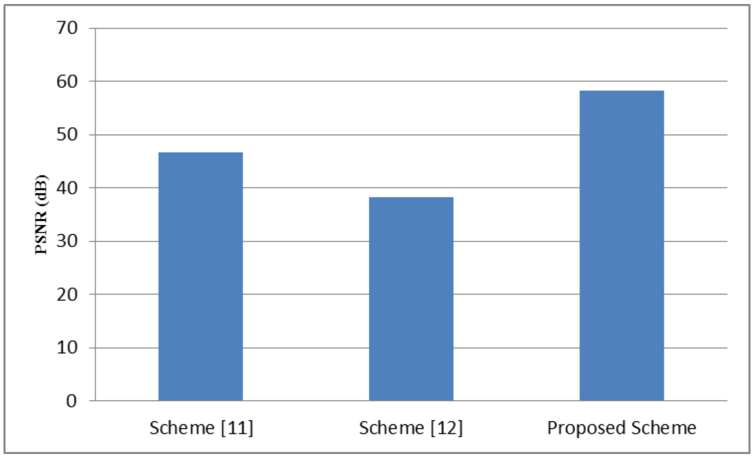

Figure 4.21: Performance comparison with respect to PSNR with schemes [11], [12]

4.5 Summary

In brain tumor classification scheme, we got classification accuracy of normal or abnormal brain image is 98.15% for GRB kernel based SVM. GRB kernel based SVM classifier provides tumor grade classification accuracy 81.63%, whereas feed forward back propagation based ANN classifier provides 85.71%. So, our proposed semi-automatic classification scheme gives promising performance for classification of normal or abnormal brain images and then low or high grade tumors. In 1st watermarking scheme, cellular automata keys and the embedding key array improve the security of proposed scheme because without these secret keys, no one can extract and descramble the watermark. Besides, NSCT and SVD assure the robustness against different distortion attacks. PSNR and NC are used to evaluate the efficacy of the watermarking scheme and this scheme presents security, imperceptibility and robustness. In 2nd watermarking scheme, multiple chaotic maps are used for scrambling patient's information and the keys that are associated with this scrambling process improve security of watermarking scheme. Here, both NSCT and DCT ensure robustness and imperceptibility of the watermarking scheme. Experimental results in terms of MSE, PSNR and NC demonstrate that our proposed watermarking scheme ensures better image quality compared to other methods.

References

[1] BRATS 2015 (Multimodal Brain Tumor Segmentation Challenges). < https://www.smir.ch/BRATS/Start2015/>

[2] B.H. Menze, A. Jakab, S. Bauer, J.K. Cramer, K. Farahani, J. Kirby, Y. Burren, N. Porz, J. Slotboom, R. Wiest, L. Lanczi,"The multimodal brain tumor image segmentation benchmark (BRATS),"*IEEE Transactions on Medical Imaging*, vol. 34 (10), pp.1993-2024, Dec. 2014.

[3] M. Kistler, S. Bonaretti, M. Pfahrer, R. Niklaus, and P. Buchler, "The virtual skeleton database: An open acess repository for biomedical research and collaboration," *Journal of Medical Internet Research,* vol. 15 (11), pp.e245, Nov. 2013.

[4] R. Ahmmed and M.F. Hossain, " Tumor detection in brain MRI image using template based K-means and Fuzzy C-means clustering algorithm," in Proc. *International Conference on Computer Communication and Informatics (ICCCI),* Jan. 2016.

[5] M. Ahmad, M.U. Hassan, I. Shafi and A. Osman, "Classification of tumors in human brain MRI using wavelet and support vector machine," *IOSR Journal of Computer Engineering (IOSRJCE)*, vol. 8(2), pp. 25-31, 2012.

[6] E.S.A. El-Dahshan, T. Hosny and A.B.M Salem, "Hybrid intelligent techniques for MRI brain images classification," *Digital Signal Processing*, vol. 20, pp. 433-441, 2010.

[7] H.B. Nandpuru, S.S. Salankar, and V.R. Bora, "MRI brain cancer classification using support vector machine," in Proc. of *IEEE Students' Conference on Electrical, Electronics and Computer Science*, March 2014.

[8] P. Kumar and B. Vijayakumar, "Brain tumor MR image segmentation and classification using by PCA and RBF kernel based support vector machine," *Middle-East Journal of Scientific Research*, vol. 23(9), pp. 2106-2116, 2015.

[9] Y.P. Lee, J.C. Lee, W.K. Chen, K.C. Chang, I.J. Su and C.P. Chang "High-payload image hiding with quality recovery using tri-way pixel-value differencing," Information Sciences, vol. 191, pp. 214-225, 2012.

[10] http://www.northcountryneurology.com/3-tesla-mri-magnetic-resonance-imaging/

[11] H.K. Lee, H.J. Kim, K.R. Kwon, and J.K. Lee, "ROI medical image watermarking using DWT and bit plane," in Proc. of *Asia-Pacific Conference on Communications,* October, 2017.

[12] J. Li, M. Huang, H. Zhang, C. Dong, and Y. Bai " The medical images watermarking using DWT and Arnold," in Proc. of *International Conference on Computer Science and Automation Engineering (CSAE)*, 2012.

[13] A.S. Nedooshan, K. Yaghmaie and R.S. Nadooshan, "Medical image watermarking based on SVD-DWT technique," *International Congress on Informatics, Environment, Energy and Applications (IEEA),* vol. 38, 2012.

[14] S.K. Bhagyashri and M.Y. Joshi, "All frequency band DWT-SVD robust watermarking technique for color images in YUV color space," in Proc. of

International Conference on Computer Science and Automation Engineering (ICCSAE), pp. 292-299, June 2011.

[15] I.A. Nasir and A.B. Abdurrman, “A robust color image watermarking scheme based on image normalization,” in Proc. of World Congress on Engineering (WCE), vol. 3, July 2013.

[16] B.L. Gunjal and S.N. Mali, “Comparative performance analysis of DWT-SVD based color image watermarking technique in YUV, RGB and YIQ color spaces,”Internatioal Journal of Computer Theory and Engineering, vol. 3, no. 6, pp. 714-179, December 2011.

CHAPTER V

CONCLUSIONS

5.1 Outcomes

In this thesis paper, brain tumor classification and watermarking of MRI using nonsubsampled contourlet transform (NSCT) has been proposed. In chapter 3, NSCT based MRI brain tumor classification using SVM and ANN is proposed. Then cellular automata based watermarking using NSCT and SVD has been proposed. Finally, MRI watermarking using multiple chaotic maps, NSCT and DCT is proposed. In chapter 4, the results and discussion of these proposed techniques are outlined. There are some promising outcomes of these three schemes that have been observed through this entire thesis. In this section, these outcomes are outlined successively which will demonstrate the entire thesis work at a glance. The outcomes are given below.

- A hybrid scheme for classification of MRI brain tumor is proposed.
- NSCT is used for extracting twelve features from segmented image because of its outstanding performance in image analysis applications.
- SVM is used in this scheme in order to classify MRI image as normal or abnormal and then to classify the grade of tumor as low or high grade.
- For GRB kernel based SVM classifier, the classification accuracy of normal or abnormal brain image is 98.15%. GRB kernel based SVM classifier provides tumor grade classification accuracy 81.63%.
- The grade of tumor is also classified using the feed forward back propagation based ANN classifier and this classifier provides tumor grade classification accuracy 85.71%.
- Cellular automata based watermarking using NSCT and SVD is proposed.

- This scheme offers security, imperceptibility and robustness against various image processing and geometric attacks like Gaussian white noise, salt and pepper noise, median filtering, JPEG compression, cropping and rotation.

- Another hybrid MRI medical images watermarking technique has been proposed in this research using chaotic maps, NSCT and DCT.

- Three chaotic maps and their four secret keys are incorporated in this watermarking technique and they are used in different ways to ameliorate the security of the scheme.

- Combination of NSCT and DCT also enhances the robustness and imperceptibility of MRI watermarking scheme.

- Experimental results in terms of MSE, PSNR and NC demonstrate that our proposed two watermarking schemes ensure better image quality compared to other existing methods.

5.2 Applications and Future Works

This proposed brain tumor classification scheme can be used to classify brain image as normal or abnormal and also to classify grade of tumor as low grade, where tumor is slowly growing or high grade, where tumor is rapidly growing. This watermarking scheme can be used to ensure security of multimedia contents while transferring through the communication channel.

In brain tumor classification scheme, some modified and advanced segmentation technique can be used in future for proper segmentation of region of interest of MRI image. Further validation of the proposed brain tumor classification scheme is needed by consideration of more standard datasets with large number of images and of various performance evaluation parameters. In this scheme, tumor is classified into two types, but further classification of tumors like grade I, II, III and IV is needed to be fulfilled which will be addressed in future works. Feed forward back propagation neural network ANN is used for classification of brain tumors, but other neural networks like self-organizing neural network can be used for elaborating results which will be fulfilled in future.

In watermarking schemes, cellular automata and multiple chaotic maps are used for improving security. In future, some more advanced image encryption or scrambling algorithm can be used. These two schemes show robustness against a limited number of noise attacks, other noise attacks like sharpening, blurring, histogram equalization can be used in future for expanding the results analysis. The performance of the schemes are evaluated by considering

MRIs, more medical images like CT, PET can be used in future. However, further validation of the proposed watermarking schemes is needed by consideration of more performance evaluating parameters and of more other promising methods for comparison which will be fulfilled in future.

5.3 Limitations

Sometimes K-means clustering is not so enough for segmenting region of interest for some brain MRIs which do not have sufficient image quality. Higher level of NSCT requires more manipulations which also rise the computational time of our tumor classification scheme. Although our method provides outstanding performance for 79 glioma images, but the real scenario is quite different because of a large number of MRIs with complicated tumor.

Cellular automata is used in first watermarking scheme and multiple chaotic maps are applied in second watermarking scheme in order to improve security, but what level of security that cellular automata and multiple chaotic maps provide in watermarking schemes, we could not measure that level. These two methods will fail to show robustness against Gaussian white noise, salt and pepper noise, speckle noise median filtering with large variance. Sometimes the extracted watermarks cannot be identified well, if the percentage of cropping and angle of rotation is increased.

List of Publications

Conference paper

1. C. Saha and M.F. Hossain, “MRI brain tumor images classification using k-means clustering, NSCT and SVM,” in Proc. of *4th Uttar Pradesh Section International Conference on Electrical, Computer and Electronics (UPCON)*, October, 2017, Mathura, India.

2. C. Saha and M.F. Hossain, Cellular automata based color image watermarking using NSCT-SVD,” in Proc. of *4th Uttar Pradesh Section International Conference on Electrical, Computer and Electronics (UPCON)*, October, 2017, Mathura, India.